

https://dspace.org/

The immunomodulatory effects of acute in vitro 1,25D3 supplementation on the metabolic profiles of monocytes and monocyte-derived macrophages

Chetty, Caitlyn Uraesha

2025-07
University of the Witwatersrand, Johannesburg
https://hdl.handle.net/10539/50201

Chetty, Caitlyn Uraesha. (2025). The immunomodulatory effects of acute in vitro 1,25D3 supplementation on the metabolic profiles of monocytes and monocyte-derived macrophages. [Master's dissertation, University of the Witwatersrand, Johannesburg]. WIReDSpace. https://hdl.handle.net/10539/50201

Downloaded from a DSpace repository. https://dspace.org/



The immunomodulatory effects of acute *in vitro* 1,25D_3 supplementation on the metabolic profiles of monocytes and monocyte-derived macrophages

by

Caitlyn Uraesha Chetty

2274031

Dissertation

Submitted in fulfilment of the requirements for the degree

Master of Science

in

Molecular and Cell Biology

in the Faculty of Science, University of the Witwatersrand, Johannesburg, South Africa

Supervisor: Dr.Vanessa Meyer

Co-supervisor: Dr. Nikki L. Gentle

July 2025

I, **Caitlyn Uraesha Chetty (2274031)**, am a student registered for the degree of **Master of Science** in the academic year **2025**.

I hereby declare the following:

- I am aware that plagiarism (the use of someone else's work without their permission and/or without acknowledging the original source) is wrong.
- I confirm that the work submitted for assessment for the above degree is my own unaided work except where explicitly indicated otherwise and acknowledged. In this context, I understand that the use of editing services is considered aided work and must be declared.
- I have not submitted this work before for any other degree or examination at this or any other University.
- The information used in the Dissertation **HAS NOT** been obtained by me while employed by, or working under the aegis of, any person or organisation other than the University.
- I have followed the required conventions in referencing the thoughts and ideas of others.
- I understand that the University of the Witwatersrand may take disciplinary action against me if there is a belief that this is not my own unaided work or that I have failed to acknowledge the source of the ideas or words in my writing.



Name: Caitlyn Uraesha Chetty Date: 08 July 2025

Monocytes and monocyte-derived macrophages (MDMs) form integral parts of the innate immune system, contributing to host defence through pathogen recognition, immune signalling, and metabolic adaptations. The immunomodulatory properties of 1,25-dihydroxyvitamin D_3 ($1,25D_3$) are well documented, yet its role in metabolic reprogramming and the potential induction of trained immunity remains largely unexplored. This study sought to evaluate the metabolic profiles of monocytes and MDMs, and assess the impact of acute *in vitro* $1,25D_3$ supplementation using an untargeted metabolomics approach. Additionally, transcriptional responses to TLR8 stimulation were examined to evaluate functional consequences at the mRNA level. Monocytes and MDMs displayed distinct metabolic profiles, with principal component analysis (PCA) revealing clear separation between these cell types. Following 4 hrs of $1,25D_3$ supplementation, monocytes exhibited a significant metabolic shift, clustering closer to MDMs. Metabolomic analysis identified fumarate and unknown metabolite 1 as key discriminatory metabolites, with fumarate being significantly elevated and unknown metabolite 1 significantly reduced in both MDMs and $1,25D_3$-supplemented monocytes. This suggests that acute $1,25D_3$ supplementation drives a metabolic state akin to MDMs, potentially priming monocytes for enhanced immune responses. Pathway analysis revealed several alterations in the tricarboxylic acid (TCA) cycle, alanine, aspartate, and glutamate (AAG) metabolism, methionine metabolism, galactose metabolism, as well as fatty acid biosynthesis pathway supporting the hypothesis of metabolic reprogramming. Gene expression analysis demonstrated that under homeostatic conditions, $1,25D_3$ significantly enhanced the expression of *CCL2* and *CXCL10* in monocytes whilst downregulating their expression in MDMs, highlighting cell-type-specific regulatory effects. Additionally, in the presence of TLR8 stimulation, expression of inflammatory markers were significantly elevated in monocytes supplemented with $1,25D_3$, further supporting the functional priming of these cells. Collectively, these findings suggest that acute $1,25D_3$ supplementation modulates monocyte metabolism and transcriptional activity in a manner consistent with the induction of trained immunity. This analysis delivers original insights into the metabolic regulation of monocyte function and the broader implications of $1,25D_3$ in immune modulation, with potential relevance for therapeutic applications in infectious and inflammatory diseases.

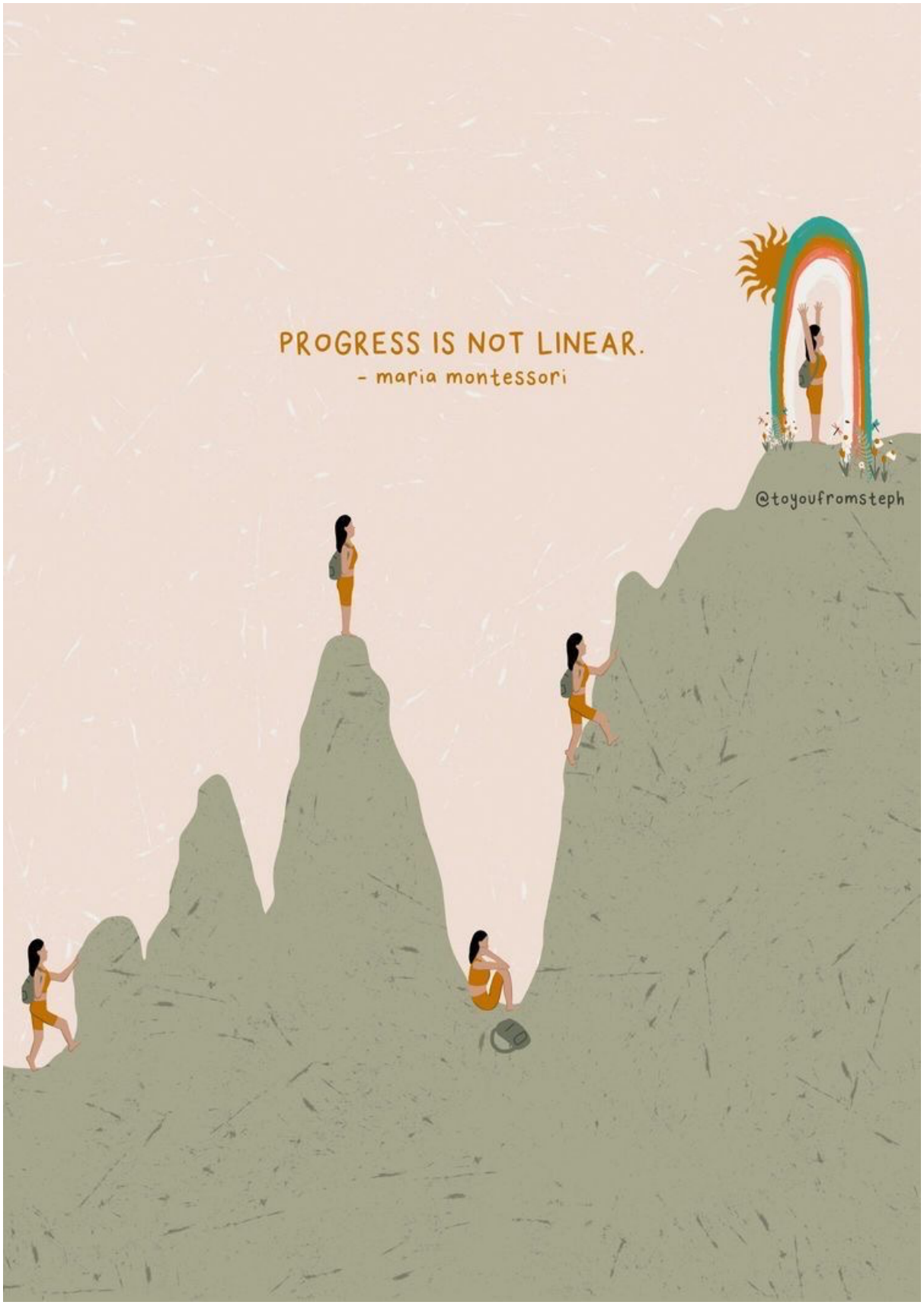
PROGRESS IS NOT LINEAR.
- maria montessori
@toyoufromsteph

I would like to acknowledge the National Research Foundation (NRF) for funding this project and the second year of my MSc degree.

Dr. Meyer, where do I even begin? Thank you for introducing me to the fascinating world of metabolomics and for believing in me from the very start. Your unwavering encouragement and guidance has inspired me to exceed my own expectations. I am truly grateful for how you've always made time to answer my calls and for patiently responding to my voice notes and messages, especially those filled with midnight thoughts. Your consistent support, thoughtful check-ins, and shared laughter have meant the world to me. Most importantly, thank you for helping me realise my potential as a scientist.

I would also like to thank my co-supervisor, Dr. Gentle for always providing insightful perspectives on my writing.

To my immediate family. My mom, Natasha, my hero—thank you for shaping me into the person I am today, for pushing me to achieve my goals, and for always reminding me that I can accomplish anything I set my mind to. I will forever cherish our long calls whenever I felt lonely in JHB, our little girls' weekends whenever you had conferences in JHB, and, most of all, for your unconditional love and support. My dad, Rubin—thank you for shaping me into the person that I am, for always challenging me to think critically, for encouraging me to follow my heart, and for your unwavering love and support. To my brother, Dr. Kyle—thank you for everything. I love you, brother dear.

To my boyfriend and best friend, Nishalan—thank you for your unwavering love and support throughout this journey. These last two years have been transformative for both of us, and I am beyond grateful for everything you've done. Thank you for encouraging me to pursue my MSc at WITS, for listening to me talk about how cool metabolomics is (even when you barely understood what I was saying), for visiting me in JHB whenever you could, and for always being there—whether it was driving me to campus, sitting in the lab with me on weekends or late nights, or simply giving me a pep talk whenever I felt like I couldn't go on. Your belief in me and your constant support have meant the world.

To my PTA family—Vigen, Vanessa, Clinton, Melissa, Khalin, Kerry, Kizzy, Trist, Aidy, and Sudeshan (whose now in Abu Dhabi)—thank you all for your unwavering support

over the last two years. Thank you for helping me move in and out of Stanley Studios, picking me up for weekend visits, temporary lodging, making an effort to always drop and pick me up from the airport, and for consistently checking in on me. Thank you for the amazing memories and, most of all, for always supporting me. To my Roodeport family—the Maistrys—thank you for always offering to take me to PMB and for being so kind and helpful in every single way. To my PMB family—the Aiyers—thank you for all your love and support throughout. I am deeply grateful for each of you.

I would also like to thank Jaivan for being such a great friend and brotherly figure during my time in JHB. Your willingness to help whenever you could has meant so much to me. I truly appreciate your support and kindness.

Lastly, I'd like to thank my labmates and friends— Janet and Palesa. To Janet, we did it! From being two outsiders stepping into WITS as postgrads, to the countless 06h00 lab mornings, laughter, and care—I appreciate it all. To Palesa, though we met later on in my journey, thank you for all the laughs, tea spills, insightful academic discussions and support; it has meant everything to me.

I am truly blessed to have such an incredible network of family, friends, and mentors by my side. Each of you has played a pivotal role in shaping this experience, and I will forever be thankful for everything you have done. This achievement is as much yours as it is mine.

- Chetty CU, Gentle NL, Meyer V. 1,25-Dihydroxyvitamin D_3 primes monocytes for macrophage function by inducing early changes in metabolism and gene expression. 3rd annual symposium of the Metabolomics South Africa (MSA) & Annual General Meeting (AGM) (17-18 September 2024), UNISA Science Campus, Johannesburg. Oral presentation by CU Chetty. Won first prize for the oral presentation category.

- Chetty CU, Gentle NL, Meyer V. 1,25-Dihydroxyvitamin D_3 primes monocytes for differentiation by inducing early changes in metabolism and gene expression. Wits Molecular Biosciences Research Thrust (MBRT) Postgraduate Research Day (05 December 2024). Public Health Auditorium, WITS Education Campus. Poster presentation by CU Chetty

Table of Contents

Declaration ..... **i**

Abstract ..... **ii**

Acknowledgements ..... **iv**

Research outputs ..... **vi**

List of figures **1**

List of tables **3**

Abbreviations **4**

Chapter 1: Literature review **7**

1.1. The immune system 7

1.2. Mononuclear phagocytes and TLR signalling 7

1.3. The role of monocytes and monocyte-derived macrophages in innate immunity 9

1.4. Vitamin D_3 and immune regulation 13

1.4.1 The molecular modes of action of 1,25D_3 14

1.4.2 The multifaceted role of 1,25D_3 in immune regulation 16

1.5. Trained immunity and metabolic memory 17

1.6. Rationale 20

Chapter 2: Methods **22**

2.1. Tissue culture and treatment protocols 22

2.1.1 THP-1 cell culture 22

2.1.2 Monocyte differentiation 22

2.1.3 Monocyte and MDM treatments 23

2.2. Trypan Blue Exclusion Assay 25

2.3. Metabolomic analysis 26

2.3.1 Metabolite extraction and preparation 26

2.3.2 GC×GC/TOF-MS analysis 26

2.3.3 Peak identification and initial data pre-processing 27

2.3.4 Chemometric analysis 28

2.3.5 Pathway enrichment and topology analysis 30

2.4. RNA Extraction 30

2.5. Agarose gel electrophoresis 31

2.6. RT-qPCR 32

2.7. Gene expression analysis 35

2.7.1 Data pre-processing 35

2.7.2 mRNA quantification 35

Chapter 3: Results **36**

3.1. Differentiation was confirmed through observed morphological changes 36

3.2. No significant alterations in cell viability were observed post-treatment 36

3.3. Supplementation with 1,25D_3 for 4 hrs in monocytes leads to a metabolic profile resembling that of MDMs in vitro 37

3.4. Elevated fumaratelevels indicate a pivotal metabolic shift during monocyte differentiation and in response to acute 1,25D_3 supplementation 39

3.5. Pathway analysis of metabolic changes in monocytes and MDMs: impact of 1,25D_3 supplementation 44

3.6. Monocytes exhibit robust fatty acid biosynthesis, which is notably modulated by 1,25D_3 supplementation 49

3.7. Increased fumarate production via the AAG metabolic pathway feeds into the TCA cycle 51

3.8. 1,25D_3 modulates mRNA expression of inflammatory markers in both monocytes and MDMs in the presence and absence of a simulated pathogenic infection 54

3.8.1 RT-qPCR quality control assessment 54

3.8.2 In vitro 1,25D_3 supplementation for 4 hrs modulates mRNA expression of inflammatory markers in both monocytes and MDMs 57

3.8.3 In the presence of TLR8 stimulation, in vitro 1,25D_3 supplementation modulates cytokine and chemokine gene expression in monocytes and MDMs at 4 hrs 59

Chapter 4: Discussion and conclusion 61

Limitations and future perspectives 68

References 70

List of figures

Figure 1.1.	Schematic illustrating an overview of TLR signalling in humans	9
Figure 1.2.	Comprehensive schematic illustrating monocyte and MDM origins and functions	12
Figure 1.3.	Schematic illustrating the conventional metabolic pathway through which the biologically active form of $1,25D_3$ is synthesised	13
Figure 1.4.	The genomic actions of $1,25D_3$	14
Figure 1.5.	The non-genomic actions of $1,25D_3$	15
Figure 1.6.	Schematic illustrating the induction of trained immunity in innate immune cells	18
Figure 2.1.	Schematic illustrating the differentiation protocol by Mol *et al*. (2024) that was used to generate MDMs from the THP-1 promonocytic cell line	23
Figure 2.2.	Schematic illustrating the different treatment conditions for monocytes and MDMs	24
Figure 2.3.	Schematic illustrating the identification of viable and non-viable cells using the trypan blue exclusion assay	25
Figure 3.1.	Morphological transition from THP-1 monocytes to MDMs	36
Figure 3.2.	Cell viability in both monocytes and MDMs was not significantly impacted by the treatment conditions	37
Figure 3.3.	1-Dimensional Total Ion Chromatogram (TIC) displaying an overview of the detected ion profiles in each sample	38
Figure 3.4.	$1,25D_3$-supplemented monocytes display a similar metabolic profile to MDMs	38
Figure 3.5.	OPLS-DA score plots illustrating metabolic differences between monocytes and MDMs, as well as between control and $1,25D_3$-supplemented monocytes	40
Figure 3.6.	Identification of the top fifteen discriminant signatory metabolites from respective OPLS-DA models derived from GC×GC/TOF-MS analysis	41
Figure 3.7.	Metabolomic pathway analysis of all GC×GC/TOF-MS derived metabolites annotated with HMDB IDs	46

Figure 3.8.	Alterations in the galactose metabolic pathway in monocytes, MDMs, and 1,25D_3-supplemented monocytes	47
Figure 3.9.	Alterations in the cysteine and methionine metabolic pathway in monocytes, MDMs, and 1,25D_3-supplemented monocytes	48
Figure 3.10.	*In vitro* supplementation with 1,25D_3 for 4 h in monocytes modulates the fatty acid biosynthesis pathway	50
Figure 3.11.	The role of the aspartate-argininosuccinate shuttle in driving increased fumarate production in MDMs and 1,25D_3-supplemented monocytes	52
Figure 3.12.	Alterations in TCA Cycle intermediates across the metabolomic profiles of monocytes, MDMs, and 1,25D_3-supplemented monocytes	53
Figure 3.13.	Confirmation of high integrity RNA extractions using agarose gel electrophoresis.	55
Figure 3.14.	Single melt peaks and gel products are indicative of primer specificity for RT-qPCR.	56
Figure 3.15.	Effect of *in vitro* 1,25D_3 supplementation on gene expression levels of inflammatory markers in monocytes and MDMs.	58
Figure 3.16.	Impact of *in vitro* 1,25D_3 supplementation on gene expression levels of inflammatory markers in monocytes and MDMs upon TLR8 stimulation.	60

Table 2.1.	Specifications of the GC columns	27
Table 2.2.	Primer sequences used for mRNA amplfication	33
Table 2.3.	cDNA synthesis reagents	34
Table 2.4.	RT-qPCR master mix components	34
Table 2.5.	CFX-96 Thermocycler incubation steps for the RT-qPCR reaction	34
Table 3.1.	Significant signatory metabolites discriminating between monocytes and MDMs	42
Table 3.2.	Significant signatory metabolites discriminating between control and 1,25D_3-supplemented monocytes	43

$1,25D_3$	1,25-dihydroxyvitamin D_3
$25D_3$	25-hydroxyvitamin D_3
AAG metabolism	alanine, aspartate, and glutamate metabolism
AMPs	antimicrobial peptides
ANOVA	analysis of variance
AP-1	activator protein-1
BCG	Bacillus Calmette-Guérin
Bhmt1	betaine-homocysteine methyltransferase 1
BMDM	bone-marrow-derived macrophages
BSTFA	N,O-bis(trimethylsilyl)trifluoroacetamide
CCL2	chemokine C-C motif ligand 2
cDNA	Complementary DNA
cMoPs	common monocyte progenitors
CMPs	common myeloid progenitors
Cq	quantification cycle
CREB	cyclic AMP-responsive element-binding protein
CXCL10	C-X-C motif chemokine ligand 10
CXCL9	C-X-C motif chemokine ligand 9
CYPs	cytochrome P450 mixed-function oxidases
DAMPs	damage-associated molecular patterns
DBP	vitamin D binding protein
EDTA	ethylenediaminetetraacetic acid
ERK	extracellular signal-regulated kinase
EtOH	100% molecular-grade ethanol
FADS2	fatty acid desaturase 2
FAO	fatty acid oxidation
FBS	foetal bovine serum
GC	gas chromatography
GC-MS	gas chromatography -mass spectrometry
GC×GC/TOF-MS	2D-gas chromatography coupled with time-of-flight mass spectrometry
GMPs	granulocyte-monocyte progenitors

HMDB IDs	human metabolome database identity number
HSCs	hematopoietic stem cells
IC_{50}	half-maximal inhibitory concentration
IL-10	interleukin-10 cytokine
IL-1β	interleukin-1β cytokine
IL-6	interleukin-6 cytokine
IRFs	interferon regulatory factors
LC-MS	liquid chromatography-mass spectrometry
LPS	lipopolysaccharide
LXR	liver X receptor
MAPK	mitogen-activated protein kinase
MDMs	monocyte-derived macrophages
MDPs	Monocyte-dendritic cell progenitors
MetPA	metaboanalyst pathway analysis
mRNA	Messenger RNA
NF-κB	nuclear factor kappa-light-chain-enhancer of activated B cells
OPLS-DA	orthogonal partial least squares discriminant analysis
oxLDL	oxidized low-density lipoproteins
OXPHOS	oxidative phosphorylation (OXPHOS
PAMPs	pathogen-associated molecular patterns
PBS	phosphate-buffered saline
PCA	principal component analysis
PERMANOVA	permutational multivariate ANOVA
PMA	phorbol-12-myristate-13-acetate
PRRs	pattern recognition receptors
PUFA	polyunsaturated fatty acid
Rf	retardation factor
RFU	relative fluorescence units
RPMI	Roswell Park Memorial Institute
RT-qPCR	reverse transcriptase-quantitative polymerase chain reaction (RT-qPCR
RXR	retinoid X receptor
TBE	Tris-borate-EDTA

TCA cycle	Tricarboxylic acid cycle
TCM	tissue culture medium
THEM4	thioesterase superfamily member 4 (THEM4)
TICs	total ion chromatograms
TLRs	toll-like receptors
TMCS	trimethylchlorosilane
TNF-α	tumour necrosis factor-α cytokine
TOFMS	time-of-flight mass spectrometer
TRMs	tissue-resident macrophages
Type 1 interferon	type I IFN
UBC	ubiquitin C
UM	unique masses
UVB	ultraviolet B
VDR	vitamin D receptor
VDR_{cyt}	cytosolic VDRs
VDREs	vitamin D response elements
VDR_{mem}	membrane bound VDR
VIP	variable importance in projection
x g	g-force
YWHAZ	tyrosine 3-monooxygenase/ tryptophan 5-monooxygenase activation protein zeta

Chapter 1: Literature review

1.1. The immune system

Broadly, immunity is a term used to describe host defence mechanisms against pathogenic infections (Pham and Mathis, 2019). The immune system encompasses a multitude of cells, chemicals, and biochemical processes that co-operate to shield the host from disease (Wang *et al*., 2024). Immunity can be largely categorised into the adaptive and innate systems. Adaptive immunity, also known as acquired or specific immunity, develops through exposure to pathogens (Marshall *et al*., 2018). It provides long-term, antigen-specific protection by generating antibodies and establishing immunological memory. Upon first exposure to an antigen, the body initiates an antibody response and retains a memory of it for future encounters. This enables a more efficient immune response upon subsequent exposures to the same antigen. Consequently, immunological memory forms the basis of vaccine efficacy, enabling the immune system to recognise and neutralise pathogens with greater precision upon re-exposure (Sallusto *et al*., 2010).

In contrast, innate immunity is rapid, non-specific, and provides immediate protection against an array of pathogens (Clark and Kupper, 2005; Wang *et al*., 2024). It is present in all multicellular organisms from birth, serving as the host's primary line of immunological defence. This initial defence system comprises anatomical and physiological barriers that act as 'shields' to inhibit pathogen entry, thereby mitigating pathogenesis (Turvey and Broide, 2010). However, if these physical barriers are compromised, internal defences are promptly activated. At the forefront of this response are leukocytes, which not only identify and eliminate pathogens, but also facilitate tissue repair, ensuring adequate host protection (Bellingan, 2000; Wang *et al*., 2024).

1.2. Mononuclear phagocytes and TLR signalling

Mononuclear phagocytes are a specialised subset of leukocytes, comprising three main types: monocytes, macrophages, and dendritic cells (Guillonneau *et al*., 2017). These cells are characterised by a single nucleus and play a vital role in detecting and phagocytosing pathogens, recruiting additional leukocytes to infection sites, and modulating inflammation (Lugo-Villarino *et al*., 2019). Although all three mononuclear

phagocyte subsets are essential for immune defence, dendritic cells primarily function in antigen presentation, while monocytes and macrophages are mainly responsible for pathogen removal (Randolph *et al*., 2008).

Amid pathogenic challenges, pattern recognition receptors (PRRs), such as toll-like receptors (TLRs) on monocytes and macrophages, recognise structurally conserved pathogen-associated molecular patterns (PAMPs) and endogenous damage-associated molecular patterns ([DAMPs], Santecchia *et al*., 2020; Li and Wu, 2021). Humans possess ten TLR subtypes (TLR1–10), which can be located extracellularly on the plasma membrane or intracellularly within endosomes (Sameer and Nissar, 2021). TLR10 was only recently identified, and its functional capabilities remain largely uncharacterised (Su *et al*., 2021). While the precise mechanisms of TLR1–9 signalling and regulation remain unclear, their dysregulation has been implicated in a diverse set of medical conditions (Duan *et al*., 2022; Wang *et al*., 2024). Regardless of which TLR is activated, the resulting signalling cascades ultimately converge to activate downstream transcription factors, including cyclic AMP-responsive element-binding protein (CREB), activator protein-1 (AP-1), nuclear factor kappa-light-chain-enhancer of activated B cells (NF-κB), and interferon regulatory factors ([IRFs]; [Fig. 1.1]; Gun *et al*., 2014; Monlish *et al*., 2016). These transcription factors then regulate the expression of inflammatory molecules (e.g. tumour necrosis factor-α [TNF-α], interleukin-1β [IL-1β]) and type I interferons (IFNs), which, in turn, stimulate the production of other cytokines and chemokines (e.g. C-X-C motif chemokine ligand 9 [CXCL9], chemokine C-C motif ligand 2 [CCL2], CXCL10, IL-10), all of which are integral for pathogen elimination and tissue repair (Kopitar-Jerala, 2017; Metzemaekers *et al*., 2018; Bhol *et al*., 2024).

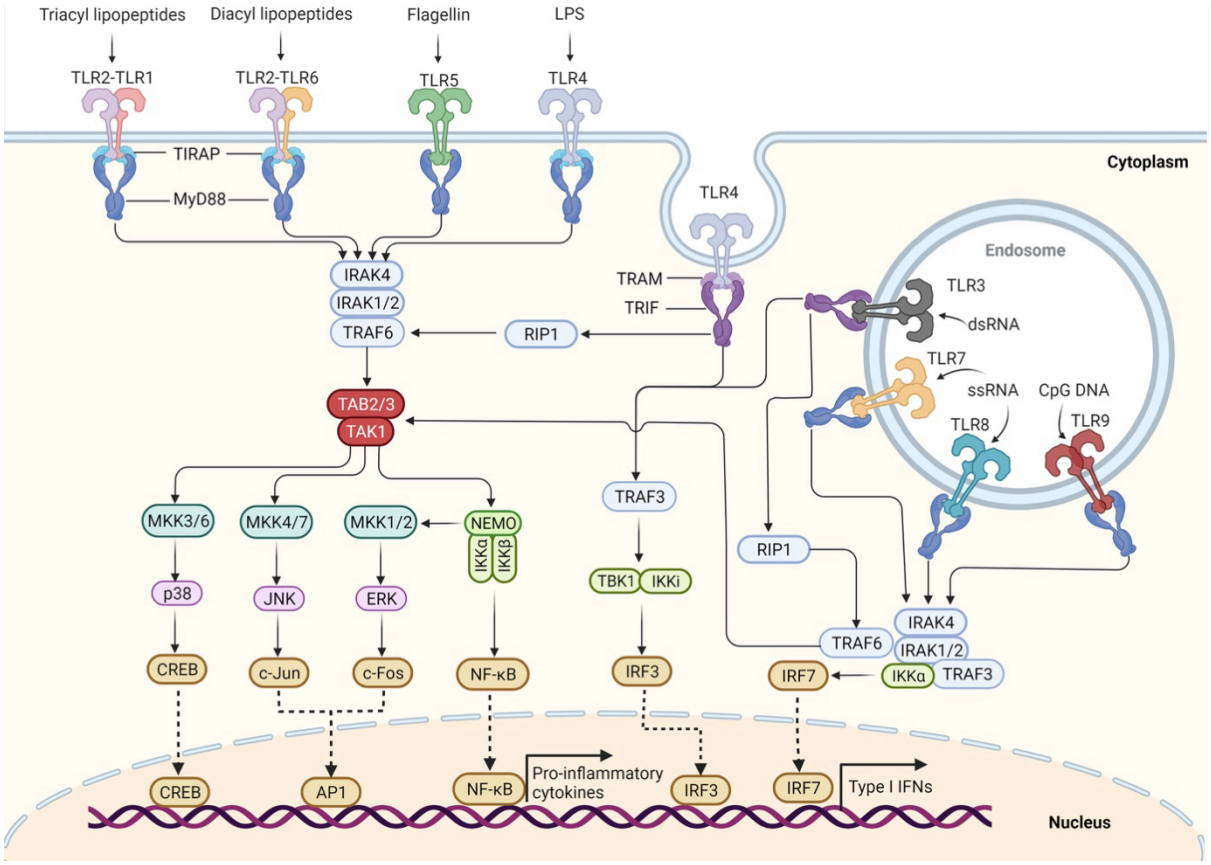

Figure 1.1. Schematic illustrating an overview of TLR signalling in humans. Regardless of which TLR is activated, all signalling pathways eventually converge to activate either CREB, AP-1, NF-κB and IRFs**.** Image obtained from Duan *et al*. (2022).

1.3. The role of monocytes and monocyte-derived macrophages in innate immunity

Although monocytes are primarily recognised as circulating precursors of macrophages under homeostatic conditions, they also play a distinct—and independent—role in pathogen removal (Serbina *et al*., 2008). Circulating monocytes are generated from bone marrow-derived hematopoietic stem cells ([HSCs]; [Fig 1.2A]; Ungefroren *et al*., 2016; Luque-Martin *et al*., 2021). These cells differentiate into common myeloid progenitors (CMPs), which give rise to granulocyte-monocyte progenitors (GMPs). Monocyte-dendritic cell progenitors (MDPs) are then produced from these GMPs and further differentiate into common monocyte progenitors (cMoPs). These cMoPs then mature and enter the bloodstream as monocytes. Monocytes display diverse phenotypes and functions depending on the relative expression of the CD14 and CD16 surface markers (Kapellos *et al*., 2019; Maher *et al*., 2022; Williams *et al*., 2023).

Classical monocytes ($CD14^{+}CD16^{-}$) are the most prevalent subset and display the highest level of phagocytic activity (Espinoza and Emmady, 2023). Upon infection,

they rapidly migrate into the tissue of the affected site, where they can differentiate into macrophages (Miyake *et al*., 2024). Moreover, classical monocytes themselves actively contribute to the regulation of inflammation. In contrast, non-classical monocytes ($CD14^{-}CD16^{+}$) primarily contribute to inflammation resolution and tissue homeostasis by patrolling the walls of blood vessels, where they continuously survey for indications of tissue damage and infection (Maher *et al*., 2022). Intermediate monocytes ($CD14^{+}CD16^{+}$) combine traits of both sunsets. In addition to this, they also participate in antigen-presentation, apoptosis regulation and angiogenesis (Nowlin *et al*., 2018; Williams *et al*., 2023).

Macrophages, in addition to their role in pathogen removal, are essential for maintaining immune homeostasis (Hirayama *et al*., 2017). Their functional characteristics are dictated by specific signals within the tissue microenvironment (Heckmann *et al*., 2017). Broadly, they can be classified as either tissue-resident macrophages (TRMs) or monocyte-derived macrophages ([MDMs]; [Fig 1.2B]; Ammarah *et al*., 2024). TRMs are self-renewing and originate from embryonic progenitors that populate tissues during development (Mu *et al*., 2021). Their primary functions include maintaining tissue homeostasis and repair, immune surveillance, and modulating inflammation (Davies *et al*., 2013). However, during pathogenesis, the existing TRM population may be insufficient to manage the inflammatory response, necessitating the recruitment of circulating monocytes. Under such conditions, an influx of circulating monocytes will infiltrate the affected tissue, differentiate into MDMs, and assist in the immune response (Shi and Pamer, 2011).

To limit the further spread of infection, MDMs phagocytose pathogens and initiate inflammatory responses (Hirayama *et al*., 2017; Saahene *et al*., 2022; Fang *et al*., 2024). Additionally, they contribute to tissue homeostasis by clearing dead cells and debris, whilst promoting repair via angiogenesis and collagen deposition (Wynn and Vannella, 2016; Mosser *et al*., 2021). Moreover, MDMs contribute significantly to the adaptive immune response by recruiting and activating immune cells through antigen presentation (Saahene *et al*., 2022). Like monocytes, MDMs exhibit significant heterogeneity in their phenotypes and functions. MDMs are broadly categorised into the pro-inflammatory (M1) and anti-inflammatory (M2) phenotypes (Zhang *et al*., 2021; Kesapragada *et al*., 2024). However, this binary classification misrepresents the

diversity of MDM functionality, as these cells exist along a spectrum of activation states, dependent on tissue-specific signals (Pizzurro and Miller-Jensen, 2023).

Although extensive research has been conducted on monocyte and MDM immune regulation, most of it focuses on genetic studies, such as gene expression profiling. However, this approach does not provide a comprehensive picture of phenotype and function, as metabolic reprogramming plays a crucial role in immune cell functionality (Chi, 2022). Immunometabolism describes the dynamic interplay between metabolic pathways and immune cell function (Chi, 2022). It has been shown that metabolic pathways such as glycolysis, tricarboxylic acid (TCA) cycle, and fatty acid oxidation (FAO) do more than simply meet the energy and biosynthesis demands of immune cells (Hu *et al*., 2022; Wculek *et al*., 2022; Hu *et al*., 2024). The metabolic intermediates generated by these pathways have been shown to profoundly influence the activation, differentiation, and immune responses of these cells, providing valuable insights into their functional proteome (Lafaye *et al*., 2005; Ganeshan and Chawla, 2014; George *et al*., 2025). As cellular metabolism is intrinsically linked to functionality, this highlights the need to investigate the metabolic profiles of both monocytes and MDMs.

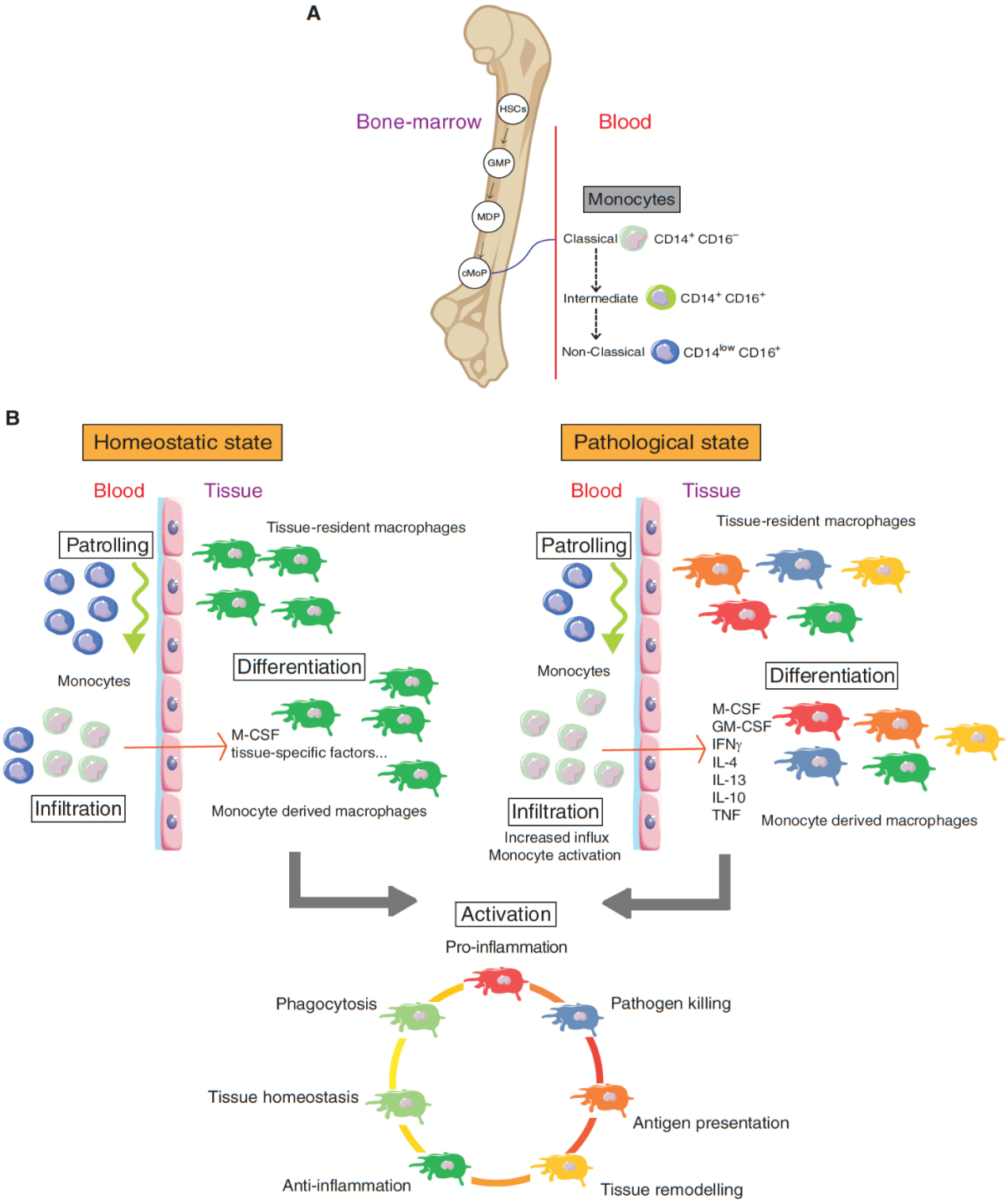

Figure 1.2. Comprehensive schematic illustrating monocyte and MDM origins and functions. HSCs populate progenitors in bone marrow to generate circulating monocytes (**A**). As determined by flow-cytometric phenotyping, monocytes are subdivided into three distinct classes. Each monocyte subset displays distinct functions and tissue distributions, with intermediate and non-classical monocytes potentially deriving from classical monocytes. Monocytes infiltrate tissue from the bloodstream and differentiate into MDMs (**B**). Under pathologic conditions both MDMs and TRMs are polarized by stimuli in the extracellular environment and exhibit distinct and specialised functions accordingly. Image obtained from Luque-Martin *et al*. (2021).

1.4. Vitamin D_3 and immune regulation

Vitamin D_3 is a secosteroid pro-hormone that humans primarily obtain through two sources: sunlight (through ultraviolet B [UVB] radiation) and dietary intake (Jeon and Shin, 2018; Olszewska and Zmijewski, 2024). Once in the bloodstream and bound to the vitamin D binding protein (DBP), vitamin D_3 is converted into its biologically active form, 1,25-dihydroxyvitamin D_3 ($1,25D_3$), by cytochrome P450 mixed-function oxidases (CYPs) through two key steps ([Fig 1.3]; Bikle, 2014; Jeon and Shin, 2018). Briefly, vitamin D_3 is hydroxylated by CYP2R1 and CYP27A1 to produce the major circulating inactive intermediate, 25-hydroxyvitamin D_3 ($25D_3$). Thereafter, $25D_3$ enters the kidneys, where it is further hydroxylated by CYP27B1 to generate $1,25D_3$. Notably, CYP27B1 is the only enzyme capable of 1α-hydroxylating $25D_3$ (Saponaro *et al*., 2020). Outside of the kidneys, CYP27B1 is expressed in immune cells such as monocytes and MDMs, enabling localised production of $1,25D_3$. This active metabolite subsequently affects cellular function via the vitamin D receptor (VDR), a nuclear receptor that governs gene expression. Interestingly, the VDR is present in most nucleated cells, albeit at varying levels (Chang and Lee, 2019; Holick *et al*., 2023).

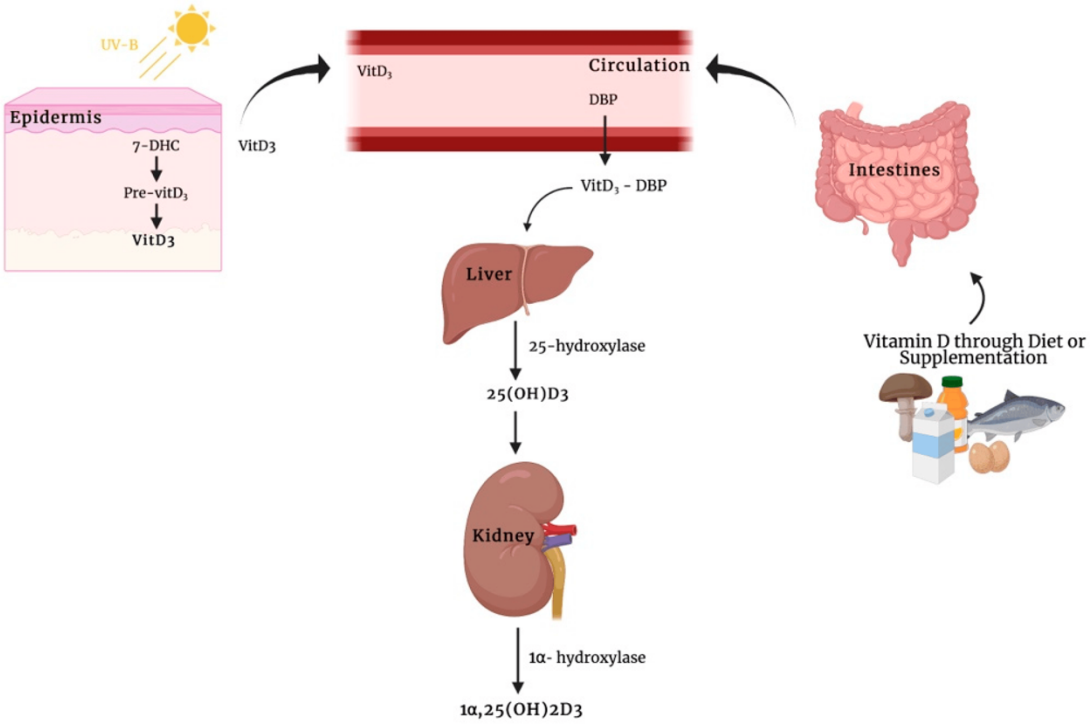

Figure 1.3. Schematic illustrating the conventional metabolic pathway through which the biologically active form of $1,25D_3$ is synthesised. Image obtained from Donati *et al*. (2022).

1.4.1 The molecular modes of action of 1,25D$_3$

The genomic molecular mechanism of 1,25D$_3$ is mediated through its interaction with cytosolic VDRs ([VDRcyt]; [Fig 1.4]; Bikle, 2014). Structurally, the VDR is composed of two primary binding domains at the C-terminal and N-terminal with a hinge region connecting both (Rochel *et al*., 2000; Pike and Meyer, 2010). After 1,25D$_3$ binds to the C-terminal of the VDR, it forms a heterodimer with the retinoid X receptor ([RXR]; Barsony and Prufer, 2002). Thereafter, as an active transcriptional unit, the VDR/RXR complex translocates into to the nucleus where the N-terminal interacts with vitamin D response elements (VDREs) in the promoter regions of target genes (Carlberg, 2023; Holick *et al*., 2023). Variations in VDRE sequences lead to the recruitment of specific co-modulators, which modulate gene transcription, influencing processes such as calcium and phosphate homeostasis, cell proliferation, differentiation, and immune responses.

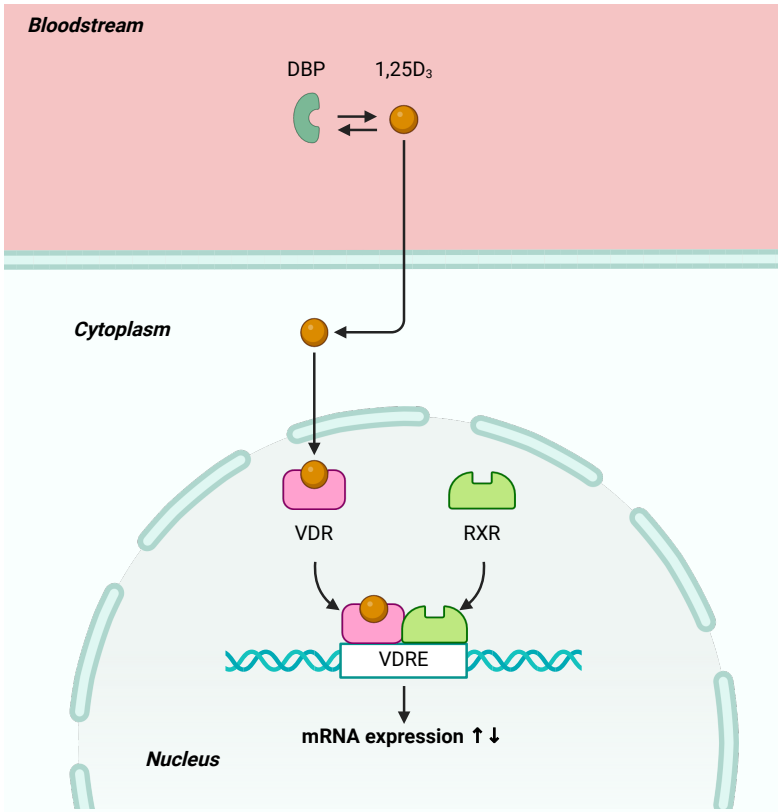

Figure 1.4. The genomic actions of 1,25D$_3$. The genomic actions of 1,25D$_3$ are facilitated by the VDRE in the nucleus. Image obtained from Pál *et al*. (2023) modified in BioRender.com.

In contrast, the non-genomic molecular mode of action of 1,25D$_3$ is characterised by its rapid onset (Donati *et al*., 2022). It involves the binding of 1,25D$_3$ to either a cellular membrane bound VDR (VDRmem), VDRcyt or other membrane-associated receptors.

Upon binding, pathways such as the mitogen-activated protein kinase (MAPK)/extracellular signal-regulated kinase (ERK) cascade are activated ([Fig 1.5]; Jeon and Shin, 2018). These signalling events lead to the modulation of calcium homeostasis and several other cellular functions. As a result, $1,25D_3$ exerts rapid effects that are independent of direct gene transcription, affecting physiological processes such as muscle contraction and immune cell activation (Ceglia, 2009; Walker and Modlin, 2009).

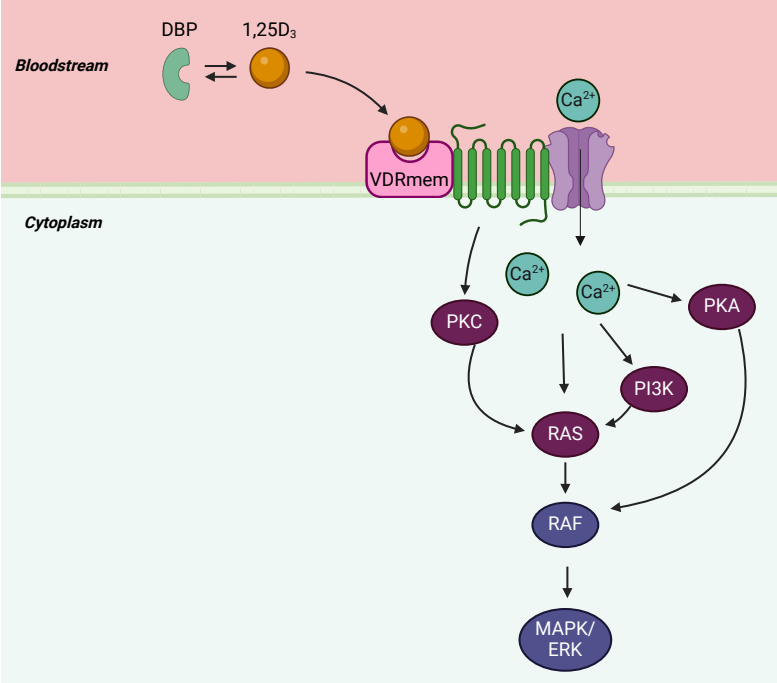

Figure 1.5. The non-genomic actions of $1,25D_3$. The non-genomic effects of $1,25D_3$ are initiated through its binding to VDR_{mem}, causing the immediate activation of signalling pathways like the MAPK/ERK pathway, calcium influx pathway and others, which in turn affect various cellular processes. Image obtained from Donati *et al*. (2021) modified in BioRender.com.

Furthermore, $1,25D_3$ has been well established as a significant regulator of epigenetic processes such as DNA methylation and histone modification (Fetahu *et al*., 2014). For example, van Megen *et al*. (2021) demonstrated that $1,25D_3$ supplementation altered the expression of autoimmune risk genes by modifying DNA methylation at promoter regions, potentially overriding genetic predisposition thereby stabilising epigenetic marks that regulate inflammatory pathways in dendritic cells. Additionally, Moore *et al*. (2018) reported that $1,25D_3$ supplementation enhances the transcription of the betaine-homocysteine methyltransferase 1 gene (*Bhmt1*) in CD4+ T cells, promoting homocysteine recycling, reducing neuronal toxicity, and replenishing methionine for DNA methylation. Furthermore, Zhang *et al*. (2012) indicated that $1,25D_3$ supplementation in both murine and human macrophages increased histone

H4 acetylation near a putative VDRE in the MKP-1 promoter, suggesting that this histone modification contributes to the regulation of gene expression by $1,25D_3$. Collectively, these findings suggest that $1,25D_3$ influences both epigenetic mechanisms and metabolic processes regulating immune cell function.

1.4.2 The multifaceted role of $1,25D_3$ in immune regulation

The regulatory role of $1,25D_3$ in the immune system is mediated by its ability to modulate immune-related gene expression (Dhanapal and Vimaleswaran, 2022; Ghaseminejad-Raeini *et al*., 2023). This regulation is vital for maintaining immune homeostasis and preventing excessive immune responses during pathogenic challenges. Consequently, $1,25D_3$ holds significant therapeutic potential for treating immune dysfunction in both inflammatory and infectious conditions.

One of the most well-established mechanisms through which $1,25D_3$ has been shown to enhance monocyte and MDM function is by increasing the production of antimicrobial peptides (AMPs), such as defensin β2 and cathelicidin (Sassi *et al*., 2018; Yaqinuddin *et al*., 2022). Furthermore, pathogen exposure has been shown to upregulate the gene expression of *CYP27B1* and *VDR* in monocytes, thereby enhancing the capacity for local synthesis of and response to $1,25D_3$ during infection (Sassi *et al*., 2018). Additionally, $1,25D_3$ has shown a significant regulatory role in MDM function. This effect is demonstrated by its ability to enhance chemotaxis, autophagy, and phagocytosis, while simultaneously reducing excessive antigen presentation during MDM-lymphocyte interactions (Yuk *et al*., 2009; Sassi *et al*., 2018; Fernández García *et al*., 2022; Yaqinuddin *et al*., 2022).

Notably, the association between TLRs and $1,25D_3$ suggest that $1,25D_3$ may exert its immunomodulatory effects by modulating TLR activity in monocytes and MDMs (Arababadi *et al*., 2018). Adams *et al*. (2014) demonstrated that TLR1 and TLR2 activation upregulates *VDR* expression and subsequently enhances CYP27B1 activity in MDMs, thereby amplifying the local production of $1,25D_3$. Conversely, Sadeghi *et al*. (2006) reported that $1,25D_3$ down-regulates *TLR2* and *TLR4* expression in monocytes. These findings are further supported by several studies suggesting that $1,25D_3$ prevents TLR overactivation, thereby controlling excessive immune activation and inflammation (Pedersen *et al*., 2007; Zhang *et al*., 2012). This feedback mechanism underscores the role of $1,25D_3$ in maintaining immune homeostasis.

Furthermore, $1,25D_3$ is well recognised for its anti-inflammatory properties. *In vitro* studies have established that $1,25D_3$ promotes the gene expression of anti-inflammatory cytokines such as *IL-10*, while reducing the expression of pro-inflammatory cytokines such as *IL-6* (Cannell *et al*., 2014; Meza-Meza *et al*., 2022; Yaqinuddin *et al*., 2022). Studies have suggested that through the target gene, thioesterase superfamily member 4 gene (*THEM4*), $1,25D_3$ inhibits the NF-κB pathway, thereby suppressing the expression of *TNF-α* and *IL-6* (Dankers *et al*., 2017; Meza-Meza *et al*., 2022). However, Yusupov *et al*. (2010) reported that $1,25D_3$ supplementation had no effect on either *TNF-α* or *IL-10* levels. These conflicting results highlight the potential for $1,25D_3$ to function in two roles in inflammation modulation, with its effects likely varying depending on the context, cell-type, and specific biological condition.

Collectively, these results reinforce the significance of $1,25D_3$ as an immunomodulator. Through the enhancement of AMP synthesis and modulation of cytokine production, $1,25D_3$ supports the functional adaptations of monocytes and MDMs during immune responses through preventing overactivation and inflammation highlighting its importance in both innate and adaptive immunity.

1.5. Trained immunity and metabolic memory

The backbone of immune defence lies in immune memory, which enables the immune system to retain information after its initial exposure to endogenous or exogenous stimuli (Netea *et al*., 2019; Ochando *et al*., 2023; Netea and Joosten, 2024). This memory allows the immune system to mount a more rapid and enhanced response upon subsequent infections, improving host survival. While immune memory has traditionally been associated with adaptive immunity, recent discoveries have revealed that innate immune cells can also exhibit a form of memory, known as trained immunity ([Fig. 1.6]; Netea *et al*., 2011). Unlike adaptive immunity, trained immunity is non-antigen-specific and driven by epigenetic modifications and metabolic reprogramming of innate immune cells, resulting in enhanced functional capabilities (Fanucchi *et al*., 2021; Ferreira *et al*., 2022; Vuscan *et al*., 2024). Trained immunity, unlike differentiation, is a reversible process wherein innate immune cells undergo functional reprogramming as a result of an initial stimulus. However, once the stimulus is removed, the cells return to their baseline function (Divangahi *et al*., 2021; Ochando

et al., 2023). This adaptability underscores the crucial role of trained immunity in enhancing the innate immune response, enabling rapid and versatile responses that complement the long-term specificity of adaptive immunity.

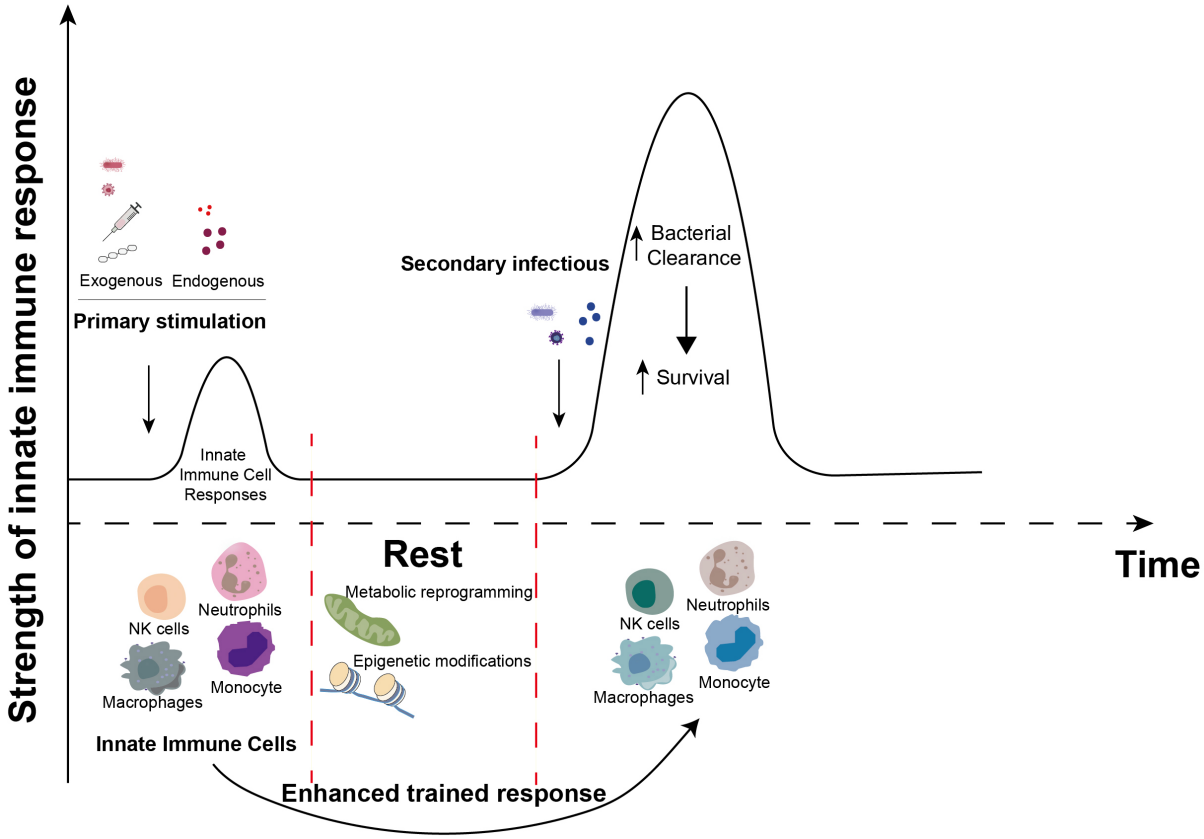

Figure 1.6. Schematic illustrating the induction of trained immunity in innate immune cells. Upon exposure to a primary stimulus, innate immune cells undergo metabolic reprogramming and epigenetic modifications allowing for a robust immune upon secondary infection. Image obtained from Wang *et al*. (2024).

Metabolic memory, a key component of trained immunity, results from metabolic reprogramming in innate immune cells following their initial exposure to a stimulus, such as a pathogen (Netea *et al*., 2019; Fanucchi *et al*., 2021; Riksen and Netea, 2021). These alterations go beyond fulfilling immediate energy demands, reprogramming the bioenergetic pathways of the cell to establish a foundation for immune memory (Ferreira *et al*., 2024).

A key pathway commonly affected during this process is glycolysis (Soto-Heredero *et al*., 2020; Xu *et al*., 2022). Although typically associated with anaerobic energy production, immune cells undergoing trained immunity have exhibited an upregulation of glycolysis over oxidative phosphorylation (OXPHOS), even in the presence of oxygen (Soto-Heredero *et al*., 2020; Ochando *et al*., 2023). This shift is attributed to

the need for faster ATP production during immune activation. While glycolysis provides a rapid energy supply, OXPHOS remains essential for sustaining long-term energy production and maintaining cellular functions throughout the immune response. Additionally, the increased glycolytic activity results in higher lactate production, which not only supports energy generation but also maintains redox homeostasis (Wang *et al*., 2021; Fang *et al*., 2024).

Moreover, upregulation of glycolysis leads to alterations in the TCA cycle through increased pyruvate production (Ferreira *et al*., 2022; Arnold and Finley, 2023). TCA cycle alterations are reflected in the amended levels of critical metabolites such as acetyl-CoA, fumarate, and α-ketoglutarate (Ferreira *et al*., 2024). Acetyl-CoA and α-ketoglutarate play well-established roles in energy production and the synthesis of essential biomolecules like lipids, proteins, and nucleotides (Arnold and Finley, 2023; Park *et al*., 2024). Furthermore, fumarate and α-ketoglutarate have been reported to influence epigenetic regulation by modifying gene expression through processes such as histone acetylation and DNA methylation (Groh *et al*., 2018). Arts *et al*. (2016) demonstrated that increased fumarate levels inhibit histone demethylases, resulting in increased trimethylation at H3K4 and acetylation at H3K27, both of which promote gene expression related to inflammation and immune activation .

Additionally, lipid metabolism plays a vital role in immune memory. Soharbi *et al*. (2020) reported that activation of liver X receptor (LXR) in human monocytes induced a long-term inflammatory response, dependent on the mevalonate pathway and fatty acid synthesis for sustained immune activation. This finding was further supported by Findeisen *et al*. (2022), who found that lipid deposition and modified lipoproteins activate PRRs in human monocytes, triggering an enhanced inflammatory response and initiating trained immunity. Specifically, LXR activation in response to oxidized low-density lipoproteins (oxLDL) priming upregulated glycolysis and fatty acid synthesis, further emphasizing the pivotal role of lipid metabolism in trained immunity. Additionally, Ferreira *et al*. (2023) reported the crucial role of long-chain polyunsaturated fatty acid (PUFA) synthesis in Bacillus Calmette-Guérin (BCG)-induced trained immunity. Inhibition of fatty acid desaturase 2 (FADS2) resulted in a significant decline in pro-inflammatory cytokine production. Furthermore, their study also highlighted the regulatory role of LXRs in lipid metabolism and inflammation,

noting that inhibition of LXR signalling led to a decreased immune response to TLR4 restimulation in BCG-trained MDMs.

Collectively, this demonstrates that metabolic reprogramming during trained immunity is a dynamic process that not only provides the necessary energy for immune activation but also supplies molecular signals essential for shaping immune memory, underscoring the intricate and multifaceted nature of metabolic reprogramming in immune function.

1.6. Rationale

Monocytes and MDMs are integral to the immune response, detecting, reacting to, and eliminating pathogenic threats. Therefore, understanding the intricacies of their immunometabolism is crucial, as their metabolic state directly impacts their functional capabilities. Notably, $1,25D_3$ is a long-standing regulator of immune cell function (Dhanapal and Vimaleswaran, 2022; Ghaseminejad-Raeini et al., 2023). It has been shown to modulate immune cell activity, influencing processes such as AMP production and cytokine secretion. These modifications may also have profound effects on cellular metabolism. Within recent decades the concept of trained immunity, has gained significant attention. This immunological mechanism comprises epigenetic and metabolic reprogramming of innate immune cells following exposure to a primary stimulus independent of antigen specificity. This process results in the development of metabolic memory enabling a prompt and robust response upon subsequent infections. Therefore, elucidating how acute exogenous $1,25D_3$ supplementation influences the metabolome –potentially inducing a trained immune state in monocytes and MDMs via metabolic reprogramming– represents a promising approach for broadening our understanding of immunometabolism. Furthermore, to provide additional insight into the functional consequences of immunometabolism and to determine whether the metabolomic shifts induced by $1,25D_3$ were reflected at the mRNA level, TLR8 stimulation was used to assess transcriptional responses.

Aim

This study focused on assessing the metabolic profiles of monocytes and MDMs, while also identifying metabolic shifts linked to the immunomodulatory effects of acute *in vitro* 1,25D_3 supplementation using an untargeted metabolomics approach.

The aim was achieved through completion of the following objectives:

1. Established and maintained the promonocytic THP-1 cell line, which was subsequently supplemented with or without 1,25D_3 for 4 hrs.
2. Differentiated THP-1 cells into MDMs, which were then supplemented with or without 1,25D_3 for 4 hrs.
3. Extracted and quantified intracellular metabolites using 2D-gas chromatography coupled with time-of-flight mass spectrometry (GC×GC/TOF-MS).
4. Performed chemometric and pathway analyses on GC×GC/TOF-MS derived metabolites to annotate variables of importance and determine key pathway alterations.
5. Validated functional changes induced by 1,25D_3 after 4 hrs by quantifying gene expression in monocytes and MDMs in the presence and absence of a TLR8 agonist.

Chapter 2: Methods

2.1. Tissue culture and treatment protocols

All tissue culture experiments were performed at a cell plating density of 5×10^5 cells/mL in 60 mm culture plates (22.1 cm² growth area) from TPP, Trasadingen, Switzerland. The experiments were incubated in a 95% humidified incubator with 5% CO_2 at 37 °C, unless otherwise specified. All consumables and reagents for tissue culture and treatment were acquired from Sigma-Aldrich, St. Louis, MO, USA, unless otherwise indicated.

2.1.1 THP-1 cell culture

The THP-1 cell line, an immortalised acute promonocytic leukaemia cell line, was isolated from human peripheral blood (Tsuchiya *et al.*, 1980). The cells are regarded as the closest model to primary monocytes and macrophages, mirroring their morphological and differentiation traits while growing as suspension cultures, making them an excellent model for *in vitro* studies of these cells (Bosshart and Heinzelmann, 2016). The THP-1 cells used in this project were provided by Dr. H. Ranchod (HIV Reagent Program ARP-9942, NICD, South Africa) and were revived at passage 23, with experimentation conducted from passages 25 to 27. The tissue culture medium (TCM) was Roswell Park Memorial Institute (RPMI) 1640 supplemented with 2 mM L-glutamine (Pan Biotech, Aidenbach, Germany), 10% (v/v) foetal bovine serum (FBS; Pan Biotech, Aidenbach, Germany), and 1% (v/v) penicillin/streptomycin to prevent bacterial contamination. FBS provided essential nutrients, growth factors, hormones, and proteins for cell growth and maintenance. Cell counts and viability assessments (section 2.2) were routinely performed to ensure cell density did not exceed 5×10^5 cells/mL (Tedesco *et al*., 2018).

2.1.2 Monocyte differentiation

Once cell confluency reached 80–90%, monocytes were differentiated into macrophages following the protocol established by Mol *et al*. (2024). Briefly, on day 1 of differentiation, monocytes were treated with both 10 nM $1,25D_3$ and 5 nM phorbol-12-myristate-13-acetate ([PMA]; Fig. 2.1). The cells were then incubated for 24 hrs to allow for differentiation process to be initiated. On day 2, the cells were washed with 2 mL phosphate-buffered saline (PBS; pH 7.4), resupplemented with fresh TCM and

10 nM 1,25D_3, and incubated for 72 hrs. Successful differentiation was confirmed on day 4 using an inverted light microscope (Thermo Fisher Scientific, Waltham, MA, USA) by observing morphological changes at 40 x magnification. Images were captured with an iPhone 13 camera (Apple Inc, Cupertino, CA, USA), and to standardise image measurements scale bars were added using ImageJ software (v. 2.16.0/1.54g; Laboratory for Optical and Computational Instrumentation, University of Wisconsin, Madison, WI, USA).

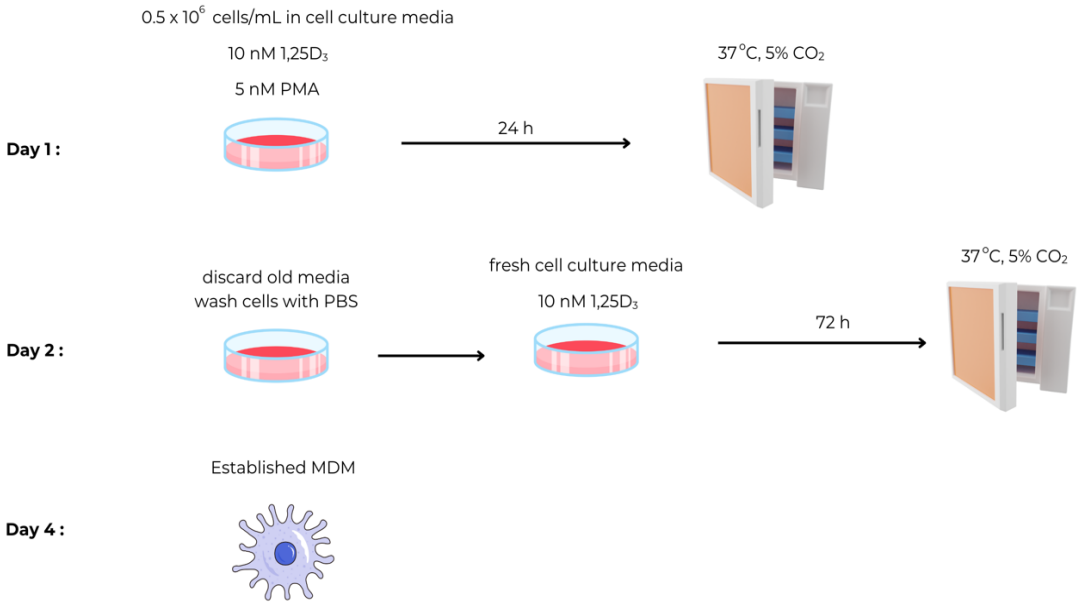

Figure 2.1. Schematic illustrating the differentiation protocol by Mol *et al*. (2024) that was used to generate MDMs from the THP-1 promonocytic cell line. Image created using Canva.com.

2.1.3 Monocyte and MDM treatments

To assess the effect of acute *in vitro* 1,25D_3 supplementation, cells were plated and treated for 4 hrs with 10 nM 1,25D_3 (dissolved in ethanol [EtOH]) or a matched vehicle control containing 0.002% EtOH and 0.01% dimethyl sulfoxide (DMSO) (Figs. 2.2A and B).The selection of 10 nM 1,25D_3 was based on its physiological relevance and minimal cytotoxicity in *in vitro* monocyte stimulation models. Previous studies have shown an inverse relationship between 1,25D_3 concentration and cell viability, with Varghese *et al*. (2020) reporting an IC_{50} of 15 µM. However, 10 nM is widely recognised as a physiologically relevant concentration for *in vitro* 1,25D_3 supplementation in primary monocytes, with no observed cytotoxic effects (Djukic *et al*., 2014; Rafique *et al*., 2019; Rao Muvva *et al*., 2020; Borojević *et al*., 2022). Therefore, 10 nM was chosen to induce measurable short-term immune effects while

maintaining cell viability. To simulate a pathogenic challenge, monocytes and MDMs were then stimulated with 5 µM motolimod (a TLR8 agonist which was dissolved in DMSO), in the presence or absence of 10 nM $1,25D_3$ for 4 hrs (Fig. 2.2B).While most studies report that TLR gene expression increases 12–24 hrs post-infection, Triantafilou *et al*. (2005) and Song *et al*. (2011) have shown that TLR8 gene expression can rise as early as 2–6 hrs (Lee *et al*., 2014; Dechamma *et al*., 2015). Given this display of rapid TLR8 gene upregulation, a 4 hr time point was selected for both the TLR8 agonist and $1,25D_3$ only treated samples (Fig. 2.2B). Furthermore, since MDMs are adherent when studied *in vitro*, trypsinisation was employed to detach the cells during harvesting. This involved adding 2 mL of 1X trypsin-EDTA to the cells and incubating for 3 min. To inactive the trypsin, 1 mL of TCM was added, and a cell scraper was used to gently scrape the cells guaranteeing complete detachment from the culture dish. The cell suspension was centrifuged at 400 x *g* for 5 min at 25 °C and the supernatant was discarded, the pellet was resuspended in 1 mL PBS for cell counting and viability assessment. In preparation for GC×GC/TOF-MS (section 2.3) and reverse transcriptase-quantitative polymerase chain reaction (RT-qPCR; section 2.6) analysis, cell samples (1 x 10^6 cells/mL) were snap-frozen and stored at -80 °C.

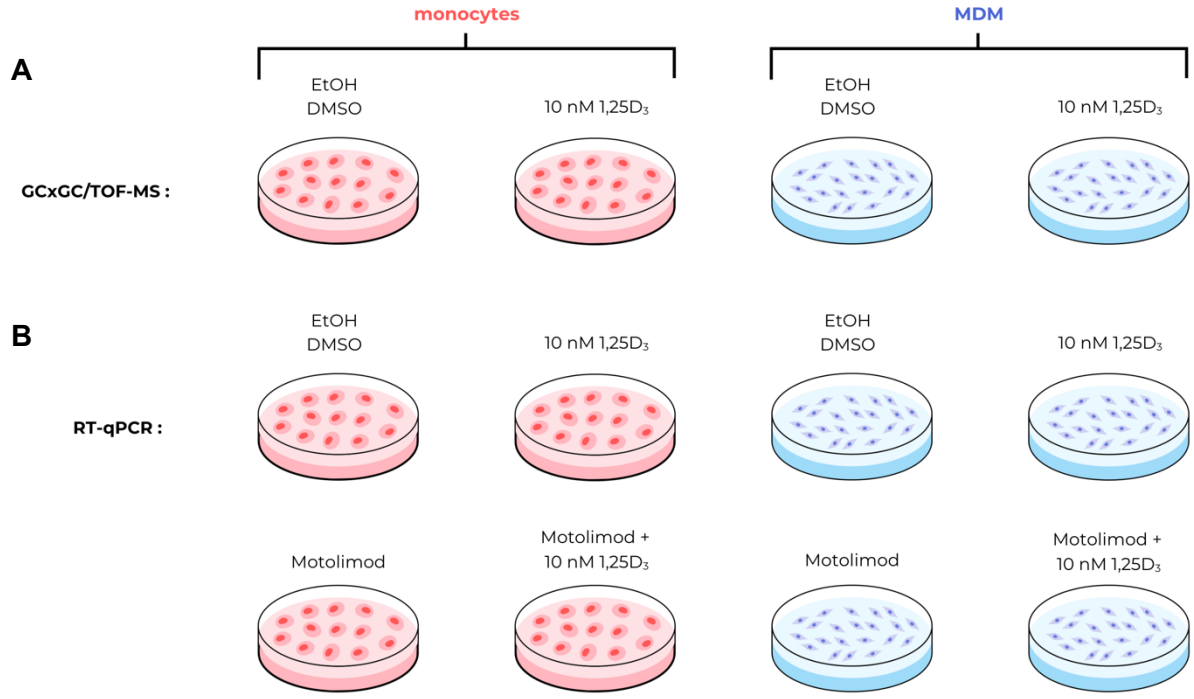

Figure 2.2. Schematic illustrating the different treatment conditions for monocytes and MDMs. Cell culture was done to collect cell pellets following the selected differing treatments at 4 hrs in preparation for GC×GC/TOF-MS (**A**) and RT-qPCR (**B**) analysis. Image created using Canva.com.

2.2. Trypan Blue Exclusion Assay

Cell viability plays an essential role in acquiring precise, accurate, and reproducible experimental results (Stoddart, 2011). Viable cells refer to metabolically active cells which maintain regular functionality (Lockshin and Zakeri, 2007; Saito *et al*., 2021). In contrast, non-viable cells are damaged, dead, or dying, rendering them incapable of sustaining life. This results in the loss of structural integrity and metabolic activity. Additionally, non-viable cells can release degraded biomolecules such as fragmented DNA, degraded RNA, and denatured proteins, which may contaminate samples and yield misleading results (Alberts *et al*., 2002). Beyond assessing general cell health, cell viability tests are crucial for identifying potential cytotoxic effects of treatments (Piccinini *et al*., 2017). To assess cell viability and cytotoxicity in this study, the trypan blue exclusion assay was employed. The basis of this assay is that dead cells have compromised cellular membranes allowing the dye to penetrate and accumulate within the cytoplasm, whereas living cells do not (Fig. 2.3). A 1:1 (v/v) mixture of cell suspension and trypan blue dye (Sigma Aldrich, St. Louis, MO, USA) was prepared by gently pipetting up and down to ensure homogeneity, and a 10 µL aliquot was loaded onto a haemocytometer. The Countess II FL Automated Cell Counter (Thermo Fisher Scientific, Waltham, MA, USA) was used to assess cell viability and total cell counts. Cells showing trypan blue staining were classified as non-viable, while cells that remained uncoloured were considered viable.

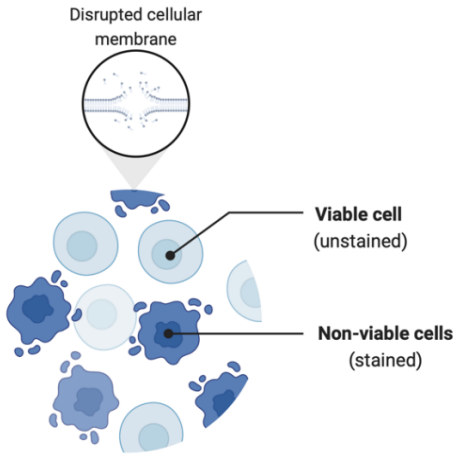

Figure 2.3. Schematic illustrating the identification of viable and non-viable cells using the trypan blue exclusion assay. Viable cells remain clear as they possess intact cellular membranes which exclude the dye. Whereas non-viable cells are stained blue due to the loss of structural integrity of their cellular membrane allowing the dye to incorporate into their cytoplasm. Image obtained from Mani and Swargiary (2023) and modified using Biorender.com.

2.3. Metabolomic analysis

Metabolite extraction, preparation, and identification for three biological replicates of each treatment was outsourced to the Centre for Human Metabolomics at North-West University (NWU), Potchefstroom, RSA. These procedures were conducted unmodified according to the protocol described by Beukes *et al*. (2019). Subsequent chemometric and pathway analyses were performed independently by Caitlyn Chetty (MSc Candidate). Intracellular metabolite extraction

2.3.1 Metabolite extraction and preparation

Briefly, high-resolution GC×GC/TOF-MS was employed for this untargeted metabolomics study, as the metabolite concentrations were anticipated to be too low for accurate detection using conventional one-dimensional GC (Fig. 2.2A). Additionally, all consumables and reagents for GC×GC/TOF-MS analysis were acquired from Honeywell International Inc., Muskegon, MI, USA unless otherwise specified. Each sample was initially quenched by adding 1 mL 100% methanol, 100 µL of an internal standard (3-phenylbutyric acid prepared in H_2O [HPLC grade, 25 ^oC], 100 ppm), and 230 µL of H_2O (HPLC grade, 25 ^oC) to a 1.5 mL DNA LoBind microcentrifuge tube. A 3 mm tungsten carbide bead was then added to the tube, and the mixture was shaken for 2 min at 30 Hz using an MM 400 mixer mill (Retsch GmbH & Co. KG, Haan, Germany) to facilitate metabolite extraction. Afterward, 330 µL of chloroform was introduced, and the samples were vortexed followed by a 10 min incubation on ice. The samples were then centrifuged at 50 x *g* for 10 min at 4 °C, and the entirety of the resulting supernatant (including the polar and non-polar phases) was transferred into a GC-MS vial and dried under a nitrogen stream. The dried samples were then derivatised by adding 50 µL of methoxyamine hydrochloride in pyridine (200 mg/10 mL) and incubating at 60 °C for 60 min. Following this, 50 µL of N,O-bis(trimethylsilyl)trifluoroacetamide (BSTFA) containing 1% trimethylchlorosilane ([TMCS]; Sigma Aldrich, St. Louis, MO, USA) was added, and the sample was incubated at 60 °C for another 60 min. The derivatised samples were thereafter placed in a glass insert within a sample vial for GC×GC/TOF-MS analysis.

2.3.2 GC×GC/TOF-MS analysis

Metabolite analysis was performed using a Pegasus 4D GC×GC-TOFMS system (Leco Corporation, St. Joseph, MI, USA), which incorporated an Agilent 7890A gas

chromatograph (Agilent, Atlanta, GA) coupled to a time-of-flight mass spectrometer ([TOFMS]; Leco Corporation, St. Joseph, MI, USA). The system was equipped with a Gerstel MultiPurpose Sampler ([MPS]; Gerstel GmbH & Co. KG, Eberhard-Gerstel-Platz 1, D-45473 Mülheim an der Ruhr) and a cryogenic cooler for enhanced performance. The derivatised samples were injected with a volume of 1 µL into the inlet of the GC columns (Restek, Bellefonte, PA, USA), which operated with a split ratio of 1:5 and at a temperature of 270 °C. Helium (He) was used as the carrier gas, with pressure gradually ramped to optimise the flow rate. The primary GC (Table 2.1) oven temperature was initially set to 70 °C for 2 min, followed by an increase at a rate of 4 °C/min to 300 °C, where it was held for 2 min. The secondary GC (Table 2.1) oven started at 85 °C for 2 min, then ramped at 4.5 °C/min to 300 °C, where it remained for 5 min. The modulator temperature began at 100 °C for 2 min, then increased at 4.5 °C/min to 310 °C, with a 12 min hold. Cryogenic modulation, assisted by nitrogen gas pulses (0.3 s every 3 sec), facilitated the transfer of effluent between the columns. For TOF-MS analysis, electron ionization was performed at 70 eV, with an ion source temperature of 200 °C and a transfer line temperature of 270 °C. The mass spectrometer was set to scan a mass range (m/z) from 50 to 950, with an acquisition rate of 200 spectra/sec following a 260 sec solvent delay. The detector was operated with a 200 V offset voltage.

Table 2.1: Specifications of the GC columns

Column	Length (m)	Internal Diameter (mm)	Phase	Filmthickness (µm)
Primary	28.2	0.25	Rxi-5Sil-MS	0.25
Secondary	1.320	0.25	Rxi-17	0.25

2.3.3 Peak identification and initial data pre-processing

Leco Corporation's ChromaTOF software (version 4.71) was used for peak detection and mass spectral deconvolution with an S/N ratio of 150, requiring a minimum of three apexing peaks. The identification of peaks was based on comparisons of mass fragmentation patterns and GC retention times with NIST spectral libraries (mainlib, replib), applying a similarity threshold of 70% for annotation. The raw data, consisting

of peak areas and annotations, were exported into MS Excel. Compounds with the same names but distinct unique masses (UM) were combined. Contaminants were identified by comparing the compounds detected in both extraction and system blanks with those present in the samples. Peaks detected in system blanks (without an injection prior to the run) were excluded if their average concentration in the samples was twenty times or less than the average in the blanks. Compounds exceeding this threshold were retained. Similarly, peaks from extraction blanks (processed with methanol but without biological material) were excluded if their sample concentration was three times or less than that of the blanks (Broadhurst *et al*., 2018). Compounds exceeding this threshold were retained for further analysis. Relative quantification was performed using the detected area of the internal standard, yielding metabolite concentrations in ng/µL. These values are relative rather than absolute, depending on the internal standard used. The final dataset was analysed in MetaboAnalyst (https://www.metaboanalyst.ca/), where batch correction was applied to account for potential instrument shifts across analytical runs. However, no correction was applied in this study, as the original data indicated minimal batch effects across sample groups.

2.3.4 Chemometric analysis

Statistical analysis was conducted on the acquire dataset, which comprised the concentrations (ng/µL) of identified metabolites, using MetaboAnalyst 6.0 (https://www.metaboanalyst.ca/MetaboAnalyst/ModuleView.xhtml). The analysis was conducted using the 'one-factor' module. The data was pre-processed using cube root transformation, median normalisation, and range scaling to ensure comparability across samples. Multivariate analysis using Principal Component Analysis (PCA) was performed as an unsupervised method to assess overall patterns and clustering among the groups (monocytes, MDMs, 1,25D_3-supplemented monocytes, and 1,25D_3-supplemented MDMs). To better understand the differences between monocytes and MDMs, as well as between control and 1,25D_3-supplemented monocytes, orthogonal partial least squares discriminant analysis (OPLS-DA) was employed as a supervised method. The r^2 (predictive accuracy) and q^2 (cross-validated predictive accuracy) values were evaluated to assess potential overfitting and the model's validity. With r^2Y and q^2 values exceeding 92% and 79%, respectively, the model was deemed valid, capturing a substantial portion of the variance in the data and suitable for further

interpretation. The analysis was conducted using the 'one-factor' module. For Principal Component Analysis (PCA), the data was normalised using median-centring, cube root transformation, and pareto scaling to highlight group trends while minimising the influence of large fold changes. PCA was performed as an unsupervised method to assess overall patterns and clustering among the groups (monocytes, MDMs, $1,25D_3$-supplemented monocytes, and $1,25D_3$-supplemented MDMs). To better understand the differences between monocytes and MDMs, as well as between control and $1,25D_3$-supplemented monocytes, orthogonal partial least squares discriminant analysis (OPLS-DA) was performed using cube root transformation, median normalisation, and range scaling. The r^2 (predictive accuracy) and q^2 (cross-validated predictive accuracy) values were evaluated to assess potential overfitting and the model's validity. With r^2Y and q^2 values exceeding 92% and 79%, respectively, the model was deemed valid, capturing a substantial portion of the variance in the data and suitable for further interpretation. OPLS-DA models were not assessed for the MDM with and without $1,25D_3$ comparison due to the significant overlap of these groups in the PCA. Univariate analysis further confirmed no metabolic changes in MDMs in response to acute $1,25D_3$ supplementation. Additionally, the orthogonal component's r^2 and q^2 values confirmed that most of the variation was aligned with the predictive component. The Variable Importance in Projection (VIP) scores were then calculated from the predictive component to identify the top 15 metabolites driving these differences. These 15 metabolites were then rigorously shortlisted using univariate statistical criteria. To ensure statistical significance of the discriminatory metabolites, T-tests were conducted, and *p* values were adjusted for multiple comparisons using the false discovery rate (FDR) method. Significant metabolites were visualised using volcano plots, with a threshold for FDR-adjusted *p* values set at 0.050 and a fold change threshold of 2.0. Cohen's *d* was employed to evaluate the effect sizes of the selected metabolites. This measure standardises the magnitude of differences between groups, allowing for the quantification of the strength of the observed metabolic alterations. Effect size calculations were performed on the normalised metabolite concentrations, which were adjusted for scaling and transformation.

2.3.5 Pathway enrichment and topology analysis

Pathway enrichment and topology analysis was conducted using the pathway analysis module in MetaboAnalyst (v. 6.0) to identify metabolic pathways associated with the observed metabolomic changes. The analysis was performed using a concentration table of detected metabolites, with rows corresponding to individual samples and columns representing specific metabolites. Pathway enrichment analysis was performed using the GlobalTest method to assess the over-representation of metabolites in known metabolic pathways from the KEGG *Homo sapiens* library (Lu *et al*., 2023; Datta *et al*., 2024). Statistical significance for each pathway was determined based on raw *p* values, which were then adjusted for multiple comparisons using the FDR method. For pathway topology analysis, relative betweenness centrality was used to evaluate the topological importance of pathways, identifying key metabolites that influence the overall pathway network. A summary table presented pathway statistics, including the total number of compounds in each pathway, the number of compounds matching those in the dataset, and the adjusted *p* values. Additionally, pathway impact scores, calculated from the topology analysis, were provided to reflect the relative importance of each pathway in the observed metabolic changes.

2.4. RNA Extraction

RNA was isolated from snap-frozen cell pellets containing 1 × 10^6 cells ([section 2.1.3]; Fig. 2.2B) using the Direct-zol™ RNA Mini-prep kit (Zymo Research, Irvine, CA, USA), following the provided guidelines. All surfaces and equipment were decontaminated with 30% (v/v) bleach and then 70% (v/v) ethanol to maintain an RNase-free environment. All experiments were performed on ice, unless otherwise stipulated. Additionally, all centrifugation steps were done at 13 000 x *g* for 1 min at 4 °C, whereafter the flow through was discarded unless otherwise specified. The frozen cell pellets were resuspended in 700 µl TRI Reagent® (Zymo Research, Irvine, CA, USA) and were vortexed for 2 min. An equal amount of EtOH was then added and vortexed for ~1 min to precipitate total RNA. The cell lysate was then transferred into a Zymo-Spin™ IIICG column placed in a collection tube and centrifuged to ensure complete removal of TRI Reagent® and EtOH. Thereafter, 400 µL of Direct-zol RNA wash buffer was added into the column, preceding centrifugation. Following centrifugation, 80 µl

of a DNase I treatment (5 µl of DNase I & 75 µl of DNA digestion buffer) was added to the column and incubated for 15 min at ~20°C. The purpose of the DNase I treatment was to prevent DNA contamination in the extracted RNA sample by ensuring complete DNA degradation. Following incubation, 400 µl of Direct-zol RNA Prewash was added to the column preceding centrifugation. The flow through was discarded and the collection tube was replaced, and this step was then repeated. Thereafter, 700 µl of Direct-zol RNA wash buffer was added to the column and centrifuged for 2 min to ensure complete removal of the wash buffer. The column was then transferred into a 2 mL RNase-free collection tube and the RNA was eluted using 25 µl of DNase/RNase-free water directly on to the column matrix preceding centrifugation. Utilizing a NanoDrop® spectrophotometer (Thermo Fisher Scientific, Waltham, MA, USA), quantification and quality assessments of the extracted RNA was done. Furthermore, RNA integrity was assessed using agarose gel electrophoresis (section 2.5). The extracted RNA was electrophoresed on a 1.5% (w/v) agarose gel for 30 min at 90 mV. A total of 500 ng of RNA was mixed with an equal volume of 6X DNA Gel Loading Dye (1:1 ratio) before loading into the gel wells. The extracted RNA was then aliquoted (1000 ng) and stored at –80°C in preparation for cDNA synthesis.

2.5. Agarose gel electrophoresis

Agarose gel electrophoresis is a method used to separate biomolecules like RNA or DNA according to their size and charge. The technique employs agarose gel, a polysaccharide derived from seaweed, as a matrix that facilitates the movement of molecules. When an electric field is applied, negatively charged molecules are attracted toward the anode (Sambrook and Russell, 2001). The speed at which these molecules travel through the gel is influenced by their size; smaller molecules move more quickly through the matrix, while larger molecules will migrate at a slower rate. A 10X TBE buffer stock (890 mM trisaminomethane, 890 mM boric acid, 50 mM ethylenediaminotetra-acetic acid [EDTA] disodium salt; pH 8; Sigma Aldrich, St. Louis, MO, USA) was diluted with dH_2O to prepare a 1X TBE working solution, which was then used for gel preparation and electrophoresis. Additionally, 10 mg/ml ethidium bromide (0.6 µg/ml; Sigma Aldrich, St. Louis, MO, USA), which is a UV-fluorescent dye, was added to the gel as it binds to nucleic acids and allows for visualisation under a UV light using the Gel Doc XR+ (Bio-Rad, Hercules, CA, USA).

2.6. RT-qPCR

Relative gene expression levels of *IL-1B*, *CCL2*, and *CXCL10* were measured using RT-qPCR (Table 2.2). All consumables, reagents, and machinery for the steps of this experiment were purchased from Thermo Fisher Scientific, Waltham, MA, USA unless otherwise specified. Furthermore, unless otherwise stipulated, all experiments were performed on ice. Lyophilized primers were reconstituted in Tris-EDTA buffer (IDT, Coralville, IA, USA) to prepare 100 µM stock solutions. These were subsequently diluted using nuclease-free water to make 10 µM stocks and were stored at -20 °C. Primers were optimized for efficiency, achieving values between 95% and 105%. Primer specificity was further confirmed by performing agarose gel electrophoresis using a 3% (w/v) agarose gel (section 2.5). For each treatment, three independent biological replicates with two technical repeats were subjected to RT-qPCR analysis for each gene.

Prior to RT-qPCR analysis, the extracted RNA (section 2.4) was first reverse transcribed into cDNA. cDNA synthesis master mixes were prepared using the RevertAid First Strand cDNA Synthesis Kit, following the manufacturer's guidelines (Table 2.3). The prepared cDNA master mix was then transferred to the SimpliAmp thermal cycler and incubated at 42 °C for 60 min. The reaction was then terminated by incubation at 70 °C for 5 min. The prepared cDNA was immediately used in RT-qPCR reactions. The master mixes for each gene were prepared using the Luna® Universal qPCR Master Mix (NEB, Ipswich, MA, USA) according to the manufacturer's instructions (Table 2.4). The prepared master mixes were then aliquoted into 96-well plates where 50 ng of cDNA template was added. The 96-well plate was then transferred to the CFX-96 Touch Real Time Thermal Cycler (Bio-Rad, Hercules, CA, USA) for subsequent amplification, quantification and melt curve analysis at the applicable cycle settings (Table 2.5).

Gene expression was standardised against the stably expressed *ubiquitin C* (*UBC)* and *tyrosine 3-monooxygenase/ tryptophan 5-monooxygenase activation protein zeta* (*YWHAZ*) genes (Vandesompele *et al*., 2002). RT-qPCR amplicon size was assessed by allowing the products to be electrophoresed (section 2.5) on a 3% (w/v) agarose gel for ~90 min at an electromotive force of 90 mV against the O'GeneRuler^{TM} Low Range DNA Ladder, ready-to-use, 0.1 µg/1 µL. Utilizing DNA Gel Loading Dye (6X),

the RT-qPCR product was added in a 1:5 ratio and the solution was transferred into the wells. Following electrophoresis, the molecular weight (MW) of the products was calculated by using a ruler to measure the migration distance from the top of the resolving gel to each band of the DNA ladder and to the dye front. This was also done for the bands of the RT-qPCR products. For each band of the DNA ladder, the Rf value was calculated as follows to generate a standard curve of the log (MW) versus Rf:

$$\text{Rf} = \frac{migration\ distance\ of\ RT{-}qPCR\ product\ (mm)}{migration\ distance\ of\ dye\ front\ (mm)}$$

From the standard curve the equation $y = mx + b$ was generated to determine the MW of the RT-qPCR products by solving for y using the measured Rf values.

Table 2.2: Primer sequences used for mRNA amplification

Gene		Primer Sequences[a]	Product Size (bp)[b]
Reference[c]	*UBC*	FP: ATT TGG GTC GCG GTT CTT G	133
		RP: TGC CTT GAC ATT CTC GAT GGT	
	YWHAZ	FP: ACT TTT GGT ACA TTG TGG CTT CAA	94
		RP: CCG CCA GGA CAA ACC AGT AT	
Target[d]	*IL-1B*	FP: AGC TCG CCA GTG AAA TGA TG	143
		RP: GGA GAT TCG TAG CTG GAT GC	
	CCL2	FP: CCC AAA GAA GCT GTG ATC TTC A	137
		RP: TGT GGA GTG AGT GTT CAA GT	
	CXCL10	FP: GTG GCA TTC AAG GAG TAC CT	199
		RP: TTG ATG GCC TTC GAT TCT GG	

[a]The forward (FP) and reverse (RP) primer sequences are given in the 5' – 3' direction.

[b]Predicted product size is based on in silico PCR (https://genome.ucsc.edu/cgi-bin/hgPcr).

[c]Primers for reference genes were obtained from Vandesompele *et al*., 2002.

[d]Primers for the target genes were designed using Primer3 (Untergasser *et al*., 2012).

Table 2.3: cDNA synthesis reagents

Component[a]	Volume per 20 µL reaction (µL)	Concentration
Total RNA	variable (for 1000 ng)	50 ng/µL
Oligo (dt) primer	1	100 µM
Nuclease-free Water	up to 12	-
5X Reaction Buffer	4	1 X
RiboLock Rnase inhibitor	1	20 U/µL
10mM dNTP mix	2	-
RevertAid M-MuLV RT	1	200 U/µL

[a]Components were added in the order of appearance.

Table 2.4: RT-qPCR master mix components

Component	Volume per 10 µL reaction (µL)	Final Concentration
Luna Universal qPCR Master Mix	5	1X
Forward primer (10 µM)	0.25	0.25 µM
Reverse primer (10 µM)	0.25	0.25 µM
Template cDNA	variable	< 100 ng
Nuclease-free Water	up to 10	-

Table 2.5: CFX-96 Thermocycler incubation steps for the RT-qPCR reaction

Cycle Step	Temperature (°C)	Time (sec)	Cycles
Initial Denaturation	95	60	1
Denaturation	95	15	40-45
Extension	60	30 (+ plate read)	40-45
Melt Curve	60-95	5	1

2.7. Gene expression analysis

2.7.1 Data pre-processing

Upon completion of RT-qPCR analysis, the baseline threshold for relative fluorescence units (RFU) was set to 50 for all runs in the Bio-Rad CFX Maestro 1.0 software (v. 4.0.2325.0418, Bio-Rad, Hercules, CA, USA). Quantification cycle (Cq) value outliers within the technical replicates were identified and removed from all datasets. Subsequently, the gene expression of each target gene was normalised using Livak's method ($2^{-\Delta\Delta Ct}$; Livak and Schmittgen, 2001). The normalised gene expression data was then exported to Microsoft Excel (v. 16.79.1(23111614)) for further analysis. Statistical significance was assessed from these values, and boxplots were generated to represent the $\log_{10}$ transformed mRNA expression levels for each gene.

2.7.2 mRNA quantification

Statistical analyses were performed using IBM SPSS Statistics [v. 29.0.2.0(20)]. To evaluate statistical significance of the gene expression changes following 4 hrs of *in vitro* $1,25D_3$ supplementation in monocytes and MDMs, and in response to TLR8 stimulation, a one-way analysis of variance (ANOVA) between groups was conducted on the normalised mRNA expression values. Levene's test for homogeneity of variance was conducted to assess whether the assumption of equal variances was met. If homogeneity was confirmed ($p > 0.050$), the classical one-way ANOVA was applied. If a significant overall difference was observed ($p < 0.050$), the Bonferroni post-hoc test was employed to account for multiple comparisons. Conversely, if homogeneity was not met ($p < 0.050$), Welch's one-way ANOVA, which accounts for unequal variances, was used. If an overall significant difference was observed ($p < 0.050$), the Tamhane post-hoc test was employed to adjust for multiple comparisons. The *p*-values presented in the text or shown in the graphs are those derived from the Tamhane test, unless otherwise specified.

Chapter 3: Results

3.1. Differentiation was confirmed through observed morphological changes

Inverted light microscopy confirmed the successful differentiation of monocytes into MDMs (Fig. 3.1). Initially, monocytes displayed a spherical morphology (Fig. 3.1A). Following 24 hrs of supplementation with PMA and 1,25D_3, succeeded by a 72 hr 'rest period' with 1,25D_3 alone, the cells spread across the culture surface, adopting a larger, elongated, and irregular morphology (Fig. 3.1B). This transition was consistently observed across all experimental replicates.

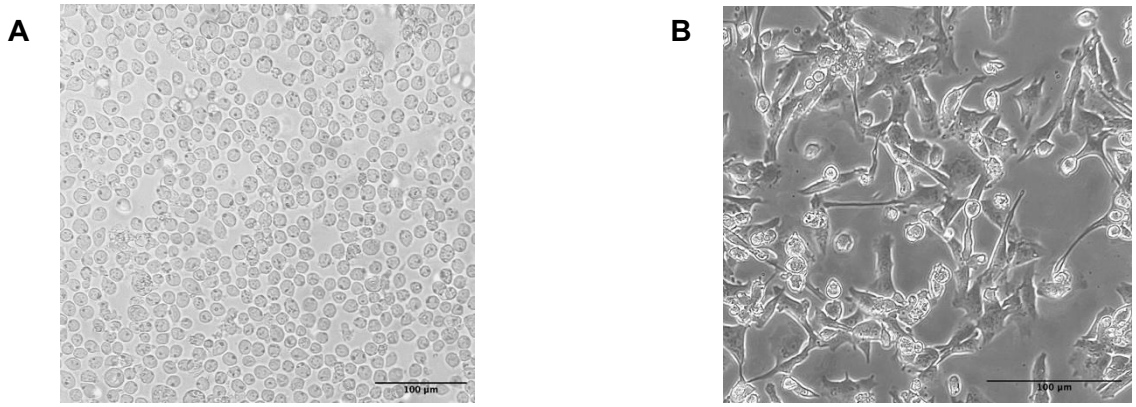

Figure 3.1. Morphological transition from THP-1 monocytes to MDMs. The images display micrographs of monocytes (**A**) and MDMs (**B**) captured at 40 x magnification. Supplementation with PMA and 1,25D_3 induced distinct morphological changes, including increased cell size, and altered cell shape. Image includes scale bar indicating 100 µm.

3.2. No significant alterations in cell viability were observed post-treatment

The trypan blue exclusion assay confirmed that cell viability was not adversely affected by any of the treatment conditions in either monocytes or MDMs. One-way ANOVA revealed no significant overall effects of the selected treatment conditions on cell viability in both cell types at 4 hrs (p > 0. 050; Fig. 3.2). Additionally, cell viability remained above 90% for both monocytes and MDMs, regardless of the treatment.

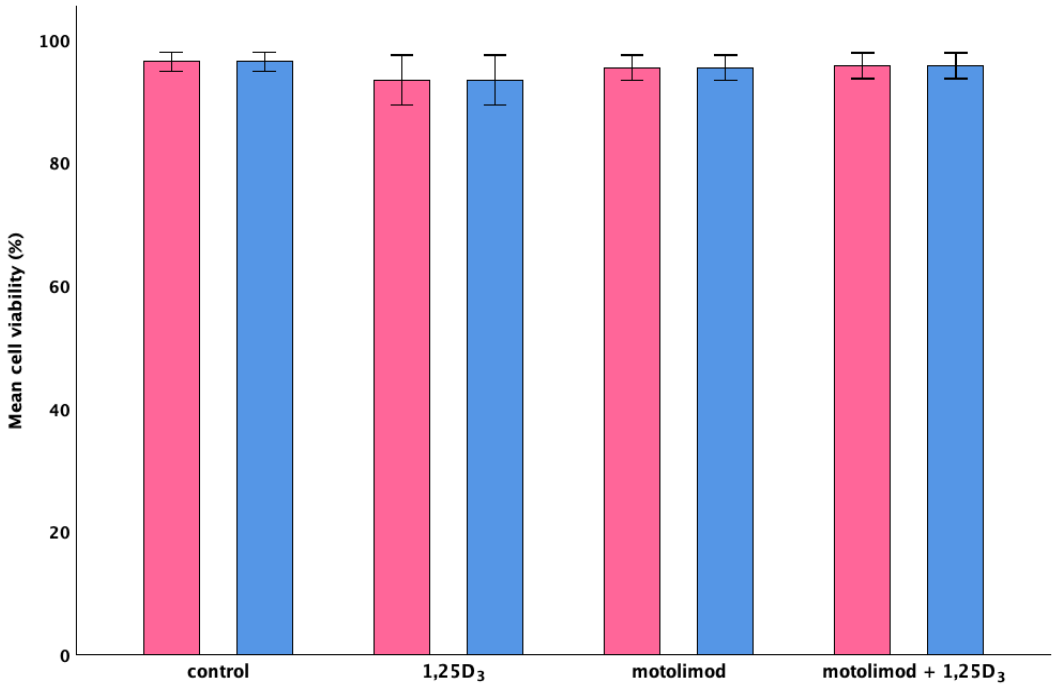

Figure 3.2. Cell viability in both monocytes and MDMs was not significantly impacted by the treatment conditions. Bar graphs illustrating the percentage cell viability as quantified by a trypan blue exclusion assay, for monocytes (**pink**) and MDMs (**blue**) in response to treatment with 10 nM $1,25D_3$, 5 µM motolimod (TLR8 agonist) or, a combination of $1,25D_3$ and motolimod for 4 hrs. Error bars indicate a ± 1 SD (n = 3).

3.3. Supplementation with $1,25D_3$ for 4 hrs in monocytes leads to a metabolic profile resembling that of MDMs *in vitro*

To evaluate the metabolic profiles of monocytes and MDMs, and the effect of 4 hrs *in vitro* supplementation with $1,25D_3$, whole cell extracts were analysed using GC×GC/TOF-MS. The resulting 1-dimensional total ion chromatograms (TICs) from each sample were first evaluated to ensure high-quality data acquisition (Fig. 3.3). These TICs provided an overview of the ion profiles, revealing complex chromatograms with numerous well-resolved peaks, each corresponding to a distinct metabolite with retention times ranging from 500 to 3500 s. This broad polarity spectrum indicated effective separation, allowing for accurate detection of subtle metabolite variations. Subsequently, PCA was applied as an unsupervised method to identify differences between cell types and to evaluate the effect of acute *in vitro* supplementation with $1,25D_3$ thereon (Fig. 3.4). In the absence of $1,25D_3$ supplementation, monocyte and MDM groups showed clear separation. While $1,25D_3$ did not significantly affect the metabolic profile of MDMs, it induced distinct metabolic shifts in monocytes, resulting in a separation from control monocytes and clustering closer to the control MDMs profile.

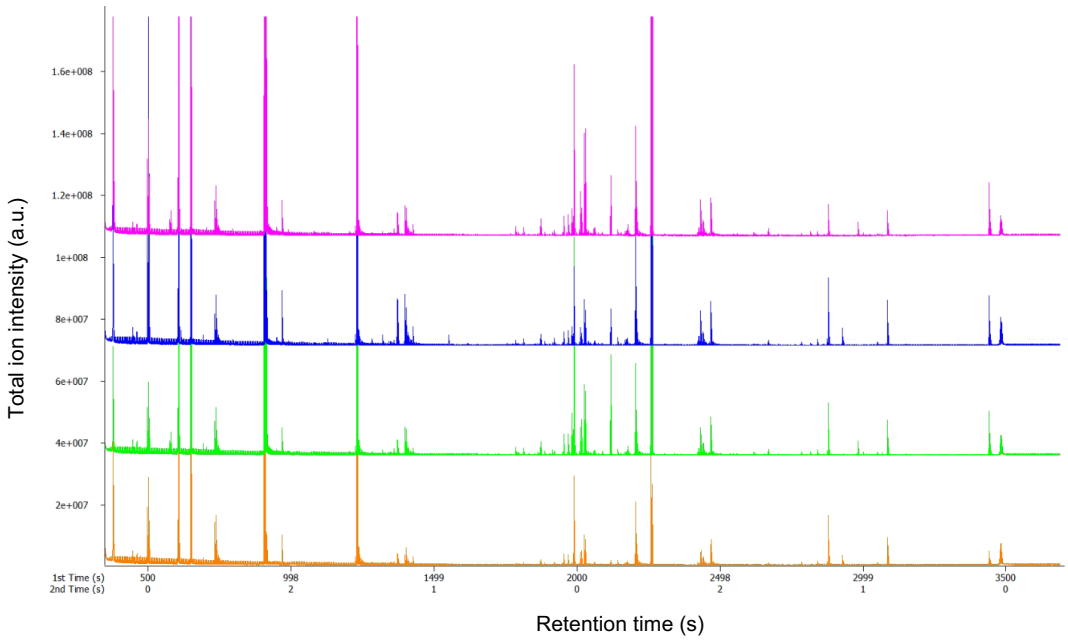

Figure 3.3. 1-Dimensional Total Ion Chromatogram (TIC) displaying an overview of the detected ion profiles in each sample. The representative image displays the total ion intensity from GC×GC/TOF-MS analysis, corresponding to a range of metabolites in monocytes (**orange**), MDMs (**green**), 1,25D_3-supplemented monocytes (**blue**), and 1,25D_3-supplemented MDMs (**pink**).

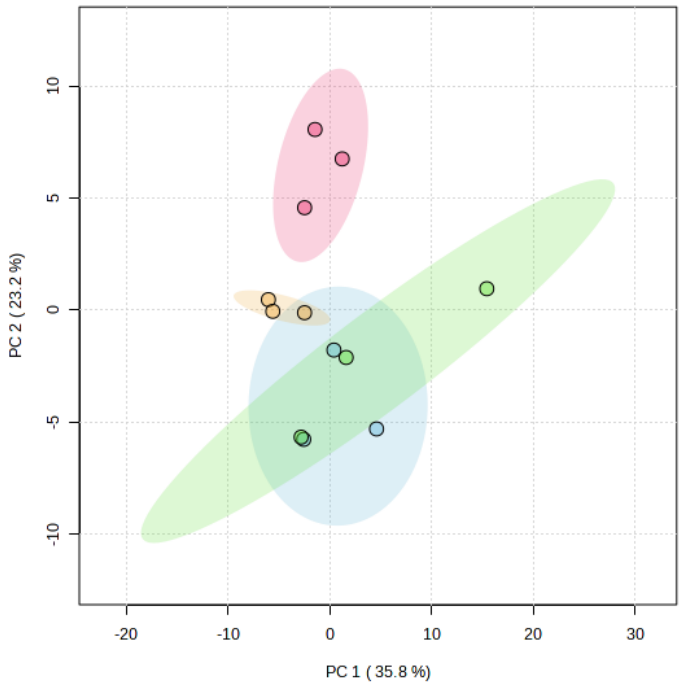

Figure 3.4. 1,25D_3-supplemented monocytes display a similar metabolic profile to MDMs. The unsupervised PCA scores scatter plot shows sample grouping of monocytes (**pink**), 1,25D_3-supplemented monocytes (**orange**), MDMs (**blue**) and 1,25D_3-supplemented MDMs (**green**) at 4 hrs. Ellipsoids represent 95% confidence intervals around the group centroids, based on the distribution of PCA scores. Along the axes, the percentage of variation explained by each principal component (PC) is provided in brackets. The statistical significance of group separation was assessed using PERMANOVA on 999 permutations (R^2 = 0.562, F-value = 3.427, p < 0.010, n = 3).

3.4. Elevated fumaratelevels indicate a pivotal metabolic shift during monocyte differentiation and in response to acute 1,25D_3 supplementation

The top fifteen discriminatory metabolites distinguishing monocytes from MDMs, as well as control monocytes from those supplemented with 1,25D_3, were identified using OPLS-DA. Both OPLS-DA models demonstrated high predictive accuracy and validity, with R^2 and q^2 values exceeding 93% and 65%, respectively (Fig. 3.5). These models were further utilised for supervised analysis to characterise the observed differences (Fig. 3.6). VIP score plots for monocytes vs. MDMs (Fig. 3.6A) and control vs. 1,25D_3-supplemented monocytes (Fig. 3.6B) highlighted fumarate, two unidentified metabolites (unknown metabolites 1 and 2), scyllo-inositol, and erythrose among the top discriminatory metabolites in both comparisons. Notably, fumarate and the two unidentified metabolites were elevated in both MDMs and 1,25D_3-supplemented monocytes compared to control monocytes. To validate the statistical significance of the discriminant metabolites, univariate analysis was carried out (Tables 3.1 and 3.2). Effect size analysis further confirmed substantial metabolic shifts, with fumarate exhibiting a large effect size in both MDMs (Cohen's d = 14.730, $p < 0.050$; Table 3.1) and 1,25D_3-supplemented monocytes (Cohen's d = 7.26, $p < 0.050$; Table 3.2). Similarly, unknown metabolite 1 showed a large effect size in both MDMs (Cohen's d = 11.110, $p < 0.05$; Table 3.1) and 1,25D_3-supplemented monocytes (Cohen's d = 2.83, $p < 0.050$; Table 3.2). Furthermore, in the comparison of monocytes and MDMs (Table 3.1), a significant metabolic shift in scyllo-inositol was observed exclusively in MDMs (Cohen's d = 5.370, $p < 0.050$), whereas monocytes exhibited significantly higher levels of monoradylglycerols (Cohen's $d > 0.8$, $p < 0.050$).

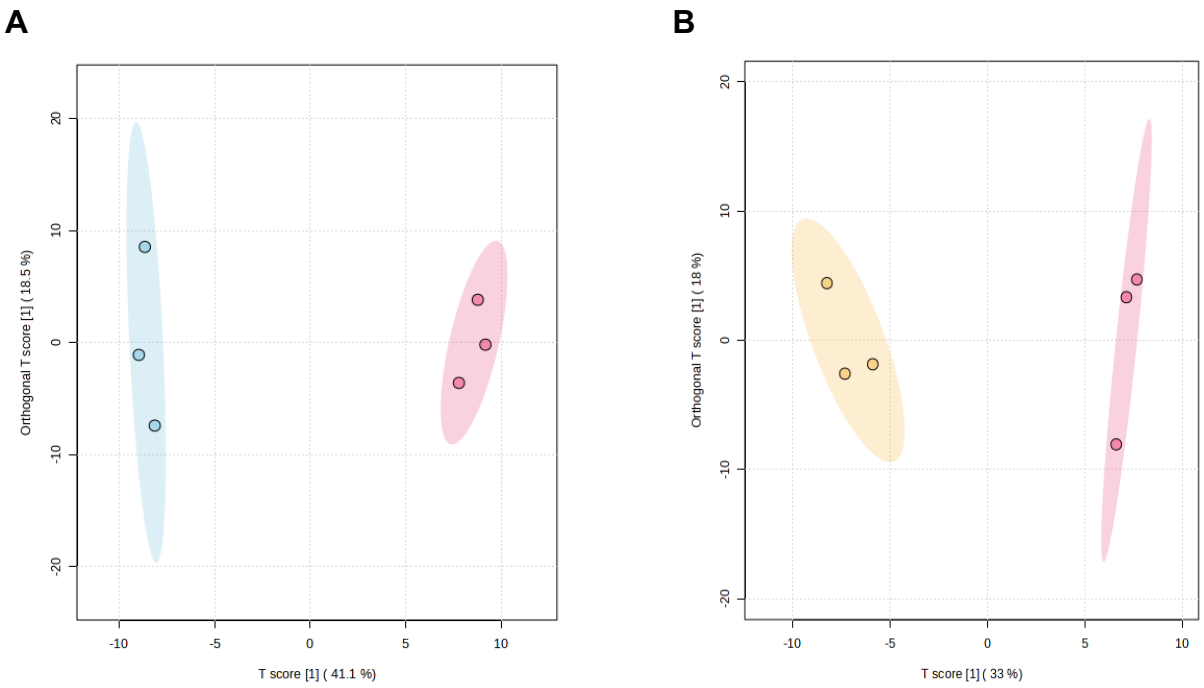

Figure 3.5. OPLS-DA score plots illustrating metabolic differences between monocytes and MDMs, as well as between control and 1,25D$_3$-supplemented monocytes. The supervised OPLS-DA model was used to determine variables responsible for differences in the metabolic profiles of monocytes (**pink**) and MDMs (**blue**) (**A**), as well as for control monocytes (**pink**) and 1,25D$_3$-supplemented monocytes (**orange**) (**B**). The 95% confidence ellipses are displayed for each group to highlight the clustering and separation within the dataset (n = 3). The scores scatter plot of T score [1] vs. orthogonal T score [1] illustrates the separation between the two classes. T score [1] represents the predictive component, which accounts for significant variance with $r^2X = 0.411$, $r^2Y = 0.921$, and $q^2 = 0.798$, indicating strong predictive ability (**A**). The orthogonal T score [1] captures orthogonal variation with $r^2X = 0.185$, $r^2Y = 0.076$, and $q^2 = 0.062$, reflecting within-class variability that is unrelated to the discrimination between the classes. The predictive component indicated strong predictive ability with $r^2X = 0.33$, $r^2Y = 0.932$, and $q^2 = 0.651$ (**B**). The orthogonal T score [1] captures orthogonal variation with $r^2X = 0.18$, $r^2Y = 0.057$, and $q^2 = 0.063$.

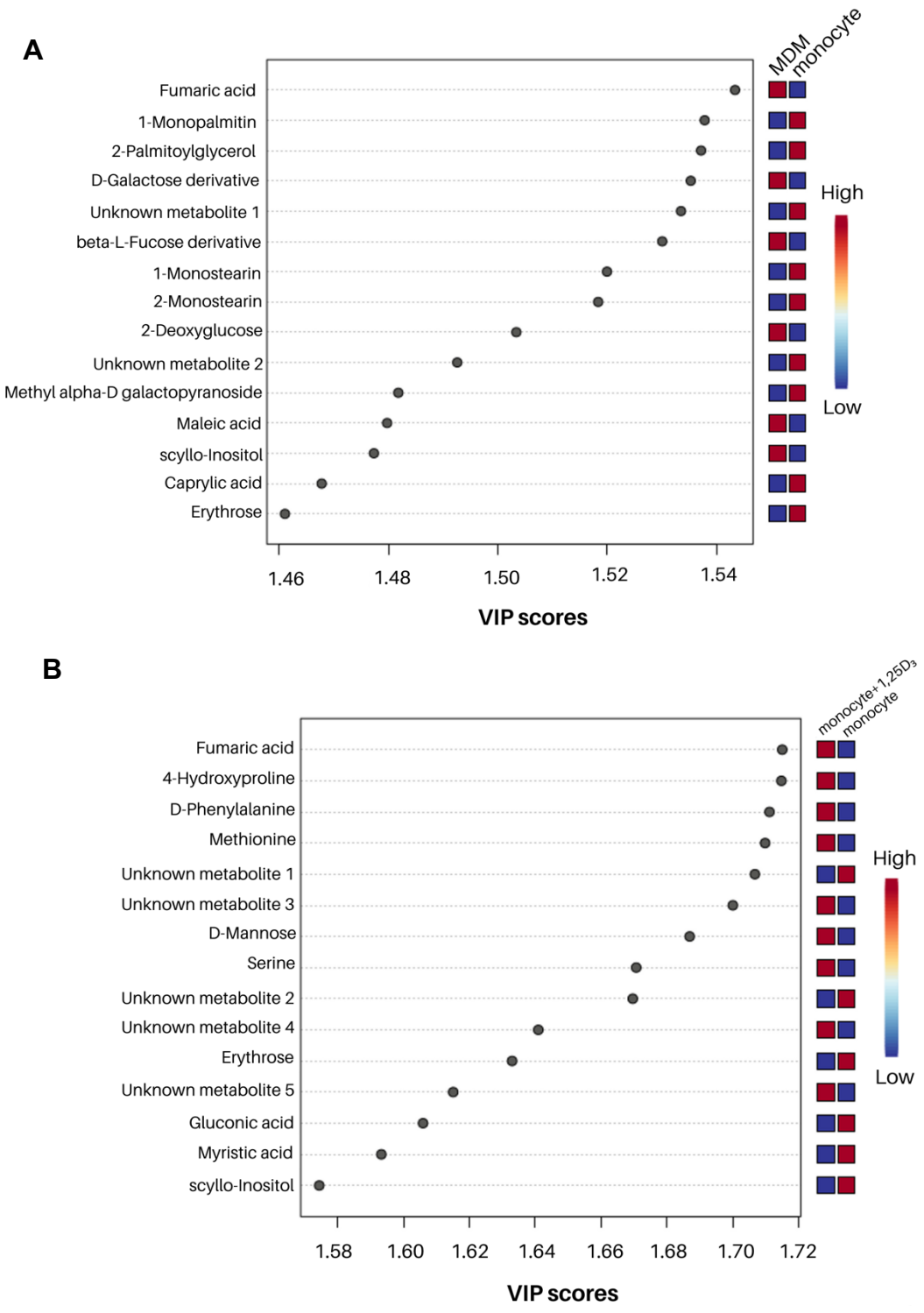

Figure 3.6. Identification of the top fifteen discriminant signatory metabolites from respective OPLS-DA models derived from GC×GC/TOF-MS analysis. The VIP scores plots highlight the most influential metabolites that contribute to the differences observed between monocytes and MDMs (**A**) and, control and 1,25D$_3$-supplemented monocytes (**B**). Top metabolites are labelled according to their relative abundance, indicating their importance.

Table 3.1: Significant signatory metabolites discriminating between monocytes and MDMs

Category	Metabolite	Mean concentration (SD) [a]		FC [b]	OPLS-DA VIP score	Cohen's *d* [c]	FDR [d]
		monocytes	MDMs				
Monoradylglycerols	2-Monostearin	43.346 (13.710)	28.835 (8.836)	3.237	1.518	7.560	0.023
	1-Monostearin	372.090 (100.780)	218.845 (68.478)	3.692	1.520	6.760	0.031
	2-Palmitoylglycerol	41.224 (10.787)	28.649 (11.255)	3.193	1.537	10.920	0.013
	1-Monopalmitin	424.851 (99.565)	213.773 (82.902)	4.412	1.538	9.200	0.019
Carbohydrates and carbohydrate conjugates	D-Galactose derivative	0.233 (0)	45.713 (25.068)	0.012	1.535	8.450	0.021
	Methyl alpha-D-galactopyranoside	3.484 (1.859)	0.165 (0)	40.945	1.482	5.660	0.049
	beta-L-Fucose derivative	0.017 (0)	19.991 (17.120)	0.002	1.530	7.790	0.023
Dicarboxylic acids and derivatives	Fumarate	0.259 (0)	7.511 (2.360)	0.077	1.543	14.730	0.012
	Maleic acid	0.118 (0)	4.927 (1.859)	0.057	1.480	5.500	0.049
Fatty alcohols	2-Deoxyglucose	0.272 (0)	10.903 (6.447)	0.056	1.503	5.600	0.049
Alcohols and polyols	scyllo-Inositol	5.133 (0.262)	36.499 (9.201)	0.306	1.477	5.370	0.049
-	Unknown metabolite 1	67.020 (32.576)	0.646 (0)	196.500	1.533	11.110	0.013

[a] pre-normalised values in ng/µL with the respective standard deviations
[b] fold change threshold of 2 is relative to monocytes
[c] calculated using normalised concentration values
[d] FDR was calculated using the Benjamini-Hochberg procedure to adjust for multiple comparisons.

Table 3.2: Significant signatory metabolites discriminating between control and 1,25D_3-supplemented monocytes

Category	Metabolite	Mean concentration (SD) [a]		FC [b]	OPLS-DA VIP score	Cohen's *d* [c]	FDR [d]
		monocytes	1,25D_3-supplemented monocytes				
Amino acids, peptides, and analogues	Methionine	0.499 (0)	4.883 (1.268)	0.27884	1.720	2.82	0.015
	D-Phenylalanine	2.292 (0.580)	61.469 (18.466)	0.10558	1.711	2.81	0.015
	4-Hydroxyproline	0.345 (0.342)	12.427 (4.645)	0.070036	1.715	6.73	0.039
Dicarboxylic acids and derivatives	Fumarate	0.259 (0)	6.661 (3.004)	0.10815	1.715	7.26	0.039
-	Unknown metabolite 1	67.012 (32.576)	0.646 (0)	255.3	1.707	2.83	0.015
-	Unknown metabolite 4	1.137 (0)	60.656 (21.392)	0.04921	1.641	2.59	0.039
-	Unknown metabolite 3	2.090 (0.033)	19.575 (7.092)	0.29601	1.700	2.66	0.039

[a] pre-normalised values in ng/µL with the respective standard deviations
[b] fold change threshold of 2 is relative to control monocytes
[c] calculated using normalised concentration values
[d] FDR was calculated using the Benjamini-Hochberg procedure to adjust for multiple comparisons

3.5. Pathway analysis of metabolic changes in monocytes and MDMs: impact of 1,25D_3 supplementation

To further investigate metabolic differences between monocytes and MDMs, as well as between control and 1,25D_3-supplemented monocytes, pathway analysis was performed using MetaboAnalyst ([MetPA]; Fig. 3.7). A normalised concentration table containing 410 detected metabolites with available HMDB IDs was used to identify pathway alterations and assess their biological relevance. This approach integrated both significant and background metabolites, providing robust confirmation of pathway changes. The analysis revealed that galactose metabolism had the highest pathway impact score when comparing monocytes and MDMs ([p < 0.001, impact score = 0.391]; Fig. 3.7A). Within this pathway, MDMs exhibited significantly higher levels of galactose and mannose compared to monocytes ([p < 0.050]; Fig. 3.8). Additionally, increased levels of fructose and glucose were also observed in MDMs relative to monocytes. Similarly, just as glucose levels were elevated in MDMs, 1,25D_3-supplemented monocytes also exhibited increased glucose levels compared to control monocytes. Furthermore, when comparing monocytes and MDMs (Fig. 3.7A), alanine, aspartate, and glutamate (AAG) metabolism (p < 0.010, impact score = 0.361) and the TCA cycle (p < 0.050, impact score = 0.268) were also significantly impacted. Similarly, when comparing control and 1,25D_3-supplemented monocytes (Fig. 3.7B), notable alterations were also observed in the TCA cycle (p < 0.010, impact score = 0.223) and AAG metabolism (p < 0.050, impact score = 0.361). Although fatty acid biosynthesis was identified as statistically significant (p < 0.050) when comparing monocytes and MDMs (Fig. 3.7A), its low impact score (0.015) suggests a limited contribution to overall metabolic changes. Similarly, in the control and 1,25D_3-supplemented monocytes comparison (Fig. 3.7B), fatty acid biosynthesis also showed a low impact score (p > 0.050, impact score = 0.015). However, further analysis revealed a detection issue in MetaboAnalyst, where HMDB IDs for monoradylglycerols were not recognised (Table 3.1). Given their established role in lipid metabolism and fatty acid biosynthesis, this highlights the need for refined pathway annotations in future studies. Furthermore, in the comparison between control and 1,25D_3-supplemented monocytes, cysteine and methionine metabolism was identified as the most impacted pathway ([p < 0.001, impact score = 0.126]; Fig. 3.7B). 1,25D_3-supplemented monocytes showed significantly higher levels of methionine and serine

in comparison to control monocytes ([$p < 0.050$]; Fig. 3.9). Collectively, these results highlight the TCA cycle, AAG metabolism, as well as fatty acid biosynthesis, as key pathways underlying metabolic differences between monocytes and MDMs, as well as the metabolic effects of acute 1,25D_3 supplementation in monocytes.

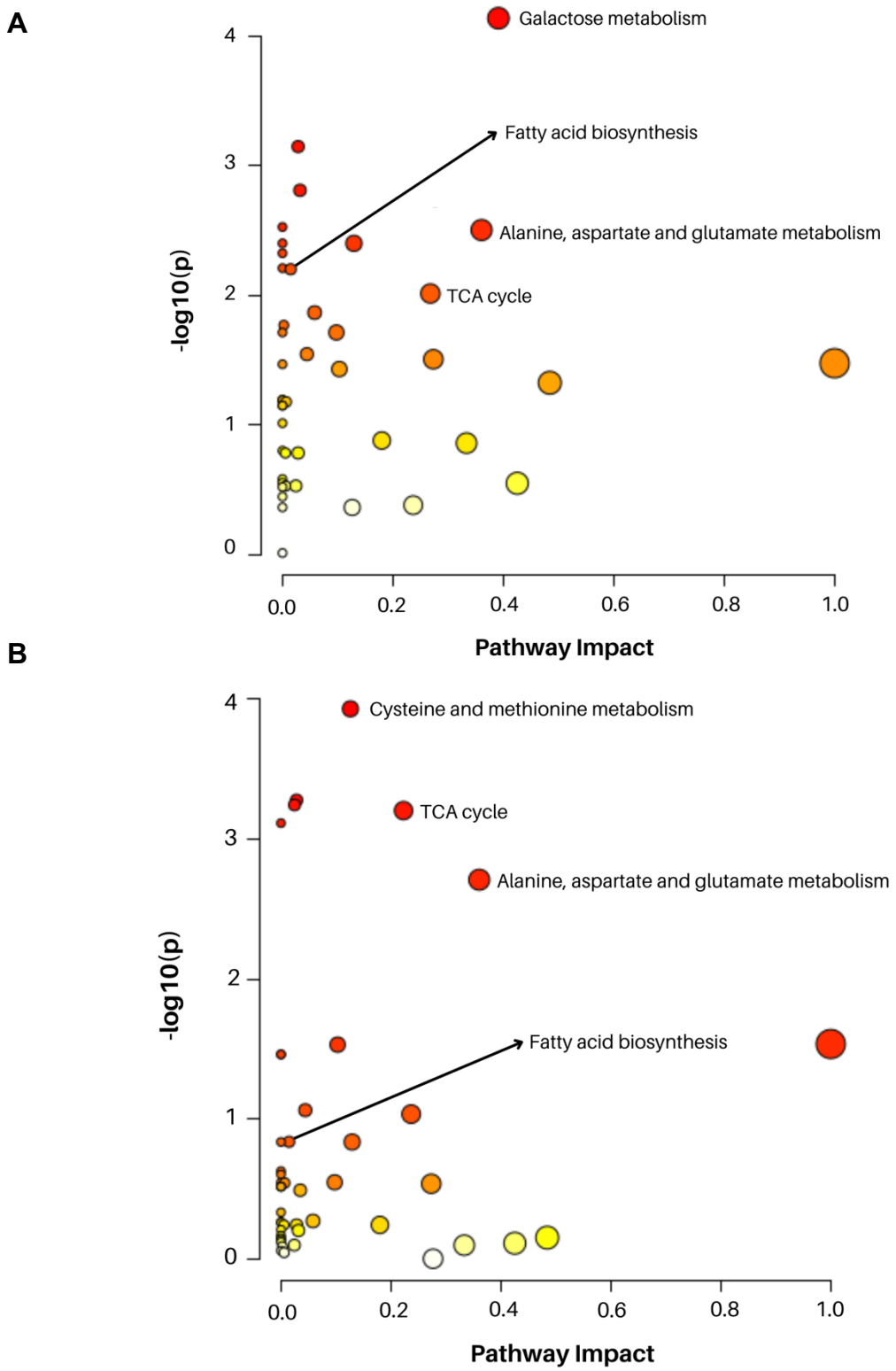

Figure 3.7. Metabolomic pathway analysis of all GC×GC/TOF-MS derived metabolites annotated with HMDB IDs. Each circle represents a potentially impacted metabolic pathway (node) identified in the comparison between monocytes and MDMs (**A**) and, control and 1,25D_3-supplemented monocytes (**B**). Pathway impact values and -log(10)*p*-values of each node are represented on the x and y axis, respectively. Larger, darker red nodes signify pathways with higher impact and greater significance, while less significant pathways transition to yellow.

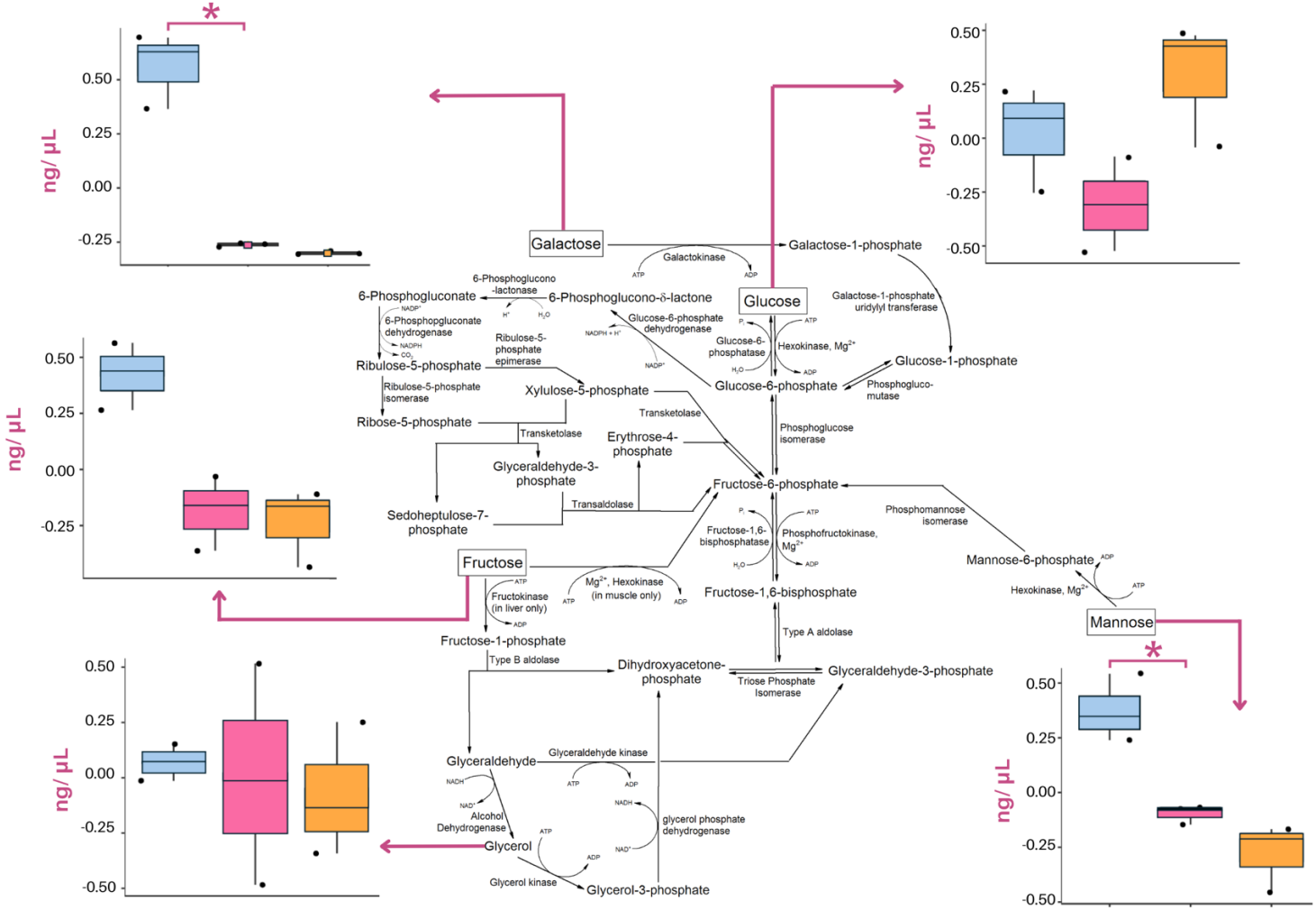

Figure 3.8. Alterations in the galactose metabolic pathway in monocytes, MDMs, and 1,25D$_3$-supplemented monocytes. The boxplots display GC×GC-TOFMS-derived metabolite levels of galactose metabolism intermediates at 4 hrs in MDMs (**blue**), monocytes (**pink**) and 1,25D$_3$-supplemented monocytes (**orange**). Significance was determined by Welch's two-sample t-Test between monocytes and MDMs, and control and 1,25D$_3$-supplemented monocytes (* $p < 0.050$, ** $p < 0.010$, *** $p < 0.001$) (n=3).

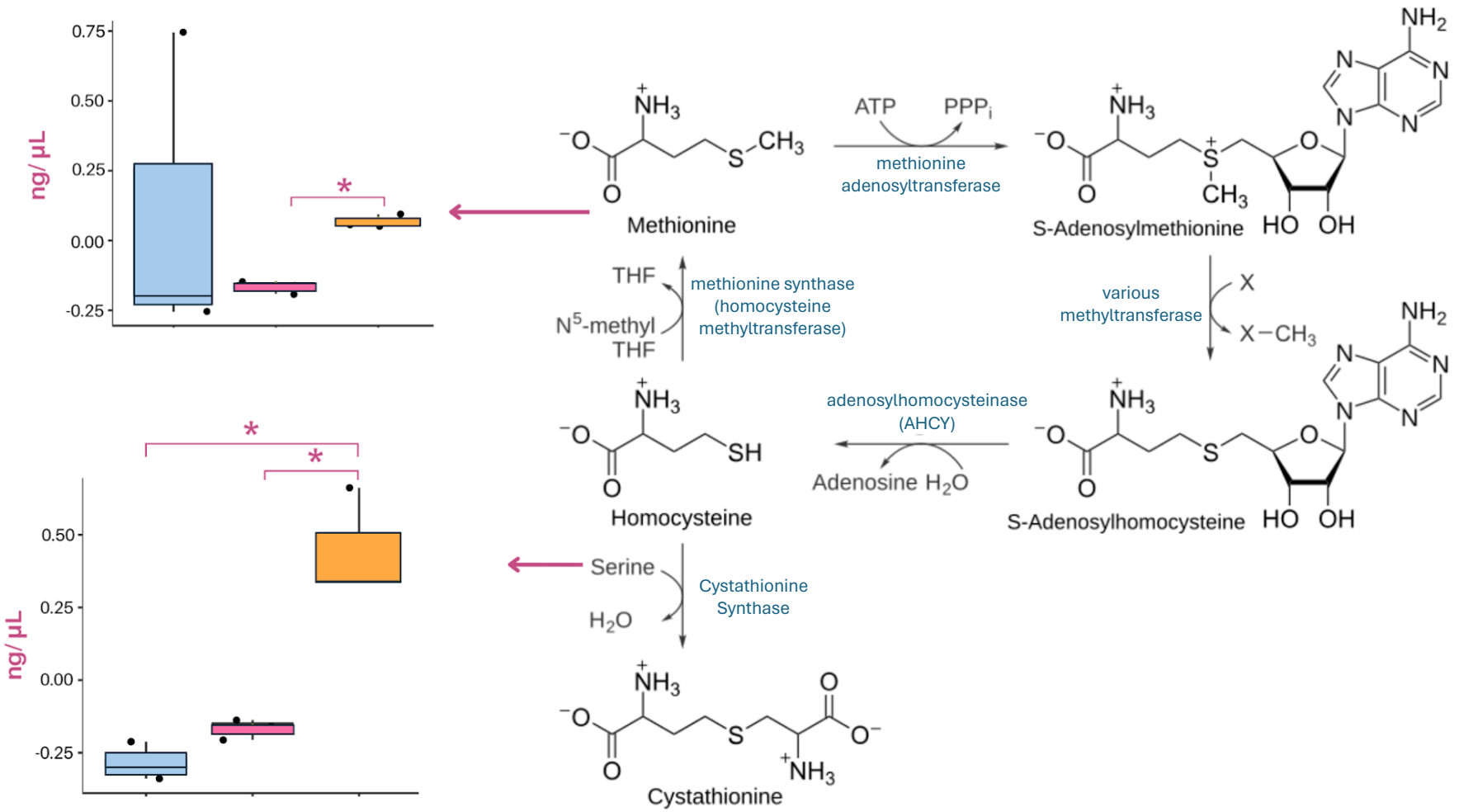

Figure 3.9. Alterations in the cysteine and methionine metabolic pathway in monocytes, MDMs, and 1,25D$_3$-supplemented monocytes. The boxplots display GC×GC-TOFMS-derived metabolite levels of cysteine and methionine metabolism intermediates at 4 hrs in MDMs (**blue**), monocytes (**pink**) and 1,25D$_3$-supplemented monocytes (**orange**). Significance was determined by Welch's two-sample t-Test between monocytes and MDMs, and control and 1,25D$_3$-supplemented monocytes (* $p < 0.050$, ** $p < 0.010$, *** $p < 0.001$) (n=3).

3.6. Monocytes exhibit robust fatty acid biosynthesis, which is notably modulated by 1,25D_3 supplementation

Although fatty acid biosynthesis was initially identified to have minimal contribution to the overall metabolic changes (Fig. 3.7), further analysis revealed its significant impact on the observed variances (Fig. 3.10). The identified metabolites: myristic acid, palmitic acid, lauric acid, and caprylic acid are associated with the fatty acid biosynthesis pathway. The T-test analysis indicated that monocytes exhibited significantly higher levels of myristic acid, lauric acid, and caprylic acid compared to MDMs ($p < 0.050$). Furthermore, supplementation with 1,25D_3 significantly reduced the levels of myristic acid and palmitic acid in monocytes ($p < 0.050$). Additionally, it was also observed that the levels of these fatty acids were not significantly different between MDMs and 1,25D_3-supplemented monocytes ($p > 0.050$).

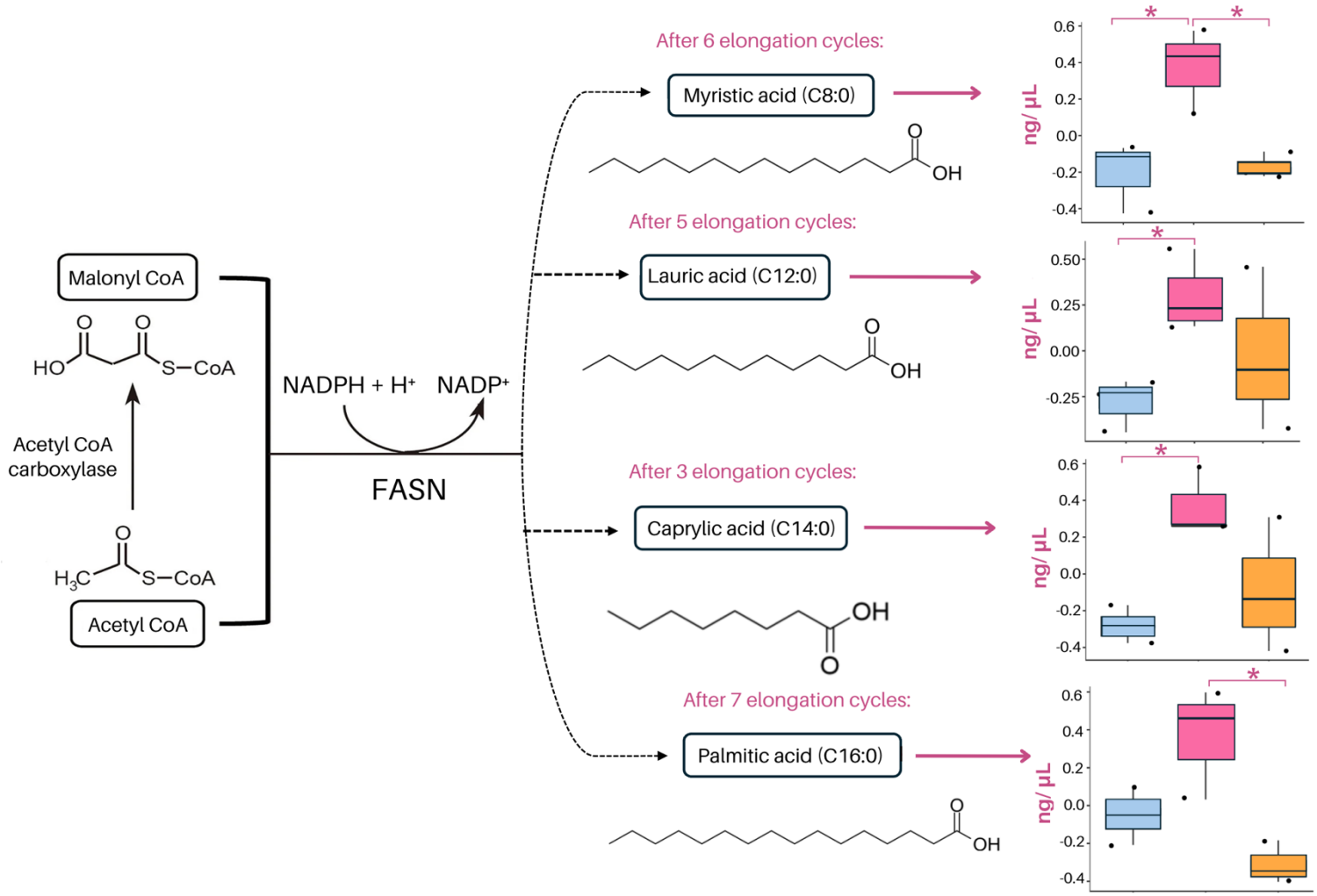

Figure 3.10. *In vitro* supplementation with 1,25D$_3$ for 4 hrs in monocytes modulates the fatty acid biosynthesis pathway. The boxplots display GC×GC-TOFMS-derived metabolite levels of fatty acid biosynthesis intermediates produced via fatty acid synthase (FASN) in MDMs (**blue**), monocytes (**pink**) and 1,25D$_3$-supplemented monocytes (**orange**). Significance was determined by Welch's two-sample t-Test between monocytes and MDMs, and control and 1,25D$_3$-supplemented monocytes (* $p < 0.050$, ** $p < 0.010$, *** $p < 0.001$) (n=3).

3.7. Increased fumarate production via the AAG metabolic pathway feeds into the TCA cycle

It is seen that AAG metabolism exhibited a pathway impact score of 0.361 in both the monocyte and MDM, as well as the control and 1,25D_3-supplemented monocyte comparisons (Fig. 3.7). Within this pathway, MDMs exhibit higher levels of aspartate compared to monocytes, though this difference is not statistically significant ([p > 0.050]; Fig. 3.11). However, it is seen that through the aspartate-argininosuccinate shuttle, there is a significant upregulation of fumarate levels in both MDMs and 1,25D_3-supplemented monocytes compared to control monocytes (p < 0.050). This increase in fumarate further contributed to its upregulation within the TCA cycle ([p < 0.050]; Fig. 3.12), highlighting a strong interplay between these metabolic pathways in both experimental conditions. Alongside fumarate, citrate was also significantly upregulated in the TCA cycle of MDMs and 1,25D_3-supplemented monocytes, highlighting broader metabolic shifts within this pathway (p < 0.050). Additionally, monocytes exhibited significantly higher levels of α-ketoglutarate compared to MDMs (p < 0.050), but this difference was not observed when compared to 1,25D_3-supplemented monocytes.

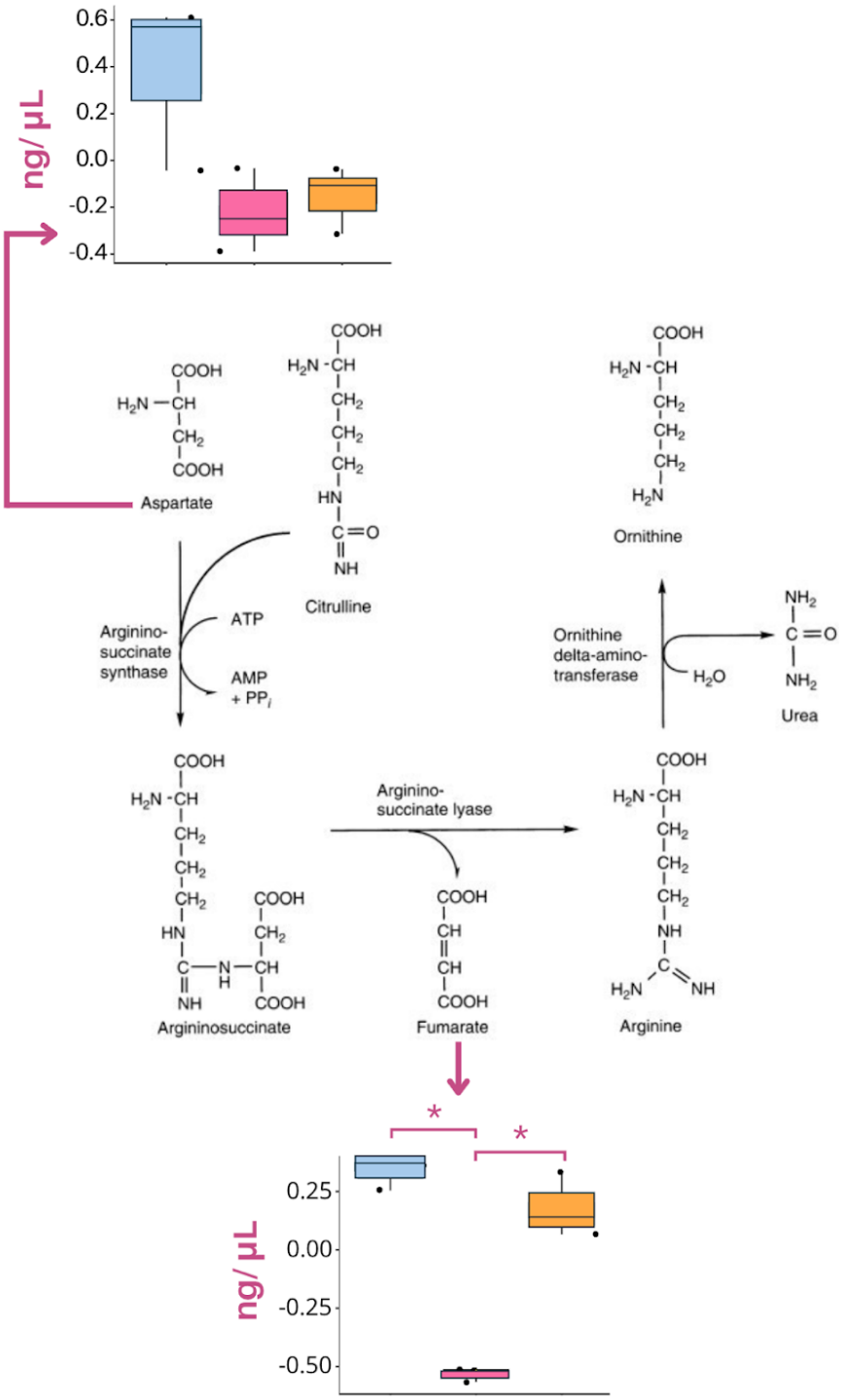

Figure 3.11. The role of the aspartate-argininosuccinate shuttle in driving increased fumarate production in MDMs and 1,25D$_3$-supplemented monocytes. The boxplots display GC×GC-TOFMS-derived metabolite levels of AAG metabolic pathway intermediates in MDMs (**blue**), monocytes (**pink**) and 1,25D$_3$-supplemented monocytes (**orange**). Significance was determined by Welch's two-sample t-Test between monocytes and MDMs, and control and 1,25D$_3$-supplemented monocytes (* $p < 0.050$, ** $p < 0.010$, *** $p < 0.001$) (n=3).

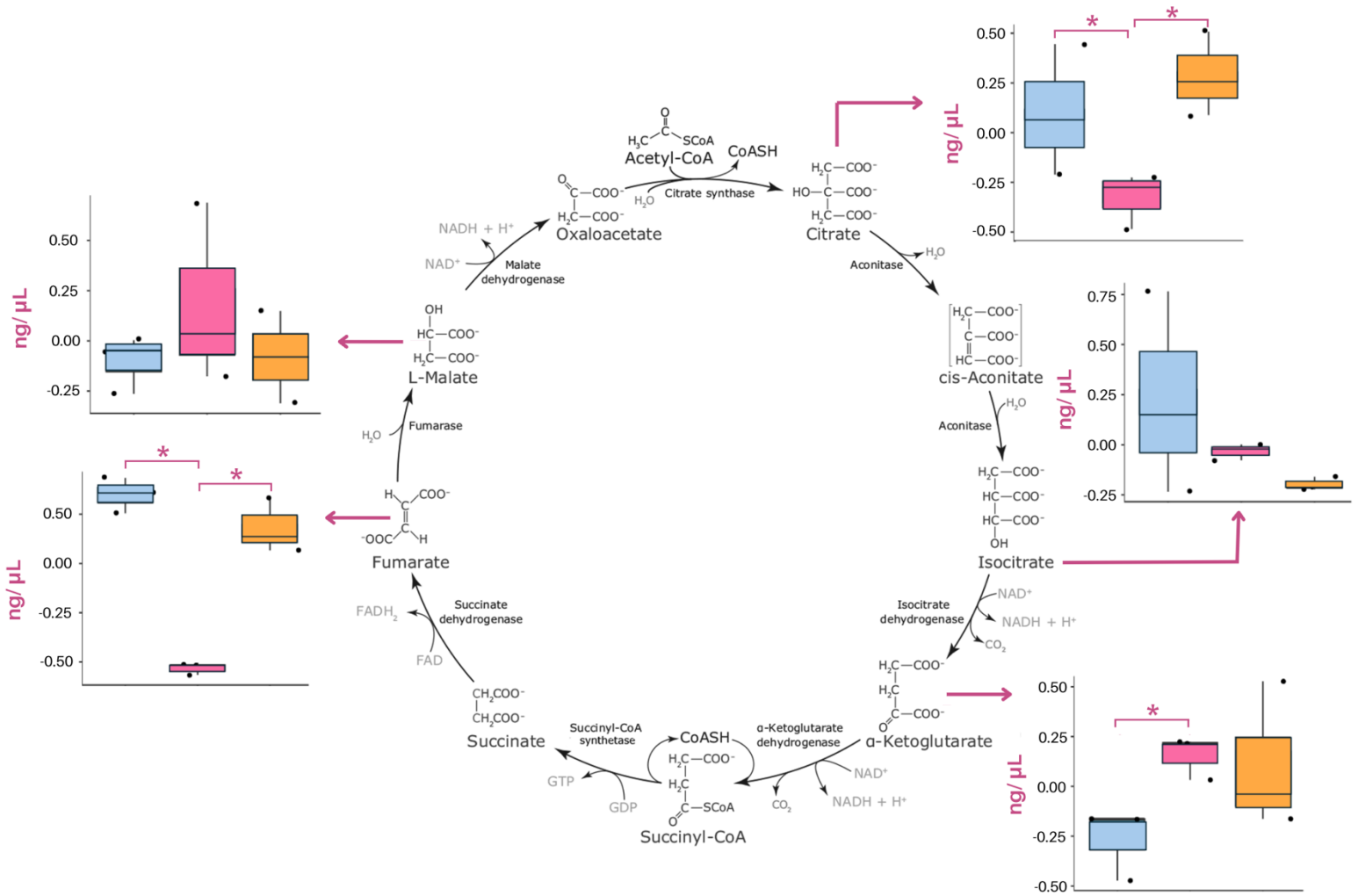

Figure 3.12. Alterations in TCA Cycle intermediates across the metabolomic profiles of monocytes, MDMs, and 1,25D$_3$-supplemented monocytes. The boxplots display GC×GC-TOFMS-derived metabolite levels of TCA cycle intermediates at 4 hrs in MDMs (**blue**), monocytes (**pink**) and 1,25D$_3$-supplemented monocytes (**orange**). Significance was determined by Welch's two-sample t-Test between monocytes and MDMs, and control and 1,25D$_3$-supplemented monocytes (* $p < 0.050$, ** $p < 0.010$, *** $p < 0.001$) (n=3).

3.8. 1,25D_3 modulates mRNA expression of inflammatory markers in both monocytes and MDMs in the presence and absence of a simulated pathogenic infection

To assess whether the metabolic changes induced by 1,25D_3 in monocytes correlate with enhanced functional capabilities, monocytes and MDMs were first supplemented with 1,25D_3 for 4 hrs. Changes in gene expression of the inflammatory markers *IL-1β*, *CCL2*, and *CXCL10* were then quantified by RT-qPCR. Thereafter, monocytes and MDMs, with and without 1,25D_3 supplementation, were exposed to a TLR8 agonist for 4 hrs, and the gene expression of the same inflammatory markers were quantified.

3.8.1 RT-qPCR quality control assessment

i. Quality of RNA extracts

Prior to cDNA synthesis, RNA extracts were tested to ensure they were of high purity and integrity. Using a NanoDrop Microvolume Spectrophotometer, the extracted RNA was quantified and assessed for DNA, protein, polysaccharide, RNase, salt, and/or organic solvent contamination. The results indicated that, on average, RNA extracts had a 260/280 and 260/230 absorbance ratio of 2.01 (range: 1.98–2.05) and 2.17 (range: 1.72–2.19), respectively. As another quality control step, agarose gel electrophoresis was used to confirm the integrity of the extracted RNA (Fig. 3.13). The RNA extracts were confirmed to be of high integrity due to minimal band smearing and be consistently intact indicated the presence of two distinct bands, which represent the ribosomal RNA subunits.

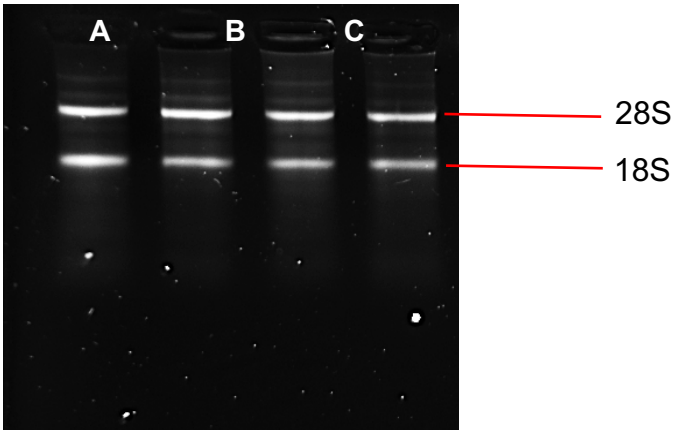

Figure 3.13. Confirmation of high integrity RNA extractions using agarose gel electrophoresis. The representative image displays bands indicating the 28S and 18S subunits of ribosomal RNA, which was extracted from monocytes following the respective treatments: control (**A**), 1,25D_3 (**B**), motolimod (TLR8 agonist) (**C**), motolimod + 1,25D_3 (**D**) on a 1.5% (w/v) agarose gel.

ii. Primers pairs were specific in targeting a single amplicon using RT-qPCR

Prior to RT-qPCR analysis, both primer specificity and efficacy were assessed. Melt-curve analysis of each target gene was done to ensure that only one product was specifically amplified in the absence of primer dimers, using the Bio-Rad CFX Maestro software (Fig. 3.14A). It was confirmed that each amplicon generated a unique peak above the threshold line on its melt curve, signifying the amplification of a single product. Furthermore, agarose gel electrophoresis was used to confirm amplicon size and absence of primer dimers (Fig. 3.14B). The observed RT-qPCR amplicon sizes corresponded to the predicted *in silico* product sizes (Chapter 2, Table 2.2). Additionally, a single solid band was visualised per target gene, confirming the absence of non-specific binding and primer dimers.

A

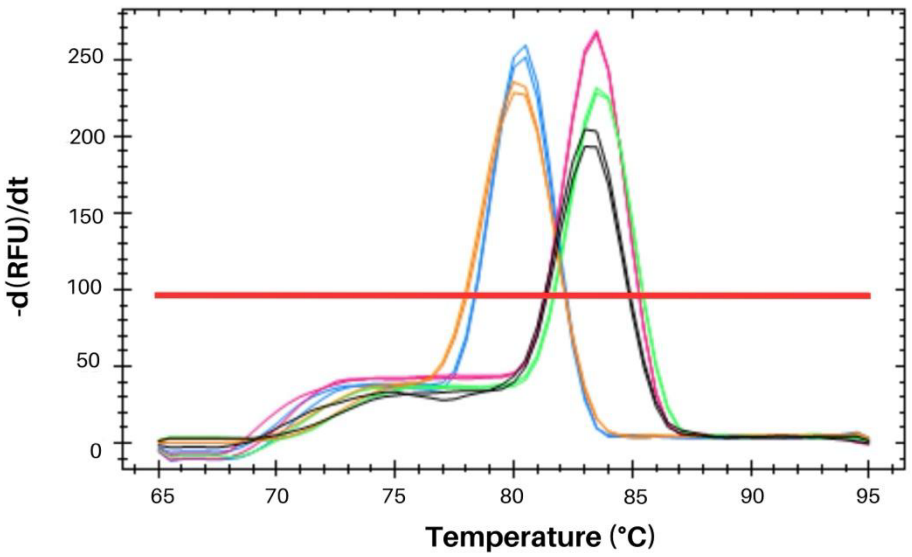

B

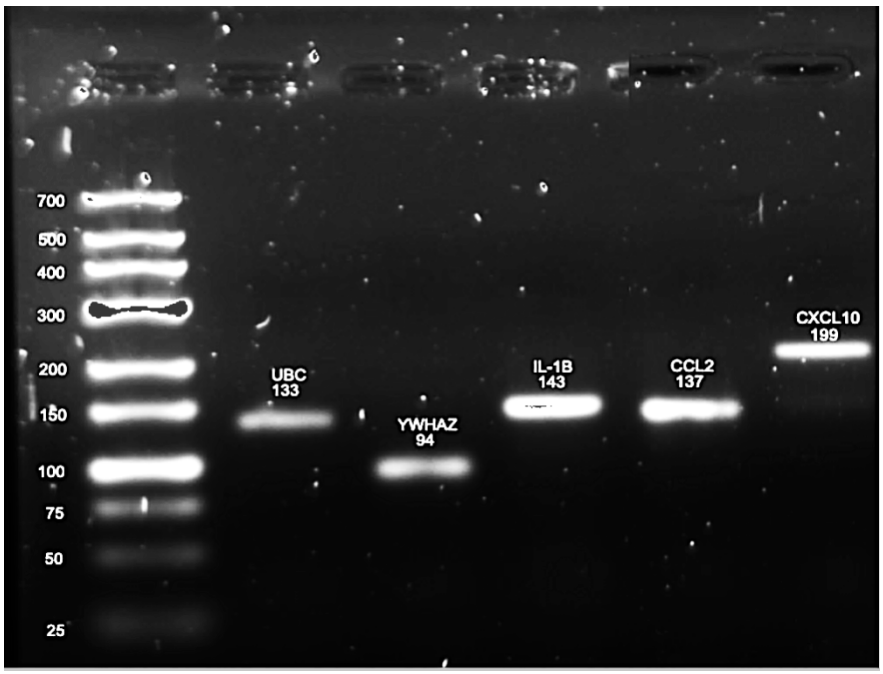

Figure 3.14. Single melt peaks and gel products are indicative of primer specificity for RT-qPCR. Each melt curve represents the change in relative fluorescence units over time (-d(RFU)/dT) against temperature (°C) (**A**). Single peaks in the melt curves were shown for the reference genes *UBC* (**black**) and *YWHAZ* (**orange**), as well as for the target genes, *IL-1β* (**green**), *CCL2* (**pink**) and *CXCL10* (**blue**). The representative gel electrophoresis image (**B**) displays each of the primer-pair products as a single band at the expected base pair (bp) size on a 3% (w/v) agarose gel.

3.8.2 *In vitro* 1,25D_3 supplementation for 4 hrs modulates mRNA expression of inflammatory markers in both monocytes and MDMs

In the absence of stimulation, *in vitro* 1,25D_3 supplementation modulated the expression of selected inflammatory genes in both monocytes and MDMs (Fig. 3.15). The variability observed between technical replicates is likely attributable to minor pipetting inconsistencies and variation in cDNA synthesis efficiency. Each biological sample was analysed in duplicate, and only technical replicates with consistent melt curves and Cq values were included in the final analysis. Despite this variability, gene expression patterns remained consistent across biological replicates, and the observed trends were statistically significant. One-way ANOVA revealed significant overall differences in *IL-1β* ([$p < 0.010$]; Fig. 3.15A), *CCL2* ([$p < 0.010$]; Fig. 3.15B), and *CXCL10* ([$p < 0.010$]; Fig. 3.15C) expression in monocytes and MDMs. Pairwise comparisons identified several significant alterations. 1,25D_3 supplementation did not significantly alter *IL-1β* expression in either monocytes or MDMs compared to their respective controls ([$p > 0.050$]; Fig. 3.15A). However, 1,25D_3 supplementation did significantly influenced the expression of *CCL2* and *CXCL10* in both monocytes and MDMs (Figs. 3.15B&C). *CCL2* expression was significantly increased in1,25D_3 supplemented monocytes ($p < 0.050$) but decreased in 1,25D_3 supplemented MDMs ($p < 0.050$) relative to their respective controls (Fig. 3.15B). Similarly, *CXCL10* expression was significantly increased in monocytes ($p < 0.010$) and decreased in MDMs ($p < 0.050$) following 1,25D_3 supplementation (Fig. 3.15C). Additionally, under control conditions, monocytes exhibited significantly lower expression levels of *IL-1β* ($p < 0.050$), *CCL2* ($p < 0.050$), and *CXCL10* ($p < 0.050$) compared to MDMs. However, 1,25D_3 supplementation increased *IL-1β* and *CCL2* expression in monocytes to levels comparable to those in MDMs, eliminating the previously observed difference ($p > 0.050$).

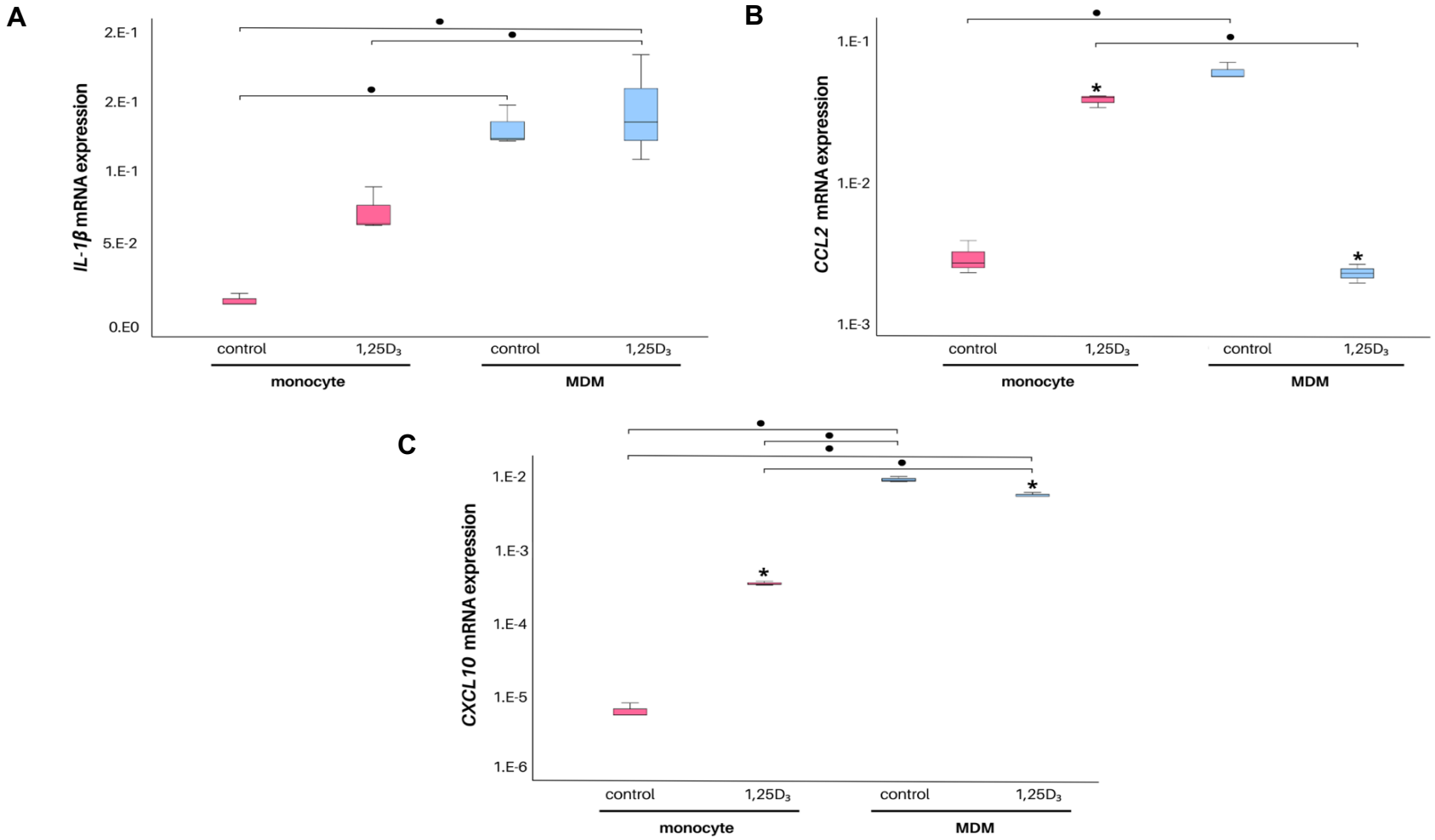

Figure 3.15. Effect of *in vitro* 1,25D$_3$ supplementation on gene expression levels of inflammatory markers in monocytes and MDMs. The boxplots display mRNA expression of *IL-1B* (**A**), *CCL2* (**B**) and *CXCL10* (**C**) in response to 4 hrs of *in vitro* 1,25D$_3$ supplementation in monocytes and MDMs. Overall significance was determined using one-way ANOVA. Pairwise comparisons were performed using Bonferroni post hoc tests for *IL-1β* (**A**) and Tamhane post hoc tests for *CCL2* (**B**) and *CXCL10* (**C**) (* $p < 0.050$, ** $p < 0.010$, *** $p < 0.001$). Black stars (*) indicate differences relative to the control. Error bars represent ± 1 SD (n=3).

3.8.3 In the presence of TLR8 stimulation, *in vitro* $1,25D_3$ supplementation modulates cytokine and chemokine gene expression in monocytes and MDMs at 4 hrs

After assessing the effects of $1,25D_3$ supplementation alone, the next step was to determine how the expression of specific inflammatory markers changed when monocytes and MDMs were exposed to a simulated pathogenic challenge via TLR8 stimulation, both in the presence and absence of $1,25D_3$ (Fig. 3.16). To investigate this, RT-qPCR analysis was performed following 4 hrs of treatment. One-way ANOVA revealed significant overall effects from the different treatments on the expression of *IL-1β* ([$p < 0.001$]; Fig. 3.16A), *CCL2* ([$p < 0.001$]; Fig. 3.16B), and *CXCL10* ([$p < 0.001$]; Fig. 3.16C) in both monocytes and MDMs. Pairwise comparisons showed that motolimod alone significantly increased the expression of only *CXCL10* in monocytes compared to the respective control ([$p < 0.050$]; Fig. 3.16C), while no significant changes were observed for *IL-1β* (Fig. 3.16A) or *CCL2* (Fig. 3.16B). In contrast, in MDMs, motolimod alone significantly upregulated the expression *IL-1β* ([$p < 0.050$]; Fig. 3.16A), *CCL2* ([$p < 0.050$]; Fig. 3.16B), and *CXCL10* ([$p < 0.050$]; Fig. 3.16C) compared to the controls. When $1,25D_3$ was combined with motolimod, monocytes exhibited significant increases in *IL-1β* ([$p < 0.050$]; Fig. 3.16A), *CCL2* ([$p < 0.050$]; Fig. 3.16B), and *CXCL10* ([$p < 0.050$]; Fig. 3.16C) expression relative to the respective controls. Furthermore, the combination of $1,25D_3$ and motolimod in monocytes significantly increased the expression of *IL-1β* ([$p < 0.050$]; Fig. 3.16A) and *CCL2* ([$p < 0.050$]; Fig. 3.16B) as compared to motolimod alone. Conversely, in MDMs, the addition of $1,25D_3$ to motolimod treatment significantly reduced *IL-1β* ([$p < 0.050$]; Fig. 3.16A) and *CCL2* ([$p < 0.050$]; Fig. 3.16B) expression compared to motolimod alone. However, no significant changes were observed for *CXCL10* expression in MDMs following $1,25D_3$ co-treatment ([$p > 0.050$]; Fig. 3.16C).

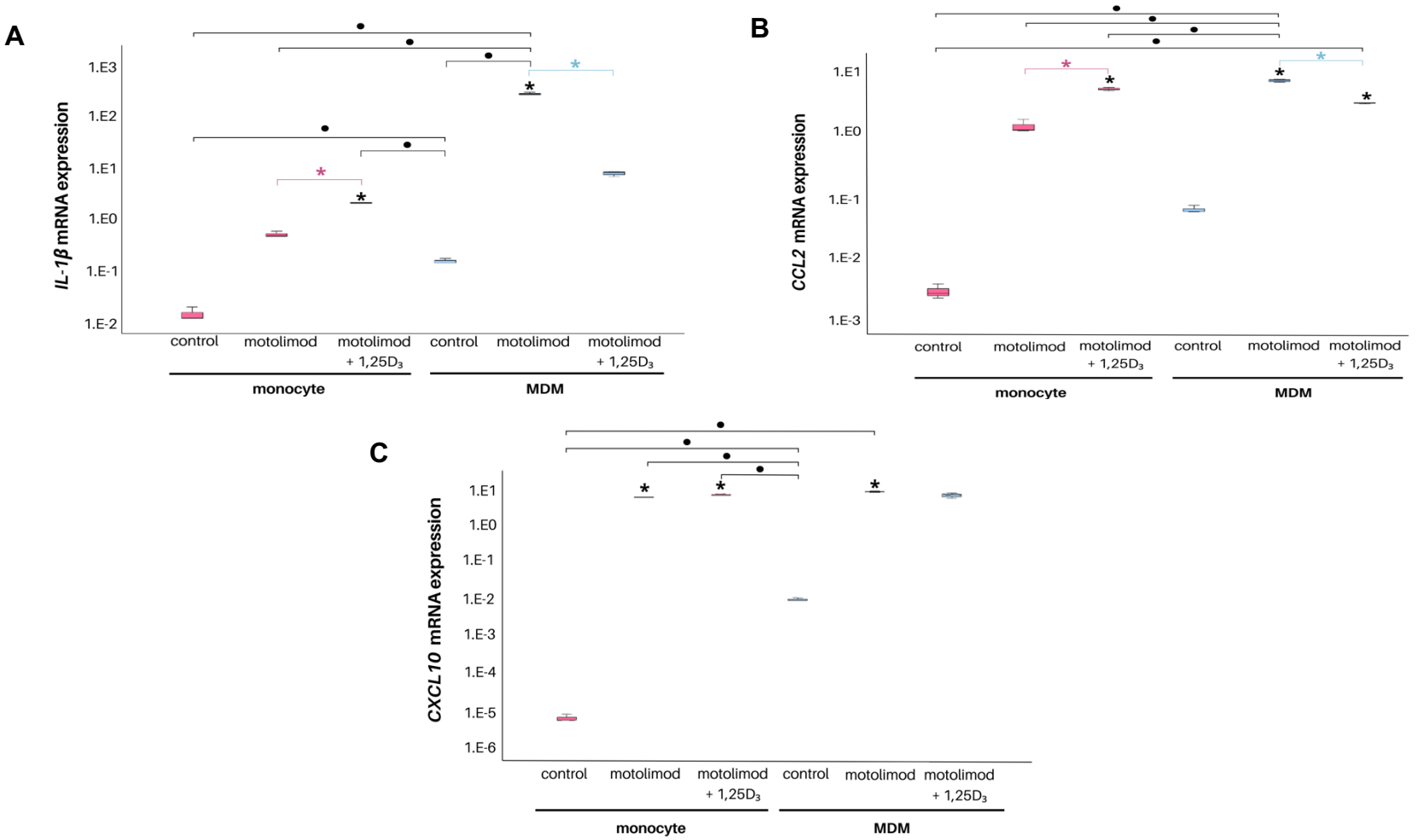

Figure 3.16. Impact of *in vitro* 1,25D$_3$ supplementation on gene expression levels of inflammatory markers in monocytes and MDMs upon TLR8 stimulation. The boxplots display mRNA expression of *IL-1β* (**A**), *CCL2* (**B**)and *CXCL10* (**C**) in response to stimulation with motolimod (a TLR8 agonist) in the presence and absence of *in vitro* 1,25D$_3$ supplementation for 4 hrs in monocytes (pink) and MDMs (blue). Overall significance was determined using one-way ANOVA. Pairwise comparisons were performed using Tamhane post hoc ($^{\bullet}$ $p < 0.050$, $^{\bullet\bullet}$ $p < 0.010$, $^{\bullet\bullet\bullet}$ $p < 0.001$). Black stars (*) indicate differences relative to the control and pink (*) and blue (*) stars represented intra-cell type differences in monocytes and MDMs respectively. Error bars represent ± 1 SD (n=3)

Chapter 4: Discussion and conclusion

This study aimed to characterise the distinct metabolic profiles of monocytes and MDMs, and to investigate how acute *in vitro* $1,25D_3$ supplementation modulates these profiles, providing insights into its potential to enhance immune function. The results obtained showed that acute $1,25D_3$ supplementation induces metabolic and functional reprogramming in monocytes, priming them for enhanced immune responses by modulating inflammatory gene expression and metabolite profiles, while having minimal effects on already differentiated MDMs.

To establish MDMs, monocytes were differentiated, and their morphological changes were monitored using light microscopy. Distinct cellular transformations indicative of successful differentiation was observed. Initially, monocytes exhibited a spherical morphology with a singular nucleus (Fig. 3.1A). Following treatment, they adopted a predominantly flattened, elongated, spindle-like, or irregular shape with an increased surface area (Fig. 3.1B). These morphological changes align with previous studies by Lee *et al*. (2012) and Baxter *et al*. (2020), albeit with the use of differing PMA-induced THP-1 differentiation protocols. Furthermore, while light microscopy provides rapid visual assessment for differentiation, it does not confirm functional maturation at the molecular level. Mol *et al*. (2024) have addressed these limitations by validating the effectiveness of this protocol using transcriptomics, cytokine secretion profiling and flow cytometry.

Monocytes and MDMs are different mononuclear phagocytes, each contributing uniquely to immune functions (Italiani and Boraschi, 2014; Stunault *et al*., 2021; Dash *et al*., 2024). Therefore, it is not surprising that the PCA plot indicated distinct ellipsoidal clustering between the two groups with regards to their metabolic profiles under homeostatic conditions (Fig. 3.4). Furthermore, $1,25D_3$ supplementation induced a shift in the metabolic profile of monocytes but had minimal impact on the metabolic profile of MDMs. Interestingly, the $1,25D_3$-supplemented monocyte group was seen to cluster closer to the MDM group, suggesting an overlap in metabolic characteristics following $1,25D_3$ exposure. These findings suggest that the metabolic shifts induced by acute *in vitro* $1,25D_3$ supplementation are specific to monocytes. One possibility is that, as a fully differentiated phenotype, MDMs exist at a functional plateau, rendering them less sensitive to $1,25D_3$. However, this is unlikely as

Cervantes *et al*. (2019), Small *et al*. (2021) and, Fernandez *et al*. (2022) among others have demonstrated that 1,25D_3 modulates MDM function to improve pathogen elimination and promote tissue homeostasis. Instead, this minimal impact may be due to experimental factors, such as the chosen supplementation period.

Additionally, several studies have reported that beyond its role in differentiation, 1,25D_3 enhances monocyte function (Djukic *et al*., 2015; Siddiqui *et al*., 2020). For instance, Edfeldt *et al*. (2010) reported that autophagy, which is process essential for phagosome maturation, was significantly increased in primary human monocytes treated with 10 nM 1,25D_3 for 18 h. A study conducted by Liu *et al*. (2006) found that 1,25D_3 upregulates the production of the cathelicidin in human monocytes controlling the proliferation of *Mycobacterium tuberculosis*. Furthermore, Tokuda and Levy (1996) reported that 1,25D_3 markedly upregulated phagocytic activity of monocytes, further supporting its role in immune defence. Considering these findings and the PCA analysis from this study, it may be suggested that acute 1,25D_3 supplementation facilitates functional "priming" of monocytes, shifting them toward a more MDM-like metabolic phenotype.

To further elucidate the key metabolic drivers of these shifts, OPLS-DA was performed to identify specific metabolites contributing to the observed separations (Fig 3.5). Fifteen discriminatory metabolites were identified for each comparison, and based on univariate criteria, were further shortlisted (Fig 3.6; Tables 3.1 and 3.2). Elevated fumaratelevels highlighted a significant metabolic event for discriminating monocytes from MDMs and were seen to similarly elevated in 1,25D_3-supplemented monocytes. The large effect size of fumarateobserved in both MDMs (Cohen's d = 14.730, $p < 0.050$) and 1,25D_3-supplemented monocytes (Cohen's d = 7.26, $p < 0.050$) underscores its role as a hallmark of monocyte differentiation and 1,25D_3 driven metabolic reprogramming. In support, Hooftman *et al*. (2023) reported that elevated fumaratelevels in bone-marrow-derived macrophages (BMDM) stimulated with lipopolysaccharide (LPS) for 4 hrs is driven by the aspartate–argininosuccinate shunt. Under homeostatic conditions, the present analysis also identified the aspartate–argininosuccinate shunt as the source of elevated fumaratelevels in both MDMs and 1,25D_3-supplemented monocytes (Fig 3.11). Furthermore, Martínez-Reyes and Chandel (2020), Wang *et al*. (2021) and Hooftman *et al*. (2023) have reported that fumarate controls type I IFN release, however the exact mechanism governing this

regulation remains unclear. Therefore, it may be postulated that the elevated fumaratelevels in 1,25D_3-supplemented monocytes is likely to modulate type I IFN release, functionally priming monocytes for enhanced pathogenic or inflammatory response (Lee and Ashkar, 2018). This may assist in adjusting immune responses to ensure robust and efficient pathogen defence, whilst preventing overactive responses that may cause tissue damage or chronic inflammation.

Given that fumarate is a key intermediate of the TCA cycle, its elevated levels in both MDMs and 1,25D_3-supplemented monocytes suggest broader metabolic adaptations beyond the aspartate–argininosuccinate shunt. This is further supported by the significant increase in both fumarate and citrate levels in MDMs and 1,25D_3-supplemented monocytes compared to control monocytes, indicating a shift in TCA cycle activity (Fig. 3.12). Citrate may indirectly contribute to histone acetylation through its conversion to acetyl-CoA, highlighting a potential epigenetic mechanism that regulates inflammatory gene transcription and immune responses (Jo *et al*., 2020; Li *et al*., 2022). Additionally, higher glucose levels observed in both macrophages and 1,25D_3-supplemented monocytes likely contribute to elevated citrate levels (Fig 3.8). Increased glucose metabolism enhances glycolytic flux, providing more pyruvate for the TCA cycle, which in turn leads to higher citrate production (Williams and O'Neill, 2018). Therefore, this metabolic shift in citrate not only supports mitochondrial energy production but also primes monocytes for more effective immune activation. Moreover, the simultaneous increase in methionine levels in 1,25D_3-supplemented monocytes (Fig 3.9) suggest additional epigenetic modifications through DNA methylation, which is critical in regulating gene expression of inflammatory markers and immune cell activation (Moore *et al*., 2018; Ji *et al*., 2019; Zhang *et al*., 2022). Collectively, acute 1,25D_3 supplementation induces metabolic reprogramming that likely primes monocytes for more robust immune responses by adapting their epigenetic landscape, enhancing both immediate activation and the potential for long-term immune memory. The elevated levels of fumarate, citrate, and methionine suggest a broader metabolic shift that supports immune functionality and likely contributes to the induction of trained immunity in monocytes.

Although pathway analysis initially suggested minimal contribution form the fatty acid biosynthesis pathway to the overall metabolic changes, further analysis revealed significant modulations (Fig. 3.10). Monocytes exhibited significantly higher levels of

myristic acid, lauric acid, and caprylic acid compared to MDMs. This corresponds with the research by Ecker *et al*. (2010), which highlighted the importance of fatty acid biosynthesis in monocytes for MDM generation. The fatty acid biosynthesis pathway is fundamental for promoting the development of key cellular structures and functions including membrane fluidity and enhanced phagocytic capacity, which are essential for MDMs biology. Notably, $1,25D_3$ supplementation drove a shift in the lipid profiles, significantly reducing the levels of myristic and palmitic acids in monocytes, making their lipid composition similar to MDMs. This metabolic remodelling underscores the broader influence of $1,25D_3$, not only in energy metabolism but also in lipid remodelling, which is crucial for macrophage differentiation and functional polarization. Collectively, acute $1,25D_3$ supplementation in monocytes induces complex metabolic and epigenetic reprogramming under homeostatic conditions, priming them for enhanced immune responses and potentially inducing trained immunity.

Gene expression analysis was used to assess whether the metabolic shifts observed in monocytes, $1,25D_3$ supplemented monocytes, and MDMs were reflected at the mRNA level. Due to its expression in both monocytes and MDMs, *IL-1β*, *CCL2*, and *CXCL10* were quantified (Vestergaard *et al*., 2004; Lopez-Castejon and Brough, 2011; Zhao *et al*., 2017). Supplementation with only $1,25D_3$ for 4 hrs exhibited distinct regulatory effects on the expression of *CCL2* and *CXCL10* under homeostatic conditions (Figs 3.15B&C). Specifically, $1,25D_3$ supplementation significantly increased *CCL2* and *CXCL10* expression in monocytes whilst significantly decreasing their expression in MDMs – highlighting potential cell type specific effects. Interestingly, these findings contrast previous studies which have reported that $1,25D_3$ has an exclusive inhibitory effect on the expression of proinflammatory chemokines in both monocytes and MDMs (Karkeni *et al*., 2015; Kraus *et al*., 2018; Alcalá-Santiago *et al*., 2024). This discrepancy highlights the influence of experimental context, suggesting that acute $1,25D_3$ supplementation under homeostatic conditions engages distinct inflammatory regulatory mechanisms as compared to prolonged or stimulated treatments. Further to its inflammatory role, *CCL2* and *CXCL10* are instrumental in recruiting other immune cells to sites of infection (Jin *et al*., 2021; Elemam *et al*., 2022; Lin *et al*., 2023). Therefore, by upregulating the expression levels of *CCL2* and *CXCL10* under homeostatic conditions, $1,25D_3$ is priming monocytes for a rapid and heightened immune response prior to infection. These findings in conjunction with

those of Valdés-López *et al*. (2022), challenge the idea that $1,25D_3$ is a purely anti-inflammatory molecule. Valdés-López *et al*. (2022) reported a similar effect at 6 h whereby $1,25D_3$ upregulated the expression of proinflammatory cytokines such as *IL-1β* in Chikungunya virus-infected monocytes. However, in this study, *IL-1β* mRNA expression was not significantly altered in either cell type following $1,25D_3$ supplementation (Fig 3.15A). This suggests that while $1,25D_3$ increases *IL-1β* expression under infectious conditions, it does not influence early *IL-1β* induction under homeostatic conditions (Valdés-López *et al*., 2022).

Therefore, these findings suggest that acute $1,25D_3$ supplementation for 4 hrs primes monocytes by significantly increasing chemokine expression, potentially preparing them for a more effective immune response, whilst not significantly altering *IL-1β* expression under homeostatic conditions. To further explore this, TLR8 was stimulated to mimic a pathogenic infection and assess how $1,25D_3$ influences the regulation of these proinflammatory mediators under inflammatory conditions. The typical concentration of motolimod used for immune cell activation ranges from 0.1 μM to 0.5 μM (Lu *et al*., 2012; Cheng *et al*., 2021). However, considering that this study primarily aimed to investigate acute immune activation at 4 hrs, a higher concentration of motolimod (5 μM) was used to ensure adequate immune cell activation. Furthermore, Dietsch *et al*. (2016) demonstrated that concentrations of up to 10 μM of motolimod were well tolerated in immune cells. This approach effectively induced short-term immune activation whilst maintaining cell viability, providing reliable conditions to mimic a pathogenic stimulus. Following TLR8 activation *IL-1β* expression increased in both monocytes and MDMs (Fig 3.16A). This is not surprising as *IL-1β* is among the first inflammasome-activated cytokines triggered during the innate immune defence (Sahoo *et al*., 2011; Jamilloux and Henry, 2013). Consistent with Valdés-López *et al*. (2022), acute $1,25D_3$ supplementation significantly increased *IL-1β* expression in TLR8 activated monocytes, supporting the hypothesis that while $1,25D_3$ does not influence *IL-1β* induction under homeostatic conditions, it enhances its expression in an inflammatory environment. These findings further highlight the context-dependent effects of $1,25D_3$ on *IL-1β* regulation. Furthermore, while $1,25D_3$ supplementation significantly decreased *IL-1β* expression in TLR8-activated MDMs (Fig 3.16A), Chen *et al*. (2017) reported that 100 nM 1,25D3 supplementation for 24 hrs significantly increased *IL-1β* in LPS-infected macrophages but significantly decreased their

phagocytic capacity. This contrast suggests that acute, low-dose $1,25D_3$ supplementation may assist MDMs maintain phagocytic abilities whilst helping regulate excessive cytokine production thereby potentially mitigating inflammatory damage (Dhawan *et al*., 2022).

Notably, TLR8 activation also led to increased *CCL2* and *CXCL10* expression in both monocytes and MDMs ([Figs 3.16B&C]; Majumdar and Murphy, 2021). Again, this is expected as both *CCL2* and *CXCL10* play essential roles in inflammatory responses and immune cell recruitment (Song *et al*., 2021). As observed under homeostatic conditions, $1,25D_3$ supplementation further upregulated *CCL2* and *CXCL10* expression in TLR8-activated monocytes. However, in MDMs $1,25D_3$ supplementation selectively decreased *CCL2* expression but did not affect *CXCL10* levels. By modulating *CCL2* expression, $1,25D_3$ supplementation is actively enhancing the immune response in monocytes, whilst limiting excessive immune cell recruitment and reducing the overall inflammatory response through MDMs. Furthermore, the preservation of *CXCL10* expression in MDMs further highlights the context-dependent nature of $1,25D_3$. This suggests that $1,25D_3$ regulates the innate immune response through modulating CCL2, while allowing the adaptive immune response to proceed unaffectedly via the increase and maintenance of *CXCL10* expression in monocytes and MDMs, respectively (Antonia *et al*., 2019).

Therefore, these findings highlight the complexities and challenge the existing knowledge regarding the immunoregulatory role of $1,25D_3$ in both the innate and adaptive responses at the mRNA level. Specifically, the normalisation of the inflammatory profile in monocytes suggests that $1,25D_3$ prepares these cells for future immune challenges, while the distinct responses observed in monocytes versus MDMs highlight how cellular differentiation influences VDR expression and downstream signalling (Martens *et al*., 2020). This variability may be driven by epigenetic modifications or differential transcriptional control, underscoring the need for further mechanistic studies. Ultimately, these findings contribute to a more refined understanding of the immunomodulatory role of $1,25D_3$.

Based on these findings, this study suggests that acute *in vitro* supplementation of 10 nM $1,25D_3$ induced significant metabolic reprogramming in monocytes, pushing them closer to a MDM-like phenotype. This was evidenced by morphological changes and

metabolomic shifts, with specific elevation of metabolites like fumarate, citrate, and methionine, which are indicative of enhanced immune activation. The observed elevation of citrate and methionine levels, in particular, suggests an epigenetic regulatory mechanism that primes monocytes for more robust immune responses. Notably, these metabolic shifts were supported by gene expression analysis, where $1,25D_3$ supplementation induced distinct regulatory effects on inflammatory gene expression in monocytes and MDMs, with a tendency to enhance immune activation in monocytes while attenuating inflammation in macrophages, particularly in the presence of TLR8 stimulation. These findings indicate that $1,25D_3$ supplementation not only reprograms the metabolism of monocytes but also enhances their immune functionality, likely contributing to the induction of trained immunity. The study emphasises the role of $1,25D_3$ in priming monocytes for an enhanced immune response, potentially offering insights into its therapeutic applications in immune modulation.

Limitations and future perspectives

When interpreting these findings, it is important to consider the limitations of this study. The use of an *in vitro* model with isolated THP-1 monocytes and MDMs does not fully capture the complexity of immune responses within a whole organism, as interactions with other cell types and tissues are excluded. *In vivo* studies are necessary to confirm the physiological relevance of these findings.

Additionally, the study assessed the effects of $1,25D_3$ at a single time point (4 hrs), limiting insights into the temporal dynamics of immune and metabolic responses. Flux studies or extended treatment durations would provide a clearer understanding of how these responses evolve over time and whether MDM responses to $1,25D_3$ are delayed or dose-dependent. The differential responses observed between monocytes and MDMs suggest that $1,25D_3$ exerts context-dependent immunomodulatory effects—enhancing immune readiness in monocytes while moderating excessive inflammation in macrophages. These findings have therapeutic implications, suggesting that $1,25D_3$ supplementation could be strategically utilised to regulate immune responses during infection or inflammation. Future studies should focus on elucidating the molecular pathways responsible for these varying effects, with a particular emphasis on VDR signalling and its associated transcriptional regulators.

Furthermore, only intracellular metabolites were analysed, limiting insights into extracellular metabolic interactions. Since immune cells secrete metabolites that influence their microenvironment and intercellular communication, the lack of extracellular metabolomic profiling restricts a full understanding of $1,25D_3$-induced metabolic crosstalk. Future studies should integrate both intracellular and extracellular metabolomics for a more comprehensive perspective on immune cell metabolism. Additionally, while scyllo-inositol was significantly altered in MDMs, its role in monocyte differentiation remains unclear, warranting further investigation into its functional significance. Given the observed increase in fumarate levels following $1,25D_3$ supplementation, future studies could explore whether this metabolic shift reflects underlying mitochondrial dysfunction. Since mitochondria play a critical role in regulating monocyte function during immune responses to treatment, inflammation, injury, and infection, investigating the impact of 10 nM $1,25D_3$ on mitochondrial

integrity and energy production via the TCA cycle may provide deeper mechanistic insights.

The study relied exclusively on GC×GC/TOF-MS for metabolomic analysis, which, despite its high-resolution capabilities, primarily detects volatile and semi-volatile compounds. This limits coverage of non-volatile metabolites, such as certain amino acids, nucleotides, and lipids. Incorporating complementary methodologies like liquid chromatography-mass spectrometry (LC-MS) would enable a more comprehensive characterisation of 1,25D_3-induced metabolic changes in monocytes and MDMs. Targeted metabolomics of key metabolic regulators (e.g. fumarate) could provide deeper mechanistic insights.

While the observed metabolic reprogramming does not necessarily equate to full differentiation, additional functional assays are needed to establish whether these metabolic shifts in monocytes enhance MDM-like activities, such as phagocytosis, cytokine secretion, or antimicrobial response.

References

Adams, J.S., Rafison, B., Witzel, S., Reyes, R.E., Shieh, A., Chun, R., Zavala, K., Hewison, M. and Liu, P.T., 2014. Regulation of the extrarenal CYP27B1-hydroxylase. The Journal of steroid biochemistry and molecular biology, 144, pp.22-27. DOI: 10.1016/j.jsbmb.2013.12.009

Alberts, B., Johnson, A., Lewis, J., Raff, M., Roberts, K. and Walter, P., 2002. Programmed cell death (apoptosis). In Molecular Biology of the Cell. 4th edition. Garland Science. Available from: https://www.ncbi.nlm.nih.gov/books/NBK26873/

Alcalá-Santiago, Á., Toscano-Sánchez, R., Márquez-López, J.C., González-Jurado, J.A., Fernández-Pachón, M.S., García-Villanova, B., Pedroche, J. and Rodríguez-Martín, N.M., 2024. The Synergic Immunomodulatory Effect of Vitamin D and Chickpea Protein Hydrolysate in THP-1 Cells: An In Vitro Approach. International journal of molecular sciences, 25(23), p.12628. DOI: 10.3390/ijms252312628

Ammarah, U., Pereira-Nunes, A., Delfini, M. and Mazzone, M., 2024. From monocyte-derived macrophages to resident macrophages—how metabolism leads their way in cancer. *Molecular Oncology*, *18*(7), pp.1739-1758. DOI: 10.1002/1878-0261.13618

Antonia, A.L., Gibbs, K.D., Trahair, E.D., Pittman, K.J., Martin, A.T., Schott, B.H., Smith, J.S., Rajagopal, S., Thompson, J.W., Reinhardt, R.L. and Ko, D.C., 2019. Pathogen evasion of chemokine response through suppression of CXCL10. Frontiers in cellular and infection microbiology, 9, p.280. DOI: 10.3389/fcimb.2019.00280

Arababadi, M.K., Nosratabadi, R. and Asadikaram, G., 2018. Vitamin D and toll like receptors. Life sciences, 203, pp.105-111. DOI: 10.1016/j.lfs.2018.03.040

Arnold, P.K. and Finley, L.W., 2023. Regulation and function of the mammalian tricarboxylic acid cycle. Journal of Biological Chemistry, 299(2). DOI: 10.1016/j.jbc.2022.102838

Arts, R.J., Novakovic, B., Ter Horst, R., Carvalho, A., Bekkering, S., Lachmandas, E., Rodrigues, F., Silvestre, R., Cheng, S.C., Wang, S.Y. and Habibi, E., 2016. Glutaminolysis and fumarate accumulation integrate immunometabolic and epigenetic programs in trained immunity. Cell metabolism, 24(6), pp.807-819. DOI: 10.1016/j.cmet.2016.10.008

Barsony, J. and Prufer, K., 2002. Vitamin D receptor and retinoid X receptor interactions in motion. DOI: 10.1016/s0083-6729(02)65071-x

Baxter, E.W., Graham, A.E., Re, N.A., Carr, I.M., Robinson, J.I., Mackie, S.L. and Morgan, A.W., 2020. Standardized protocols for differentiation of THP-1 cells to macrophages with distinct M (IFNγ+ LPS), M (IL-4) and M (IL-10) phenotypes. Journal of immunological methods, 478, p.112721. DOI: 10.1016/j.jim.2019.112721

Becker, C., Hammerle-Fickinger, A., Riedmaier, I. and Pfaffl, M.W., 2010. mRNA and microRNA quality control for RT-qPCR analysis. Methods, 50(4), pp.237-243. DOI: 10.1016/j.ymeth.2010.01.010

Bellingan, G., 2000. Leukocytes: friend or foe. Intensive care medicine, 26(Suppl 1), pp.S111-S118. DOI: 10.1007/s001340051127

Beukes, D., Du Preez, I. and Loots, D.T., 2019. Total metabolome extraction from mycobacterial cells for GC-MS metabolomics analysis. Microbial Metabolomics: Methods and Protocols, pp.121-131. DOI: 10.1007/978-1-4939-8757-3_6

Bhol, N.K., Bhanjadeo, M.M., Singh, A.K., Dash, U.C., Ojha, R.R., Majhi, S., Duttaroy, A.K. and Jena, A.B., 2024. The interplay between cytokines, inflammation, and antioxidants: Mechanistic insights and therapeutic potentials of various antioxidants and anti-cytokine compounds. Biomedicine & Pharmacotherapy, 178, p.117177. DOI: 10.1016/j.biopha.2024.117177

Bikle, D.D., 2014. Vitamin D metabolism, mechanism of action, and clinical applications. Chemistry & biology, 21(3), pp.319-329. DOI: 10.1016/j.chembiol.2013.12.016

Borojević, A., Jauković, A., Kukolj, T., Mojsilović, S., Obradović, H., Trivanović, D., Živanović, M., Zečević, Ž., Simić, M., Gobeljić, B. and Vujić, D., 2022. Vitamin D3 stimulates proliferation capacity, expression of pluripotency markers, and osteogenesis of human bone marrow mesenchymal stromal/stem cells, partly through SIRT1 signaling. Biomolecules, 12(2), p.323. DOI: 10.3390/biom12020323

Bosshart, H. and Heinzelmann, M., 2016. THP-1 cells as a model for human monocytes. Annals of translational medicine, 4(21). DOI: 10.21037/atm.2016.08.53

Broadhurst, D., Goodacre, R., Reinke, S.N., Kuligowski, J., Wilson, I.D., Lewis, M.R. and Dunn, W.B., 2018. Guidelines and considerations for the use of system suitability and quality control samples in mass spectrometry assays applied in untargeted clinical metabolomic studies. Metabolomics, 14, pp.1-17. DOI: 10.1007/s11306-018-1367-3

Cannell, J.J., Grant, W.B. and Holick, M.F., 2014. Vitamin D and inflammation. Dermato-endocrinology, 6(1), p.e983401. DOI: 10.4161/19381980.2014.983401

Carlberg, C., 2023. Genomic signaling of vitamin D. Steroids, 198, p.109271. DOI: 10.1016/j.steroids.2023.109271

Ceglia, L., 2009. Vitamin D and its role in skeletal muscle. Current Opinion in Clinical Nutrition & Metabolic Care, 12(6), pp.628-633. DOI: 10.1097/MCO.0b013e328331c707

Cervantes, J.L., Oak, E., Garcia, J., Liu, H., Lorenzini, P.A., Batra, D., Chhabra, A., Salazar, J.C. and Roca, X., 2019. Vitamin D modulates human macrophage response to Mycobacterium tuberculosis DNA. Tuberculosis, 116, pp.S131-S137. DOI: 10.1016/j.tube.2019.04.021

Chen, L., Eapen, M.S. and Zosky, G.R., 2017. Vitamin D both facilitates and attenuates the cellular response to lipopolysaccharide. Scientific reports, 7(1), p.45172. DOI: 10.1038/srep45172

Cheng, Y., Borcherding, N., Ogunsakin, A., Lemke-Miltner, C.D., Gibson-Corley, K.N., Rajan, A., Choi, A.B., Wongpattaraworakul, W., Chan, C.H., Salem, A.K. and Weiner, G.J., 2021. The anti-tumor effects

of cetuximab in combination with VTX-2337 are T cell dependent. Scientific reports, 11(1), p.1535. DOI: 10.1038/s41598-020-80957-z

Chi, H., 2022. Immunometabolism at the intersection of metabolic signaling, cell fate, and systems immunology. Cellular & molecular immunology, 19(3), pp.299-302. DOI: 10.1038/s41423-022-00840-x

Clark, R. and Kupper, T., 2005. Old meets new: the interaction between innate and adaptive immunity. Journal of Investigative Dermatology, 125(4), pp.629-637. DOI: 10.1111/j.0022-202X.2005.23856.x

Coillard, A. and Segura, E., 2019. In vivo differentiation of human monocytes. Frontiers in immunology, 10, p.1907. DOI: 10.3389/fimmu.2019.01907

Dabrowski, P., Rasmus, M., Jundzill, A., Drewa, T. and Pokrywczynska, M., 2024. A comparison of five methods to maximize RNA and DNA isolation yield from adipose tissue. PeerJ, 12, p.e17071. DOI: 10.7717/peerj.17071

Dankers, W., Colin, E.M., Van Hamburg, J.P. and Lubberts, E., 2017. Vitamin D in autoimmunity: molecular mechanisms and therapeutic potential. Frontiers in immunology, 7, p.697. DOI: 10.3389/fimmu.2016.00697

Dash, S.P., Gupta, S. and Sarangi, P.P., 2024. Monocytes and macrophages: Origin, homing, differentiation, and functionality during inflammation. Heliyon, 10 (8), e29686. DOI:10.1016/j.heliyon.2024.e29686

Datta, I., Zahoor, I., Ata, N., Rashid, F., Cerghet, M., Rattan, R., Poisson, L.M. and Giri, S., 2024. Utility of an untargeted metabolomics approach using a 2D GC-GC-MS platform to distinguish relapsing and progressive multiple sclerosis. Metabolites, 14(9), p.493. DOI: 10.1101/2024.02.07.579252

Davies, L.C., Jenkins, S.J., Allen, J.E. and Taylor, P.R., 2013. Tissue-resident macrophages. Nature immunology, 14(10), pp.986-995. DOI: https://doi.org/10.1038/ni.2705

Dechamma, M.M., Rajeish, M., Maiti, B., Mani, M.K. and Karunasagar, I., 2015. Expression of Toll-like receptors (TLR), in lymphoid organ of black tiger shrimp (Penaeus monodon) in response to Vibrio harveyi infection. *Aquaculture Reports*, *1*, pp.1-4. DOI: https://doi.org/10.1016/j.aqrep.2015.02.002

Dhanapal, A.C.T.A. and Vimaleswaran, K.S., 2022. Vitamin D supplementation and immune-related markers: an update from nutrigenetic and nutrigenomic studies. British Journal of Nutrition, 128(8), pp.1459-1469. DOI: 10.1017/S000711452200366X

Dhawan, M., Priyanka and Choudhary, O.P., 2022. Immunomodulatory and therapeutic implications of vitamin D in the management of COVID-19. Human Vaccines & Immunotherapeutics, 18(1), p.2025734. DOI: 10.1080/21645515.2022.2025734

Dietsch, G.N., Lu, H., Yang, Y., Morishima, C., Chow, L.Q., Disis, M.L. and Hershberg, R.M., 2016. Coordinated activation of toll-like receptor8 (TLR8) and NLRP3 by the TLR8 agonist, VTX-2337, ignites tumoricidal natural killer cell activity. PloS one, 11(2), p.e0148764. DOI: 10.1371/journal.pone.0148764

Divangahi, M., Aaby, P., Khader, S.A., Barreiro, L.B., Bekkering, S., Chavakis, T., van Crevel, R., Curtis, N., DiNardo, A.R., Dominguez-Andres, J. and Duivenvoorden, R., 2021. Trained immunity, tolerance, priming and differentiation: distinct immunological processes. Nature immunology, 22(1), pp.2-6. DOI: 10.1038/s41590-020-00845-6

Djukic, M., Onken, M.L., Schütze, S., Redlich, S., Götz, A., Hanisch, U.K., Bertsch, T., Ribes, S., Hanenberg, A., Schneider, S. and Bollheimer, C., 2014. Vitamin D deficiency reduces the immune response, phagocytosis rate, and intracellular killing rate of microglial cells. Infection and immunity, 82(6), pp.2585-2594. DOI: 10.1128/IAI.01814-14

Djukic, M., Sostmann, N., Bertsch, T., Mecke, M., Nessler, S., Manig, A., Hanisch, U.K., Triebel, J., Bollheimer, L.C., Sieber, C. and Nau, R., 2015. Vitamin D deficiency decreases survival of bacterial meningoencephalitis in mice. Journal of Neuroinflammation, 12, pp.1-11. DOI: 10.1186/s12974-014-0208-1

Donati, S., Palmini, G., Aurilia, C., Falsetti, I., Miglietta, F., Iantomasi, T. and Brandi, M.L., 2022. Rapid nontranscriptional effects of calcifediol and calcitriol. Nutrients, 14(6), p.1291. DOI: 10.3390/nu14061291

Donati, S., Palmini, G., Romagnoli, C., Aurilia, C., Miglietta, F., Falsetti, I., Marini, F., Zonefrati, R., Galli, G., Marcucci, G. and Iantomasi, T., 2021. In vitro non-genomic effects of calcifediol on human preosteoblastic cells. Nutrients, 13(12), p.4227. DOI:10.3390/nu13124227

Duan, T., Du, Y., Xing, C., Wang, H.Y. and Wang, R.F., 2022. Toll-like receptor signaling and its role in cell-mediated immunity. Frontiers in immunology, 13, p.812774. DOI: 10.3389/fimmu.2022.812774

Ecker, J., Liebisch, G., Englmaier, M., Grandl, M., Robenek, H. and Schmitz, G., 2010. Induction of fatty acid synthesis is a key requirement for phagocytic differentiation of human monocytes. Proceedings of the National Academy of Sciences, 107(17), pp.7817-7822. DOI: 10.1073/pnas.0912059107

Edfeldt, K., Liu, P.T., Chun, R., Fabri, M., Schenk, M., Wheelwright, M., Keegan, C., Krutzik, S.R., Adams, J.S., Hewison, M. and Modlin, R.L., 2010. T-cell cytokines differentially control human monocyte antimicrobial responses by regulating vitamin D metabolism. Proceedings of the National Academy of Sciences, 107(52), pp.22593-22598. DOI: 10.1073/pnas.1011624108

Elemam, N.M., Talaat, I.M. and Maghazachi, A.A., 2022. CXCL10 chemokine: a critical player in RNA and DNA viral infections. Viruses, 14(11), p.2445. DOI: 10.3390/v14112445

Espinoza, V.E. and Emmady, P.D., 2023. Histology, monocytes. In: StatPearls [Internet]. Treasure Island (FL): StatPearls Publishing; 2025 Jan-. Available from: https://www.ncbi.nlm.nih.gov/books/NBK557618/

Eun, H.M., 1996. Enzymology primer for recombinant DNA technology. Elsevier. Available from: https://www.sciencedirect.com/book/9780122437403/enzymology-primer-for-recombinant-dna-technology

Fang, X.H., Li, Z.J., Liu, C.Y., Mor, G. and Liao, A.H., 2024. Macrophage memory: Types, mechanisms, and its role in health and disease. Immunology, 171(1), pp.18-30. DOI: 10.1111/imm.13697

Fang, Y., Li, Z., Yang, L., Li, W., Wang, Y., Kong, Z., Miao, J., Chen, Y., Bian, Y. and Zeng, L., 2024. Emerging roles of lactate in acute and chronic inflammation. Cell Communication and Signaling, 22(1), p.276. DOI: 10.1186/s12964-024-01624-8

Fanucchi, S., Domínguez-Andrés, J., Joosten, L.A., Netea, M.G. and Mhlanga, M.M., 2021. The intersection of epigenetics and metabolism in trained immunity. Immunity, 54(1), pp.32-43. DOI: 10.1016/j.immuni.2020.10.011

Fernandez, G.J., Ramírez-Mejía, J.M. and Urcuqui-Inchima, S., 2022. Vitamin D boosts immune response of macrophages through a regulatory network of microRNAs and mRNAs. The Journal of Nutritional Biochemistry, 109, p.109105. DOI: 10.1016/j.jnutbio.2022.109105

Ferreira, A.V., Alarcon-Barrera, J.C., Domínguez-Andrés, J., Bulut, Ö., Kilic, G., Debisarun, P.A., Röring, R.J., Özhan, H.N., Terschlüsen, E., Ziogas, A. and Kostidis, S., 2023. Fatty acid desaturation and lipoxygenase pathways support trained immunity. Nature Communications, 14(1), p.7385. DOI: 10.1038/s41467-023-43315-x

Ferreira, A.V., Domiguéz-Andrés, J. and Netea, M.G., 2022. The role of cell metabolism in innate immune memory. *Journal of Innate Immunity*, *14*(1), pp.42-50. DOI: 10.1159/000512280

Ferreira, A.V., Domínguez-Andrés, J., Merlo Pich, L.M., Joosten, L.A. and Netea, M.G., 2024, August. Metabolic regulation in the induction of trained immunity. In *Seminars in Immunopathology* (Vol. 46, No. 3, p. 7). Berlin/Heidelberg: Springer Berlin Heidelberg.

Fetahu, I.S., Höbaus, J. and Kállay, E., 2014. Vitamin D and the epigenome. *Frontiers in physiology*, *5*, p.164. DOI: 10.3389/fphys.2014.00164

Findeisen, H.M., Voges, V.C., Braun, L.C., Sonnenberg, J., Schwarz, D., Körner, H., Reinecke, H. and Sohrabi, Y., 2022. LXRα regulates oxLDL-induced trained immunity in macrophages. International Journal of Molecular Sciences, 23(11), p.6166. DOI: 10.3390/ijms23116166

Ganeshan, K. and Chawla, A., 2014. Metabolic regulation of immune responses. *Annual review of immunology*, *32*(1), pp.609-634. DOI: 10.1146/annurev-immunol-032713-120236

George, N.P., Kwon, M., Jang, Y.E., Kim, S.G., Hwang, J.S., Lee, S.S. and Lee, G., 2025. Integrative Analysis of Metabolome and Proteome in the Cerebrospinal Fluid of Patients with Multiple System Atrophy. *Cells*, *14*(4), p.265. DOI: 10.3390/cells14040265

Ghaseminejad-Raeini, A., Ghaderi, A., Sharafi, A., Nematollahi-Sani, B., Moossavi, M., Derakhshani, A. and Sarab, G.A., 2023. Immunomodulatory actions of vitamin D in various immune-related disorders: a comprehensive review. Frontiers in Immunology, 14, p.950465. DOI: 10.3389/fimmu.2023.950465

Groh, L., Keating, S.T., Joosten, L.A., Netea, M.G. and Riksen, N.P., 2018. Monocyte and macrophage immunometabolism in atherosclerosis. In Seminars in immunopathology (Vol. 40, pp. 203-214). Springer Berlin Heidelberg. DOI: 10.1007/s00281-017-0656-7

Guillonneau, X., Eandi, C.M., Paques, M., Sahel, J.A., Sapieha, P. and Sennlaub, F., 2017. On phagocytes and macular degeneration. Progress in retinal and eye research, 61, pp.98-128. DOI: 10.1016/j.preteyeres.2017.06.002

Hashemipetroudi, S.H., Nematzadeh, G., Ahmadian, G., Yamchi, A. and Kuhlmann, M., 2018. Assessment of DNA contamination in RNA samples based on ribosomal DNA. Journal of visualized experiments: JoVE, (131), p.55451. DOI: 10.3791/55451

Heckmann, B.L., Boada-Romero, E., Cunha, L.D., Magne, J. and Green, D.R., 2017. LC3-associated phagocytosis and inflammation. Journal of molecular biology, 429(23), pp.3561-3576. DOI: 10.1016/j.jmb.2017.08.012

Hirayama, D., Iida, T. and Nakase, H., 2017. The phagocytic function of macrophage-enforcing innate immunity and tissue homeostasis. International journal of molecular sciences, 19(1), p.92. DOI: 10.3390/ijms19010092

Holick, M.F., Mazzei, L., García Menéndez, S., Martín Giménez V.M., Al Anouti F. and Manucha W., 2023. Genomic or non-genomic? A question about the pleiotropic roles of vitamin D in inflammatory-based diseases. Nutrients, 15: 767. DOI: 10.3390/nu15030767

Hooftman, A., Peace, C.G., Ryan, D.G., Day, E.A., Yang, M., McGettrick, A.F., Yin, M., Montano, E.N., Huo, L., Toller-Kawahisa, J.E., Zecchini, V., Ryan T.A.J., Bolado-Carrancio A., Casey A.M., Prag H.A., Costa A.S.H., De Los Santos G., Ishimori M., Wallace D.J., Venuturupalli S., Nikitopoulou E., Frizzell N., Johansson C., Von Kriegsheim A., Murphy M.P., Jefferies C., Frezza C. and O'Neill L.A.J., 2023. Macrophage fumarate hydratase restrains mtRNA-mediated interferon production. Nature, 615(7952), pp.490-498. DOI: 10.1038/s41586-023-05720-6

Hu, C., Xuan, Y., Zhang, X., Liu, Y., Yang, S. and Yang, K., 2022. Immune cell metabolism and metabolic reprogramming. *Molecular biology reports*, *49*(10), pp.9783-9795. DOI: 10.1007/s11033-022-07474-2

Hu, T., Liu, C.H., Lei, M., Zeng, Q., Li, L., Tang, H. and Zhang, N., 2024. Metabolic regulation of the immune system in health and diseases: mechanisms and interventions. *Signal Transduction and Targeted Therapy*, *9*(1), p.268. DOI: 10.1038/s41392-024-01954-6

Italiani, P. and Boraschi, D., 2014. From monocytes to M1/M2 macrophages: phenotypical vs. functional differentiation. Frontiers in immunology, 5, p.514. DOI: 10.3389/fimmu.2014.00514

Jamilloux, Y. and Henry, T., 2013. The inflammasomes: platforms of innate immunity. Medecine Sciences: M/S, 29(11), pp.975-984. DOI: 10.1051/medsci/20132911013

Jeon, S.M. and Shin, E.A., 2018. Exploring vitamin D metabolism and function in cancer. *Experimental & molecular medicine*, *50*(4), pp.1-14. DOI: 10.1038/s12276-018-0038-9

Ji, J., Xu, Y., Zheng, M., Luo, C., Lei, H., Qu, H. and Shu, D., 2019. Methionine attenuates lipopolysaccharide-induced inflammatory responses via DNA methylation in macrophages. Acs Omega, 4(1), pp.2331-2336. DOI: 10.1021/acsomega.8b03571

Jin, J., Lin, J., Xu, A., Lou, J., Qian, C., Li, X., Wang, Y., Yu, W. and Tao, H., 2021. CCL2: an important mediator between tumor cells and host cells in tumor microenvironment. Frontiers in Oncology, 11, p.722916. DOI: 10.3389/fonc.2021.722916

Jo, C., Park, S., Oh, S., Choi, J., Kim, E.K., Youn, H.D. and Cho, E.J., 2020. Histone acylation marks respond to metabolic perturbations and enable cellular adaptation. Experimental & molecular medicine, 52(12), pp.2005-2019. DOI: https://doi.org/10.1038/s12276-020-00539-x

Joseph, L.J., 2016. Setting up a laboratory. In Genetic Diagnosis of Endocrine Disorders (pp. 409-426). Academic Press.

Kapellos, T.S., Bonaguro, L., Gemünd, I., Reusch, N., Saglam, A., Hinkley, E.R. and Schultze, J.L., 2019. Human monocyte subsets and phenotypes in major chronic inflammatory diseases. Frontiers in immunology, 10, p.2035. DOI: 10.3389/fimmu.2019.02035

Karkeni, E., Marcotorchino, J., Tourniaire, F., Astier, J., Peiretti, F., Darmon, P. and Landrier, J.F., 2015. Vitamin D limits chemokine expression in adipocytes and macrophage migration in vitro and in male mice. Endocrinology, 156(5), pp.1782-1793. DOI: 10.1210/en.2014-1647

Kesapragada, M., Sun, Y.H., Zlobina, K., Recendez, C., Fregoso, D., Yang, H.Y., Aslankoohi, E., Isseroff, R., Rolandi, M., Zhao, M. and Gomez, M., 2024. Deep learning classification for macrophage subtypes through cell migratory pattern analysis. Frontiers in Cell and Developmental Biology, 12, p.1259037. DOI: 10.3389/fcell.2024.1259037

Kopitar-Jerala, N., 2017. The role of interferons in inflammation and inflammasome activation. Frontiers in immunology, 8, p.873. DOI: 10.3389/fimmu.2017.00873

Kraus, A.U., Penna-Martinez, M., Meyer, G. and Badenhoop, K., 2018. Vitamin D effects on monocytes' CCL-2, IL6 and CD14 transcription in Addison's disease and HLA susceptibility. The Journal of steroid biochemistry and molecular biology, 177, pp.53-58. DOI: 10.1016/j.jsbmb.2017.07.026

Lafaye, A., Junot, C., Pereira, Y., Lagniel, G., Tabet, J.C., Ezan, E. and Labarre, J., 2005. Combined proteome and metabolite-profiling analyses reveal surprising insights into yeast sulfur metabolism. *Journal of Biological Chemistry*, *280*(26), pp.24723-24730. DOI: 10.1074/jbc.M502285200

Lebuhn, M., Derenkó, J., Rademacher, A., Helbig, S., Munk, B., Pechtl, A., Stolze, Y., Prowe, S., Schwarz, W.H., Schlüter, A. and Liebl, W., 2016. DNA and RNA extraction and quantitative real-time PCR-based assays for biogas biocenoses in an interlaboratory comparison. Bioengineering, 3(1), p.7. DOI: 10.3390/bioengineering3010007

Lee, A.J. and Ashkar, A.A., 2018. The dual nature of type I and type II interferons. Frontiers in immunology, 9, p.2061. DOI: 10.3389/fimmu.2018.02061

Lee, H.S., Stachelek, S.J., Tomczyk, N., Finley, M.J., Composto, R.J. and Eckmann, D.M., 2013. Correlating macrophage morphology and cytokine production resulting from biomaterial contact. Journal of biomedical materials research Part A, 101(1), pp.203-212. DOI: 10.1002/jbm.a.34309

Lee, S.M., Kok, K.H., Jaume, M., Cheung, T.K., Yip, T.F., Lai, J.C., Guan, Y., Webster, R.G., Jin, D.Y. and Peiris, J.M., 2014. Toll-like receptor 10 is involved in induction of innate immune responses to influenza virus infection. *Proceedings of the National Academy of Sciences*, *111*(10), pp.3793-3798. DOI: 10.1073/pnas.1324266111

Li, D. and Wu, M., 2021. Pattern recognition receptors in health and diseases. *Signal transduction and targeted therapy*, *6*(1), p.291. DOI: 10.1038/s41392-021-00687-0

Li, X., Ye, Y., Peng, K., Zeng, Z., Chen, L. and Zeng, Y., 2022. Histones: The critical players in innate immunity. Frontiers in immunology, 13, p.1030610. DOI: 10.3389/fimmu.2022.1030610

Li, X., Zhang, P., Wang, H. and Yu, Y., 2022. Genes expressed at low levels raise false discovery rates in RNA samples contaminated with genomic DNA. BMC genomics, 23(1), p.554. DOI: 10.1186/s12864-022-08785-1

Lin, Z., Shi, J.L., Chen, M., Zheng, Z.M., Li, M.Q. and Shao, J., 2023. CCL2: An important cytokine in normal and pathological pregnancies: A review. Frontiers in Immunology, 13, p.1053457. DOI: 10.3389/fimmu.2022.1053457

Liu, P.T., Stenger, S., Li, H., Wenzel, L., Tan, B.H., Krutzik, S.R., Ochoa, M.T., Schauber, J., Wu, K., Meinken, C. and Kamen, D.L., 2006. Toll-like receptor triggering of a vitamin D-mediated human antimicrobial response. Science, 311(5768), pp.1770-1773. DOI: 10.1126/science.1123933

Livak, K.J. and Schmittgen, T.D., 2001. Analysis of relative gene expression data using real-time quantitative PCR and the 2− ΔΔCT method. methods, 25(4), pp.402-408. DOI: 10.1006/meth.2001.1262

Lockshin, R.A. and Zakeri, Z., 2007. Cell death in health and disease. Journal of cellular and molecular medicine, 11(6), pp.1214-1224. DOI: 10.1111/j.1582-4934.2007.00150.x

Lopez-Castejon, G. and Brough, D., 2011. Understanding the mechanism of IL-1β secretion. Cytokine & growth factor reviews, 22(4), pp.189-195. DOI: 10.1016/j.cytogfr.2011.10.001

Lu, H., Dietsch, G.N., Matthews, M.A.H., Yang, Y., Ghanekar, S., Inokuma, M., Suni, M., Maino, V.C., Henderson, K.E., Howbert, J.J. and Disis, M.L., 2012. VTX-2337 is a novel TLR8 agonist that activates NK cells and augments ADCC. Clinical cancer research, 18(2), pp.499-509. DOI: 10.1158/1078-0432.CCR-11-1625

Lu, Y., Pang, Z. and Xia, J., 2023. Comprehensive investigation of pathway enrichment methods for functional interpretation of LC–MS global metabolomics data. Briefings in Bioinformatics, 24(1), p.bbac553. DOI: 10.1093/bib/bbac553

Lucena-Aguilar, G., Sánchez-López, A.M., Barberán-Aceituno, C., Carrillo-Avila, J.A., López-Guerrero, J.A. and Aguilar-Quesada, R., 2016. DNA source selection for downstream applications based on DNA quality indicators analysis. Biopreservation and biobanking, 14(4), pp.264-270. DOI: 10.1089/bio.2015.0064

Lugo-Villarino, G., Cougoule, C., Meunier, E., Rombouts, Y., Vérollet, C. and Balboa, L., 2019. The mononuclear phagocyte system in infectious disease. Frontiers in Immunology, 10, p.1443. DOI: 10.3389/fimmu.2019.01443

Luque-Martin, R., Mander, P.K., Leenen, P.J. and Winther, M.P., 2021. Classic and new mediators for in vitro modelling of human macrophages. Journal of Leucocyte Biology, 109(3), pp.549-560. DOI: 10.1002/JLB.1RU0620-018R

Maher, A.K., Burnham, K.L., Jones, E.M., Tan, M.M., Saputil, R.C., Baillon, L., Selck, C., Giang, N., Argüello, R., Pillay, C. and Thorley, E., 2022. Transcriptional reprogramming from innate immune functions to a pro-thrombotic signature by monocytes in COVID-19. Nature Communications, 13(1), p.7947. DOI: 10.1038/s41467-022-35638-y

Majumdar, S. and Murphy, P.M., 2021. Chemokine regulation during epidemic coronavirus infection. Frontiers in Pharmacology, 11, p.600369. DOI: 10.3389/fphar.2020.600369

Mani, S. and Swargiary, G., 2023. In vitro cytotoxicity analysis: MTT/XTT, trypan blue exclusion. In Animal cell culture: principles and practice (pp. 267-284). Cham: Springer International Publishing. DOI: https://doi.org/10.1007/978-3-031-19485-6_18

Marshall, J.S., Warrington, R., Watson, W. and Kim, H.L., 2018. An introduction to immunology and immunopathology. Allergy, Asthma & Clinical Immunology, 14, pp.1-10. DOI: 10.1186/s13223-018-0278-1

Martens, P.J., Gysemans, C., Verstuyf, A. and Mathieu, C., 2020. Vitamin D's effect on immune function. Nutrients, 12(5), p.1248. DOI: 10.3390/nu12051248

Martínez-Reyes, I. and Chandel, N.S., 2020. Mitochondrial TCA cycle metabolites control physiology and disease. Nature communications, 11(1), p.102. DOI: 10.1038/s41467-019-13668-3

Metzemaekers, M., Vanheule, V., Janssens, R., Struyf, S. and Proost, P., 2018. Overview of the mechanisms that may contribute to the non-redundant activities of interferon-inducible CXC chemokine receptor 3 ligands. Frontiers in immunology, 8, p.1970. DOI: 10.3389/fimmu.2017.01970

Meza-Meza, M.R., Ruiz-Ballesteros, A.I. and de la Cruz-Mosso, U., 2022. Functional effects of vitamin D: From nutrient to immunomodulator. Critical reviews in food science and nutrition, 62(11), pp.3042-3062. DOI: 10.1080/10408398.2020.1862753

Miyake, K., Ito, J., Takahashi, K., Nakabayashi, J., Brombacher, F., Shichino, S., Yoshikawa, S., Miyake, S. and Karasuyama, H., 2024. Single-cell transcriptomics identifies the differentiation trajectory from inflammatory monocytes to pro-resolving macrophages in a mouse skin allergy model. Nature communications, 15(1), p.1666. DOI: 10.1038/s41467-024-46148-4

Mol, B.A., Wasinda, J.J., Xu, Y.F., Gentle, N.L. and Meyer, V., 2024. 1, 25-dihydroxyvitamin D3 augments low-dose PMA-based monocyte-to-macrophage differentiation in THP-1 cells. Journal of Immunological Methods, 532, p.113716. DOI: 10.1016/j.jim.2024.113716

Monlish, D.A., Bhatt, S.T. and Schuettpelz, L.G., 2016. The role of toll-like receptors in hematopoietic malignancies. Frontiers in immunology, 7, p.390. DOI: 10.3389/fimmu.2016.00390

Moore, J.R., Hubler, S.L., Nelson, C.D., Nashold, F.E., Spanier, J.A. and Hayes, C.E., 2018. 1, 25-Dihydroxyvitamin D3 increases the methionine cycle, CD4+ T cell DNA methylation and Helios+ Foxp3+ T regulatory cells to reverse autoimmune neurodegenerative disease. Journal of Neuroimmunology, 324, pp.100-114. DOI: 10.1016/j.jneuroim.2018.09.008

Mosser, D.M., Hamidzadeh, K. and Goncalves, R., 2021. Macrophages and the maintenance of homeostasis. Cellular & molecular immunology, 18(3), pp.579-587. DOI: 10.1038/s41423-020-00541-3

Mu, X., Li, Y. and Fan, G.C., 2021. Tissue-resident macrophages in the control of infection and resolution of inflammation. Shock, 55(1), pp.14-23. DOI: 10.1097/SHK.0000000000001601

Munro, J., Gillen, S.L., Mitchell, L., Laing, S., Karim, S.A., Rink, C.J., Waldron, J.A. and Bushell, M., 2023. Optimisation of sample preparation from primary mouse tissue to maintain RNA integrity for methods examining translational control. Cancers, 15(15), p.3985. DOI: 10.3390/cancers15153985

Netea, M.G. and Joosten, L.A., 2024. Trained innate immunity: concept, nomenclature and future perspectives. *Journal of Allergy and Clinical Immunology*. DOI: 10.1016/j.jaci.2024.09.005

Netea, M.G., Quintin, J. and Van Der Meer, J.W., 2011. Trained immunity: a memory for innate host defense. Cell host & microbe, 9(5), pp.355-361. DOI: 10.1016/j.chom.2011.04.006

Netea, M.G., Schlitzer, A., Placek, K., Joosten, L.A. and Schultze, J.L., 2019. Innate and adaptive immune memory: an evolutionary continuum in the host's response to pathogens. Cell host & microbe, 25(1), pp.13-26. DOI: 10.1016/j.chom.2018.12.006

Nouvel, A., Laget, J., Duranton, F., Leroy, J., Desmetz, C., Servais, M.D., de Préville, N., Galtier, F., Nocca, D., Builles, N. and Rebuffat, S., 2021. Optimization of RNA extraction methods from human metabolic tissue samples of the COMET biobank. Scientific reports, 11(1), p.20975. DOI: 10.1038/s41598-021-00355-x

Nowlin, B.T., Wang, J., Schafer, J.L., Autissier, P., Burdo, T.H. and Williams, K.C., 2018. Monocyte subsets exhibit transcriptional plasticity and a shared response to interferon in SIV-infected rhesus macaques. Journal of leukocyte biology, 103(1), pp.141-155. DOI: 10.1002/JLB.4A0217-047R

Ochando, J., Mulder, W.J., Madsen, J.C., Netea, M.G. and Duivenvoorden, R., 2023. Trained immunity—basic concepts and contributions to immunopathology. *Nature Reviews Nephrology*, *19*(1), pp.23-37. DOI: 10.1038/s41581-022-00633-5

Pál, É., Ungvári, Z., Benyó, Z. and Várbíró, S., 2023. Role of vitamin D deficiency in the pathogenesis of cardiovascular and cerebrovascular diseases. Nutrients, 15(2), p.334. DOI:10.3390/nu15020334

Pappenheimer, A.M., 1917. Experimental studies upon lymphocytes: I. The reactions of lymphocytes under various experimental conditions. The Journal of experimental medicine, 25(5), p.633. DOI: 10.1084/jem.25.5.633

Park, E.J., Yoon, S., Oh, E.J., Hong, S.H., Kim, C.G. and Dai Park, S., 1996. A simplified electrophoresis method for analyses of high molecular weight RNA. Molecules and Cells, 6(1), pp.23-26. DOI: https://doi.org/10.1016/S1016-8478(23)10963-0

Park, H.J., Kim, S.M., Choi, U.Y. and Kim, L.K., 2024. Multifaceted roles of trained immunity in diverse pathological contexts. *BMB reports*, *57*(10), p.431. DOI: 10.5483/BMBRep.2024-0045

Pedersen, L.B., Nashold, F.E., Spach, K.M. and Hayes, C.E., 2007. 1, 25-dihydroxyvitamin D3 reverses experimental autoimmune encephalomyelitis by inhibiting chemokine synthesis and monocyte trafficking. Journal of neuroscience research, 85(11), pp.2480-2490. DOI: 10.1002/jnr.21382

Pham, G.S. and Mathis, K.W., 2019. Autoimmunity, estrogen, and lupus. In Sex Differences in Cardiovascular Physiology and Pathophysiology (pp. 219-237). Academic Press.

Piccinini, F., Tesei, A., Arienti, C. and Bevilacqua, A., 2017. Cell counting and viability assessment of 2D and 3D cell cultures: expected reliability of the trypan blue assay. Biological procedures online, 19, pp.1-12. DOI: 10.1186/s12575-017-0056-3

Pike, J.W. and Meyer, M.B., 2010. The vitamin D receptor: new paradigms for the regulation of gene expression by 1, 25-dihydroxyvitamin D3. Endocrinology and Metabolism Clinics, 39(2), pp.255-269. DOI: 10.1016/j.ecl.2010.02.007

Pizzurro, G.A. and Miller-Jensen, K., 2023. Reframing macrophage diversity with network motifs. *Trends in Immunology*, *44*(12), pp.965-970. DOI: 10.1016/j.it.2023.10.009

Rafique, A., Rejnmark, L., Heickendorff, L. and Møller, H.J., 2019. 25 (OH) D3 and 1.25 (OH) 2D3 inhibits TNF-α expression in human monocyte derived macrophages. PLoS One, 14(4), p.e0215383. DOI: 10.1371/journal.pone.0215383

Randolph, G.J., Jakubzick, C. and Qu, C., 2008. Antigen presentation by monocytes and monocyte-derived cells. Current opinion in immunology, 20(1), pp.52-60. DOI: 10.1016/j.coi.2007.10.010

Rao Muvva, J., Parasa, V.R., Lerm, M., Svensson, M. and Brighenti, S., 2020. Polarization of human monocyte-derived cells with vitamin D promotes control of Mycobacterium tuberculosis infection. Frontiers in Immunology, 10, p.3157. DOI: 10.3389/fimmu.2019.03157

Riksen, N.P. and Netea, M.G., 2021. Immunometabolic control of trained immunity. *Molecular aspects of medicine*, *77*, p.100897. DOI: 10.1016/j.mam.2020.100897

Rochel, N., Wurtz, J.M., Mitschler, A., Klaholz, B. and Moras, D., 2000. The crystal structure of the nuclear receptor for vitamin D bound to its natural ligand. Molecular cell, 5(1), pp.173-179. DOI: 10.1016/s1097-2765(00)80413-x

Saahene, R.O., Barnes, P. and Nuvor, S.V., 2022. The Interactive Role of Macrophages in Innate Immunity. In Macrophages-Celebrating 140 Years of Discovery. IntechOpen. DOI: 10.5772/INTECHOPEN.103924

Sadeghi, K., Wessner, B., Laggner, U., Ploder, M., Tamandl, D., Friedl, J., Zügel, U., Steinmeyer, A., Pollak, A., Roth, E. and Boltz-Nitulescu, G., 2006. Vitamin D3 down-regulates monocyte TLR expression and triggers hyporesponsiveness to pathogen-associated molecular patterns. European journal of immunology, 36(2), pp.361-370. DOI: 10.1002/eji.200425995

Sahoo, M., Ceballos-Olvera, I., del Barrio, L. and Re, F., 2011. Role of the inflammasome, IL-1β, and IL-18 in bacterial infections. The Scientific World Journal, 11(1), pp.2037-2050. DOI: 10.1100/2011/212680

Saito, K., Mishra, S., Warrier, T., Cicchetti, N., Mi, J., Weber, E., Jiang, X., Roberts, J., Gouzy, A., Kaplan, E. and Brown, C.D., 2021. Oxidative damage and delayed replication allow viable Mycobacterium tuberculosis to go undetected. Science translational medicine, 13(621), p.eabg2612. DOI: 10.1126/scitranslmed.abg2612

Sallusto, F., Lanzavecchia, A., Araki, K. and Ahmed, R., 2010. From vaccines to memory and back. Immunity, 33(4), pp.451-463. DOI: 10.1016/j.immuni.2010.10.008

Sambrook J, Russel DW. (2001). Molecular Cloning: A Laboratory Manual, 3rd Ed. Cold Spring Harbor Laboratory Press: New York, NY.

Sameer, A.S. and Nissar, S., 2021. Toll-like receptors (TLRs): structure, functions, signaling, and role of their polymorphisms in colorectal cancer susceptibility. BioMed Research International, 2021(1), p.1157023. DOI: 10.1155/2021/1157023

Santecchia, I., Ferrer, M.F., Vieira, M.L., Gómez, R.M. and Werts, C., 2020. Phagocyte escape of Leptospira: the role of TLRs and NLRs. Frontiers in immunology, 11, p.571816. DOI: 10.3389/fimmu.2020.571816

Sassi, F., Tamone, C. and D'Amelio, P., 2018. Vitamin D: nutrient, hormone, and immunomodulator. Nutrients, 10(11), p.1656. DOI: 10.3390/nu10111656

Serbina, N.V., Jia, T., Hohl, T.M. and Pamer, E.G., 2008. Monocyte-mediated defense against microbial pathogens. Annu. Rev. Immunol., 26(1), pp.421-452. DOI: 10.1146/annurev.immunol.26.021607.090326

Shi, C. and Pamer, E.G., 2011. Monocyte recruitment during infection and inflammation. Nature reviews immunology, 11(11), pp.762-774. DOI: 10.1038/nri3070

Siddiqui, M., Manansala, J.S., Abdulrahman, H.A., Nasrallah, G.K., Smatti, M.K., Younes, N., Althani, A.A. and Yassine, H.M., 2020. Immune modulatory effects of vitamin D on viral infections. Nutrients, 12(9), p.2879. DOI: 10.3390/nu12092879

Small, A.G., Harvey, S., Kaur, J., Putty, T., Quach, A., Munawara, U., Perveen, K., McPhee, A., Hii, C.S. and Ferrante, A., 2021. Vitamin D upregulates the macrophage complement receptor immunoglobulin in innate immunity to microbial pathogens. Communications biology, 4(1), p.401. DOI: 10.1038/s42003-021-01943-3

Sohrabi, Y., Sonntag, G.V., Braun, L.C., Lagache, S.M., Liebmann, M., Klotz, L., Godfrey, R., Kahles, F., Waltenberger, J. and Findeisen, H.M., 2020. LXR activation induces a proinflammatory trained innate immunity-phenotype in human monocytes. Frontiers in immunology, 11, p.353. DOI: 10.3389/fimmu.2020.00353

Song, B.M., Kang, Y.M., Kim, H.S. and Seo, S.H., 2011. Induction of inflammatory cytokines and toll-like receptors in human normal respiratory epithelial cells infected with seasonal H1N1, 2009 pandemic H1N1, seasonal H3N2, and highly pathogenic H5N1 influenza virus. *Viral immunology*, *24*(3), pp.179-187. DOI: 10.1089/vim.2010.0125

Song, X., Gao, X., Wang, Y., Raja, R., Zhang, Y., Yang, S., Li, M., Yao, Z. and Wei, L., 2021. HCV core protein induces chemokine CCL2 and CXCL10 expression through NF-κB signaling pathway in macrophages. Frontiers in immunology, 12, p.654998. DOI: 10.3389/fimmu.2021.654998

Soto-Heredero, G., Gómez de Las Heras, M.M., Gabandé-Rodríguez, E., Oller, J. and Mittelbrunn, M., 2020. Glycolysis–a key player in the inflammatory response. The FEBS journal, 287(16), pp.3350-3369. DOI: 10.1111/febs.15327

Stoddart, M.J., 2011. Cell viability assays: introduction. Methods in molecular biology (Clifton, N.J.), 740, p1–6. DOI: 10.1007/978-1-61779-108-6_1

Stunault, M.I., Bories, G., Guinamard, R.R. and Ivanov, S., 2018. Metabolism plays a key role during macrophage activation. Mediators of Inflammation, 2018(1), p.2426138. DOI: 10.1155/2018/2426138

Su, S.B., Tao, L., Deng, Z.P., Chen, W., Qin, S.Y. and Jiang, H.X., 2021. TLR10: Insights, controversies and potential utility as a therapeutic target. *Scandinavian Journal of Immunology*, *93*(4), p.e12988. DOI: 10.1111/sji.12988

Tedesco, S., De Majo, F., Kim, J., Trenti, A., Trevisi, L., Fadini, G.P., Bolego, C., Zandstra, P.W., Cignarella, A. and Vitiello, L., 2018. Convenience versus biological significance: are PMA differentiated THP-1 cells a reliable substitute for blood-derived macrophages when studying in vitro polarization? Frontiers in pharmacology, 9, p.71. DOI: 10.3389/fphar.2018.00071

Tokuda, N. and Levy, R.B., 1996. 1, 25-dihydroxyvitamin D3 stimulates phagocytosis but suppresses HLA-DR and CD13 antigen expression in human mononuclear phagocytes. Proceedings of the Society for Experimental Biology and Medicine, 211(3), pp.244-250. DOI: 10.3181/00379727-211-43967

Triantafilou, K., Vakakis, E., Orthopoulos, G., Ahmed, M.A.E., Schumann, C., Lepper, P.M. and Triantafilou, M., 2005. TLR8 and TLR7 are involved in the host's immune response to human parechovirus 1. *European journal of immunology*, *35*(8), pp.2416-2423. DOI: 10.1002/eji.200526149

Tsuchiya, S., Yamabe, M., Yamaguchi, Y., Kobayashi, Y., Konno, T. and Tada, K., 1980. Establishment and characterization of a human acute monocytic leukemia cell line (THP-1). International journal of cancer, 26(2), pp.171-176. DOI: 10.1002/ijc.2910260208

Ungefroren, H., Hyder, A., Schulze, M., Fawzy El-Sayed, K.M., Grage-Griebenow, E., Nussler, A.K. and Fändrich, F., 2016. Peripheral blood monocytes as adult stem cells: molecular characterization and improvements in culture conditions to enhance stem cell features and proliferative potential. Stem cells international, 2016(1), p.7132751. DOI: 10.1155/2016/7132751

Untergasser, A., Cutcutache, I., Koressaar, T., Ye, J., Faircloth, B.C., Remm, M. and Rozen, S.G., 2012. Primer3—new capabilities and interfaces. Nucleic acids research, 40(15), pp.e115-e115. DOI: 10.1093/nar/gks596

Valdés-López, J.F., Velilla, P. and Urcuqui-Inchima, S., 2022. Vitamin D modulates the expression of Toll-like receptors and pro-inflammatory cytokines without affecting Chikungunya virus replication, in monocytes and macrophages. Acta Tropica, 232, p.106497. DOI: 10.1016/j.actatropica.2022.106497

van Megen, K.M., Chen, Z., Joosten, A.M., Laban, S., Zwaginga, J.J., Natarajan, R., Nikolic, T. and Roep, B.O., 2021. 1, 25-dihydroxyvitamin D3 induces stable and reproducible therapeutic tolerogenic dendritic cells with specific epigenetic modifications. Cytotherapy, 23(3), pp.242-255. DOI: 10.1016/j.jcyt.2020.12.003

Vandesompele, J., De Preter, K., Pattyn, F., Poppe, B., Van Roy, N., De Paepe, A. and Speleman, F., 2002. Accurate normalization of real-time quantitative RT-PCR data by geometric averaging of multiple internal control genes. Genome biology, 3, pp.1-12. DOI: https://doi.org/10.1186/gb-2002-3-7-research0034

Varghese, J.E., Shanmugam, V., Rengarajan, R.L., Meyyazhagan, A., Arumugam, V.A., Al-Misned, F.A. and El-Serehy, H.A., 2020. Role of vitamin D3 on apoptosis and inflammatory-associated gene in colorectal cancer: An in vitro approach. Journal of King Saud University-Science, 32(6), pp.2786-2789.

Versmessen, N., Van Simaey, L., Negash, A.A., Vandekerckhove, M., Hulpiau, P., Vaneechoutte, M. and Cools, P., 2024. Comparison of DeNovix, NanoDrop and Qubit for DNA quantification and impurity detection of bacterial DNA extracts. Plos one, 19(6), p.e0305650. DOI: 10.1371/journal.pone.0305650

Vestergaard, C., Just, H., Baumgartner Nielsen, J., Thestrup-Pedersen, K. and Deleuran, M., 2004. Expression of CCR2 on monocytes and macrophages in chronically inflamed skin in atopic dermatitis and psoriasis. Acta dermato-venereologica, 84(5). DOI: 10.1080/00015550410034444

Vuscan, P., Kischkel, B., Joosten, L.A. and Netea, M.G., 2024. Trained immunity: General and emerging concepts. *Immunological Reviews*. DOI: 10.1111/imr.13326

Walker, V.P. and Modlin, R.L., 2009. The vitamin D connection to pediatric infections and immune function. Pediatric research, 65(7), pp.106-113. DOI: 10.1203/PDR.0b013e31819dba91

Wang, K., Huang, H., Zhan, Q., Ding, H. and Li, Y., 2024. Toll-like receptors in health and disease. MedComm, 5(5), p.e549. DOI: 10.1002/mco2.549

Wang, W., Ma, L., Liu, B. and Ouyang, L., 2024. The role of trained immunity in sepsis. *Frontiers in Immunology*, *15*, p.1449986. DOI: 10.3389/fimmu.2024.1449986

Wang, Y., Li, N., Zhang, X. and Horng, T., 2021. Mitochondrial metabolism regulates macrophage biology. Journal of Biological Chemistry, 297(1). DOI: 10.1016/j.jbc.2021.100904

Wang, Z.H., Peng, W.B., Zhang, P., Yang, X.P. and Zhou, Q., 2021. Lactate in the tumour microenvironment: From immune modulation to therapy. EBioMedicine, 73. DOI: 10.1016/j.ebiom.2021.103627

Wculek, S.K., Dunphy, G., Heras-Murillo, I., Mastrangelo, A. and Sancho, D., 2022. Metabolism of tissue macrophages in homeostasis and pathology. *Cellular & molecular immunology*, *19*(3), pp.384-408. DOI: 10.1038/s41423-021-00791-9

Williams, H., Mack, C., Baraz, R., Marimuthu, R., Naralashetty, S., Li, S. and Medbury, H., 2023. Monocyte differentiation and heterogeneity: inter-subset and interindividual differences. International Journal of Molecular Sciences, 24(10), p.8757. DOI: 10.3390/ijms24108757.

Williams, N.C. and O'Neill, L.A., 2018. A role for the Krebs cycle intermediate citrate in metabolic reprogramming in innate immunity and inflammation. Frontiers in immunology, 9, p.141. DOI: 10.3389/fimmu.2018.00141

Wynn, T.A. and Vannella, K.M., 2016. Macrophages in tissue repair, regeneration, and fibrosis. Immunity, 44(3), pp.450-462. DOI: 10.1016/j.immuni.2016.02.015

Xu, Y., Chen, Y., Zhang, X., Ma, J., Liu, Y., Cui, L. and Wang, F., 2022. Glycolysis in innate immune cells contributes to autoimmunity. Frontiers in Immunology, 13, p.920029. DOI: 10.3389/fimmu.2022.920029

Yaqinuddin, A., Ambia, A.R. and Alaujan, R.A., 2022. Immunomodulatory effects of vitamin D and vitamin C to improve immunity in COVID-19 patients. Journal of Health and Allied Sciences NU, 12(01), pp.1-6. DOI: 10.1055/s-0041-1730084

Yuk, J.M., Shin, D.M., Lee, H.M., Yang, C.S., Jin, H.S., Kim, K.K., Lee, Z.W., Lee, S.H., Kim, J.M. and Jo, E.K., 2009. Vitamin D3 induces autophagy in human monocytes/macrophages via cathelicidin. Cell host & microbe, 6(3), pp.231-243. DOI: 10.1016/j.chom.2009.08.004

Yusupov, E., Li-Ng, M., Pollack, S., Yeh, J.K., Mikhail, M. and Aloia, J.F., 2010. Vitamin D and serum cytokines in a randomized clinical trial. *International journal of endocrinology*, *2010*(1), p.305054. DOI: 10.1155/2010/305054

Zepeda, B. and Verdonk, J.C., 2022. RNA extraction from plant tissue with homemade acid guanidinium thiocyanate phenol chloroform (AGPC). Current Protocols, 2(1), p.e351.

Zhang, C., Yang, M. and Ericsson, A.C., 2021. Function of macrophages in disease: current understanding on molecular mechanisms. Frontiers in immunology, 12, p.620510. DOI: 10.3389/fimmu.2021.620510

Zhang, S., Meng, Y., Zhou, L., Qiu, L., Wang, H., Su, D., Zhang, B., Chan, K.M. and Han, J., 2022. Targeting epigenetic regulators for inflammation: Mechanisms and intervention therapy. MedComm, 3(4), p.e173. DOI: 10.1002/mco2.173

Zhang, Y., Leung, D.Y., Richers, B.N., Liu, Y., Remigio, L.K., Riches, D.W. and Goleva, E., 2012. Vitamin D inhibits monocyte/macrophage proinflammatory cytokine production by targeting MAPK phosphatase-1. The Journal of Immunology, 188(5), pp.2127-2135. DOI: 10.4049/jimmunol.1102412

Zhao, Q., Kim, T., Pang, J., Sun, W., Yang, X., Wang, J., Song, Y., Zhang, H., Sun, H., Rangan, V. and Deshpande, S., 2017. A novel function of CXCL10 in mediating monocyte production of proinflammatory cytokines. Journal of Leukocyte Biology, 102(5), pp.1271-1280. DOI: 10.1189/jlb.5A0717-302